TÉCNICO LISBOA

Coaxial to Microstrip Transition Modeling and Characterization

Rita Dias Carreira

Thesis to obtain the Master of Science Degree in

Electrical and Computer Engineering

Supervisors: Prof. João Manuel Torres Caldinhas Simões Vaz

Examination Committee

Chairperson: Prof. Francisco André Corrêa Alegria

Supervisor: Prof. João Manuel Torres Caldinhas Simões Vaz

Members of the Committee: Prof. António Luís Campos da Silva Topa

January 2021

Declaration

I declare that this document is an original work of my own authorship and that it fulfils all the requirements of the Code of Conduct and Good Practices of the Universidade de Lisboa.

Acknowledgments

The author would like to recognize everyone who played a role in her academic journey.

First of all, a special thanks to her parents Carlos Carreira and Jacinta Castelão who's support and confidence walked with her until the end, to her sister, Zita Carreira, who's path in Instituto Superior Técnico, way to be, stubbornness and constant support allowed the author to drive almost smoothly through not only thesis but life. Author would also like to show special gratitude to her soon to be brother-in-law, Jorge Arromba, for not giving up on THE corrections of this thesis. The author would like to express her deep gratitude to Daniel Fortunato for the help in this work especially in its final steps. Their presence and contributions were essential and the author will be forever in debt.

Secondly, the author appreciates professor João Caldinhas Vaz for the help, guidance and support through this dissertation.

Finally the author would also like to thank all of her good friends for the support, wisdom, company and ultimately friendship.

To all parts involved, the author warmly thank them, without their guidance and help, this dissertation would not have been possible.

Abstract

Experimental characterization is an important step in high frequency circuits design. For that, an electrical connection between the device under test and the measurement equipment will be required. This affects the measured results. To subtract the electrical connection influence from measured results and obtain the device under test data, several de-embedding techniques can be used.

This work defines, tests and models two commonly used connections to a transmission line: welded Sub-Miniature version A (SMA) connectors and test fixture with SMA connectors.

Transmission line types were studied and, after an in-depth analysis, the microstrip line was the one chosen to work with. Two PCBs with seven transmission lines, with the same length but different widths, were designed and simulated with the Advanced Design System (ADS) software. The seven lines had theoretical characteristic impedance close to 50 Ω. An experimental analyse of the characteristic impedances of these lines was performed to choose the most matched one. The first PCB had welded SMA connectors to its transmission line and the second Printed Circuit Board (PCB) was placed on a test fixture for testing. The SMA connectors and the test fixture's SMA connectors were connected to a calibrated 2-port VNA. S-parameters were obtained with a frequency sweep ranging from 100MHz to 14GHz.

The obtained results from the VNA, had both transmission line and SMA connector/test fixture's SMA connectors included. The comparison between the theoretical results and the experimental results enabled the creation of a model for the SMA connector. Due to the poor quality of the ground planes, a model of the test fixture's SMA connectors could not be obtained.

Keywords

Transmission lines, microstrip, S-parameters, Calibration, PCB, VNA, SMA connector, test fixture, de-

embedding

Resumo

A caracterização experimental é um passo importante na concepção de circuitos de alta frequência. Para tal, será necessária uma ligação eléctrica entre o dispositivo em teste e o equipamento de medição, o que afecta os resultados medidos. Para subtrair a influência da ligação eléctrica dos resultados medidos e obter o dispositivo em teste, podem ser usadas várias técnicas de de-embedding.

Este trabalho define, testa e faz a modelação de duas ligações a uma linha de transmissão normalmente utilizadas : conectores SMA soldados e test fixtures com conectores SMA.

Vários tipos de linha de transmissão foram estudados e, após uma análise aprofundada, a linha microstrip foi a escolhida para trabalhar. Dois PCBs com sete linhas de transmissão - com o mesmo comprimento mas com larguras diferentes - foram concebidos e simuladas com o software Advanced Design System (ADS). As sete linhas tinham uma impedância característica teórica próxima de 50 Ω. Foi realizada uma análise experimental das características destas linhas para escolher a mais adaptada. O primeiro PCB tinha conectores SMA soldados à sua linha de transmissão e o segundo PCB foi colocado numa test fixture para teste.

Os conectores SMA e os conectores SMA do test fixture foram ligados a um VNA de 2 portos calibrado e foram obtidos com um varrimento de frequência de 100MHz a 14GHz. A comparação entre os resultados teóricos e os resultados experimentais permitiu a criação de um modelo para o conector SMA. Devido à má qualidade dos planos de massa, não foi possível obter um modelo dos conectores SMA do test fixture.

Palavras Chave

Linhas de transmissão, microstrip, S-parameters, Calibration, PCB, VNA, SMA connector , test fixture, de-embedding

Contents

List of Figures

List of Tables

Acronyms

ADS	Advanced Design System
CPW	Coplanar Waveguide
DUT	Device Under Test
GCPW	Grounded Coplanar Waveguide
GT	Transducer Power Gain
K	Stability Factor
LSNA	Large Signal Network Analyzer
MAG	Maximum Available Gain
MMICs	Microwave Monolithically Integrated Circuits
MSG	Maximum Stable Gain
PCB	Printed Circuit Board
RF	Radio Frequency
RFICs	Radio Frequency Integrated Circuits
SMA	Sub-Miniature version A
SNA	Scalar Network Analyzer
SOLT	Short-Open-Load-Thru
TDR	Time Domain Response
TE	Transverse Electromagnetic Mode
TEM	Transverse Electromagnetic Mode
TM	Transverse Magnetic Mode
TRL	Thru-Reflect-Line
VNA	Vector Network Analyzer

1

Introduction

Contents

Introduction

1.1 Purpose and motivation

There are many ways to test a PCB with mounted components. The usual way is to connect the PCB to the exterior by using a welded SMA connector. The second most used approach for testing PCBs and its mounted components, is the test fixture.

Several published works tried to describe SMA connector to microstrip transition effect on the measures (for example in [1] or in [2]). The problem of these works is the lack of consistency, because, the description of a SMA connector in lumped model topology is not the same in all these works. The same problem is present in the test fixtures.

1.2 Goals and challenges

The objectives of this work are to develop models both for SMA connector and for test fixture and to justify the discrepancy of the results between theoretical, simulated and experimental data.

This main objectives of this work are the modeling of a Sub-Miniature version A (SMA) connector and of a test Fixture. The available test fixture was manufactured by Argumen (now HMS). To accomplish these goals a PCB with some elements will be developed.

The emerging challenges are the unfamiliarity with the equipment (VNA), the development of a PCB capable of obtaining favorable results that enables the correct modulation of the SMA connector and of the test fixture.

1.3 Document organisation

This report can be divided in seven sections.

Chapter 2 reviews the theory of transmission lines and its associated equations. Considering that this thesis primarily works with high frequency, this chapter focuses on types of transmission lines that are used in high frequency applications. Losses in transmission lines are also mentioned in this chapter.

A summary of the advantages and the disadvantages between transmission lines and a comparison between each type is presented at the end of this chapter.

Chapter 4 is divided in 3 sections: theory of the S-parameters, calibration of the equipment VNA and, De-embedding S-parameters. It explains the theory of the S-parameters since a large part of the results introduced are in the form of S-parameters. Procedures for VNA calibration are is mentioned. After the calibration of the VNA, measurements can be performed. Since these measurements include connections to the exterior through the SMA connectors, the theory of de-embedding and embedding S-parameters is also described.

Chapter 6 is divided into two major sections: development of SMA connector and SMA connector from test fixture models. This chapter presents simulations made with program Advanced Design System (ADS), followed by the development of a PCB in ADS. Comparisons between simulated data and experimental data are also presented. This process is made both with test fixture and with the SMA connector. Finally, two lumped models are presented: the SMA connector model and the SMA connector model from test fixture model.

Chapter 8 concludes the work and discusses the validity of the proposed models as well as future work.

2

Transmission Lines

Contents

Transmission Lines

This chapter introduces the most used elements in high frequency: transmission lines.

A line with infinitesimal length, dy, can be approximated by Figure 2.1 as referred in [3]

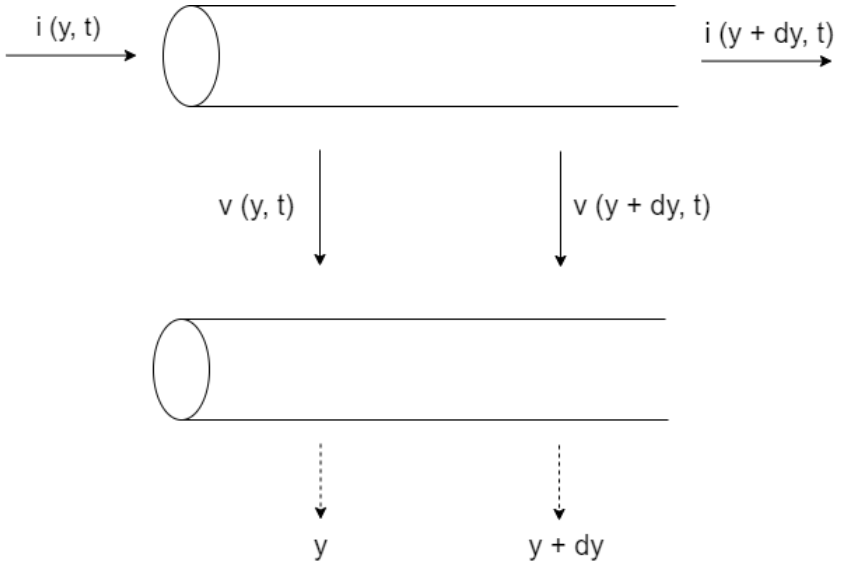

Figure 2.1: Line with infinitesimal length

and it is equivalent to 2.2.

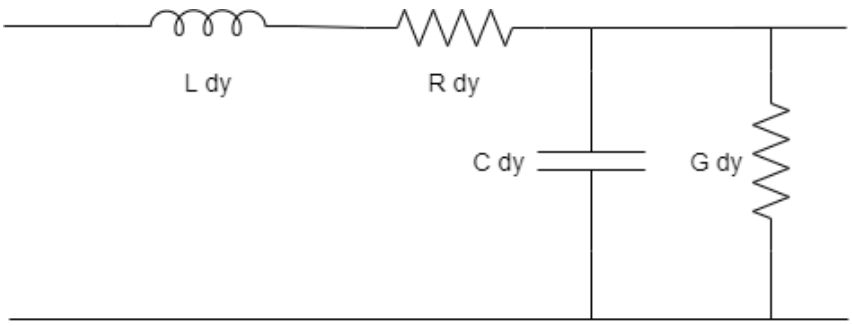

Figure 2.2: Equivalent lumped-element circuit

In equation 2.2, R represents resistance, L inductance, C capacitance and G conductance. Com-

paring the previous figures and applying Kirchoff's voltage laws the following equations can be obtained:

$$v(y,t) - v(y+dy,t) = Ri(y,t)dy + L(\frac{\delta i(y,t)}{\delta t})dy, \tag{2.1}$$

$$i(y,t) - i(y+dy,t) = Gv(y,t)dy + C(\frac{\delta v(y,t)}{\delta t})dy. \tag{2.2}$$

Combining 2.1 and 2.2, results in:

$$\frac{\delta v(y,t)}{\delta y} = -Ri(y,t) - L\frac{\delta i(y,t)}{\delta t}, \tag{2.3}$$

$$\frac{\delta i(y,t)}{\delta y} = -Gv(y,t) - C\frac{\delta v(y,t)}{\delta t}. \tag{2.4}$$

Fourier equations are applied to the equations 2.1 and 2.2 as follows:

$$\frac{\delta V(y)}{\delta y} = -(R + j\omega L)I(y); \tag{2.5}$$

$$\frac{\delta I(y)}{\delta y} = -(G + j\omega C)V(y). \tag{2.6}$$

Combining equations 2.5 and 2.6, line voltage and current can be expressed by the next differential equations:

$$\frac{\delta^2 V(y)}{\delta y^2} = (R + j\omega L)(G + j\omega C)V(y); \tag{2.7}$$

$$\frac{\delta^2 I(y)}{\delta y^2} = (R + j\omega L)(G + j\omega C)I(y); \tag{2.8}$$

Equation 2.7 has for solution,

$$V(y) = V^+ e^{-\gamma y} + V^- e^{\gamma y}, \tag{2.9}$$

where $\gamma(y)$ is the propagation constant given by equation 2.10.

$$\gamma \simeq \sqrt{(R + j\omega L)(G + j\omega C)} = \sqrt{(RG - \omega^2 LC) + j\omega(RC + GL)} = \alpha + j\beta \tag{2.10}$$

V^+ and V^- are the complex amplitudes of the voltage that propagate on the line, $e^{-\gamma y}$ represents the propagation of the wave in the positive direction and $e^{\gamma y}$ on the opposite direction.
Thereby, V can be considered as an overlap of two waves, one that follows direction y and the other its

opposite.

Considering equation 2.8, current I can be expressed by equation 2.11.

$$I(y) = -\frac{1}{R + j\omega L}\frac{\delta V(y)}{\delta y} \tag{2.11}$$

Combining equations 2.11 and 2.9, equation 2.12 is obtained.

$$I(y) = \frac{1}{Z_0}(V^+ e^{-\gamma y} + V^- e^{\gamma y}). \tag{2.12}$$

If an infinite line is considered, the terms containing $e^{\gamma y}$ are nullified. The ratio voltage current is called characteristic impedance of the line (Z_0):

$$Z_0 = \frac{R + j\omega L}{\gamma} = \sqrt{\frac{R + j\omega L}{G + j\omega C}}. \tag{2.13}$$

Note that the propagation constant and the characteristic impedance depend on R, L, G, C and ω but do not depend on the length of the line.

Equation 2.13 is only valid for a general line, including its loss effects. Therefore, the propagation constant and the characteristic impedance are complex.

Considering R and G equal zero (case with no losses), equation 2.14 is obtained.

$$\gamma = j\omega\sqrt{LC} = j\omega t_{pd} = j\beta, \tag{2.14}$$

$$Z_0 = \sqrt{\frac{L}{C}}. \tag{2.15}$$

in which t_{tp} is the propagation time in the line per length unit, the inverse of phase velocity v_P. The wavelength is defined as the distance between two successive maximums or minimums of the wave and is given by the coefficient between phase velocity and frequency, as follows,

$$\gamma = \frac{v_P}{f} = \frac{2\pi}{\beta}. \tag{2.16}$$

It results that the voltage (2.9) and the current (2.11) can be expressed as:

$$V(y) = V^+ e^{-j\beta y} + V^- e^{-j\beta y}, \tag{2.17}$$

$$I(y) = \frac{1}{Z_0}(V^+ e^{-j\beta y} + V^- e^{-j\beta y}). \tag{2.18}$$

Most used transmission lines are planar types which can be produced using low-cost printed circuit

board materials and processes. Some of the multiconductor transmission lines have a solid dielectric substrate including one or two layers of metallization with the signal and ground currents running in separate conductors.

Transmission lines with planar structure used in microwave connection can be divided in those who can brace a Transverse Electromagnetic Mode (TEM) of propagation - both electric and magnetic fields are perpendicular to the direction of propagation - and those who cannot.

When analysing several type of transmission line it is important to refer that every transmission line behaves like a high-pass filter, meaning that each line has an upper frequency limit, also referred to as cutoff frequency.

Most common types of transmission lines are presented in Figure 2.3 .

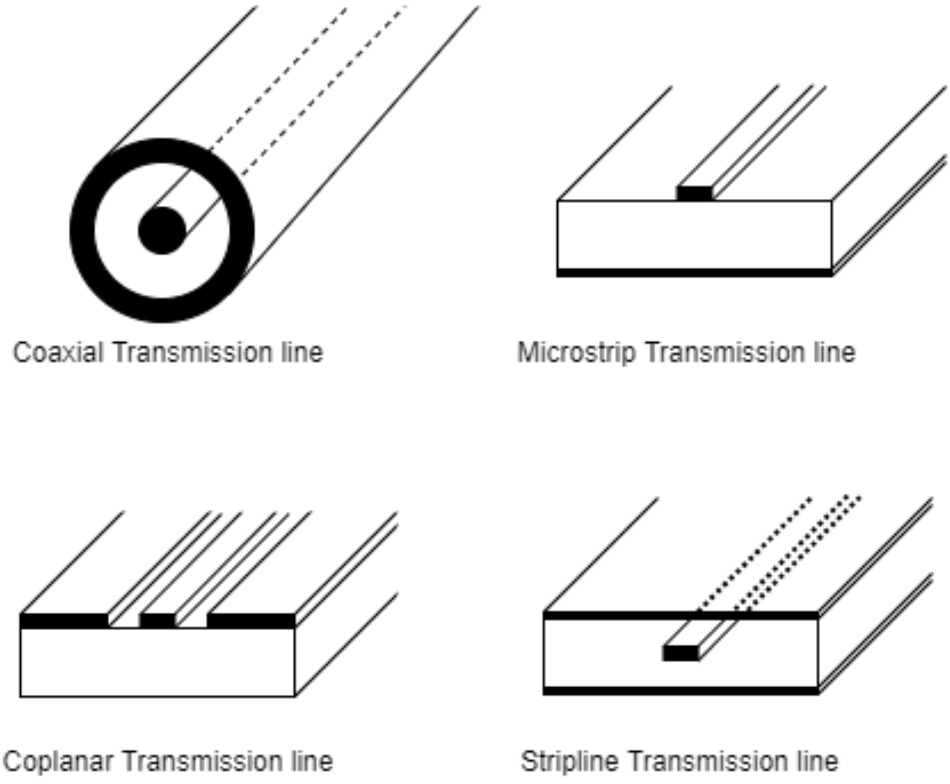

Figure 2.3: Typical transmission Lines [4].

A coaxial cable consists in two cylindrical conductors separated by a dielectric material, which has shield property. Its typical applications are Radio Frequency (RF) signal distribution networks and equipment for high-frequency measurements, like oscilloscopes and spectrum analysers. For the purpose of the present work, the coaxial cable will only be referred to as a reference. Other transmission lines will be analyzed in section 2.2, 2.3 and 2.4.

2.1 Transverse modes of electromagnetic waves

To understand waveguides, the wave concept must be addressed. The wave that concerns coaxial transmission line, microstrip and stripline is the Transverse Electromagnetic Mode (TEM). In order to look further at waveguides, the Transverse Electromagnetic Mode (TE) and Transverse Magnetic Mode (TM) must also be mentioned:

- Transverse Electromagnetic Mode (TE) - no electric field in the direction of propagation. E_z = 0 , $H_z \neq 0$. TE waves can be supported between two or more conductors or inside closed ones.
- Transverse Magnetic Mode (TM) - no magnetic field in the direction of the propagation. $E_z \neq 0$, H_z = 0. Similar to TE, TM waves can be supported between two or more conductors or inside closed ones.
- Transverse Electromagnetic Mode (TEM) - Both electric and magnetic fields are perpendicular to the direction of propagation. E_z = 0, H_z = 0.
- Quasi-Transverse Electromagnetic Mode (TEM) - Hybrid mode. $E_z \neq 0$, $H_z \neq 0$. Combination of Transverse Electromagnetic Mode (TE) and Transverse Magnetic Mode (TM). Field propagates both in air and dielectric media.

There are some unique characteristics of the TEM mode. At least two not connected conductors and a single insulator are necessary for TEM to exist, its cut-off frequency is zero Hertz.

2.2 Strip transmission line

According to Pozar [5], stripline was invented by R. Barrett in the 50s.

Stripline requires three layers of conductors: the internal (”hot” conductor), while the other two layers are the ”cold” or ”ground” conductor, consequently is also referred to as tri-plate, as mentioned in [6].

Stripline is close to a flexible and semi-rigid cable, it evolved from the coaxial cables. If pressure is applied to a coaxial cable, top and bottom, the circular structure starts to deform and goes to a elongated form. Stripline has a more operational form for higher frequencies and more efficient in Radio Frequency (RF) and microwave applications. This type of efficiency of the transmission line can be addressed to isolation. Stripline offers a good electro-magnetic shield and supports several layers, in a more easier way than some of the other transmission lines. This characteristics are due to its central metal structure.

The ”hot” conductor (central stripline’s conductor) is embedded in a homogeneous and isotropic dielectric. Unlike the next type of transmission line addressed in the present work - microstrip - in

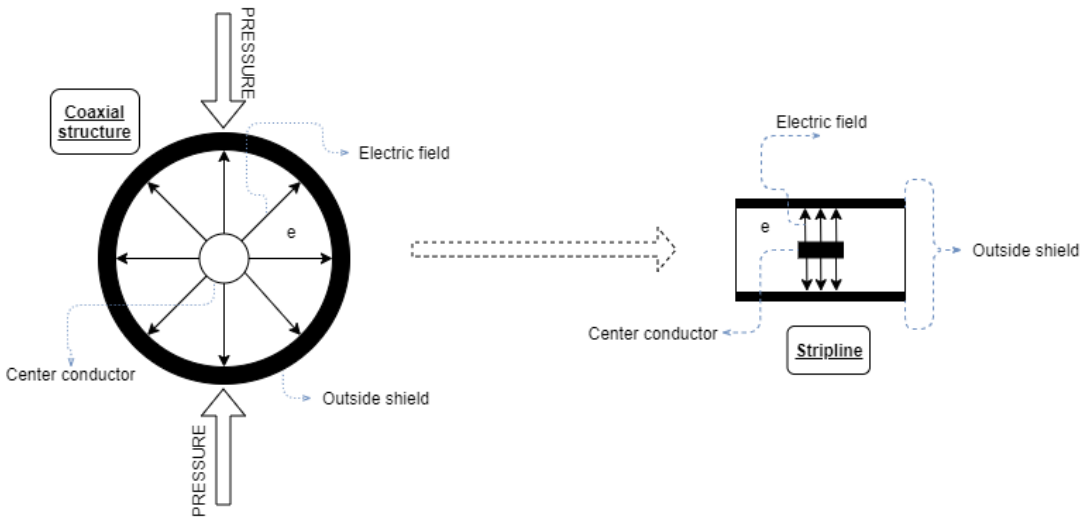

Figure 2.4: Evolution of stripline [6].

stripline, the term substrate cannot be properly used since the dielectric completely involves the ”hot” conductor.

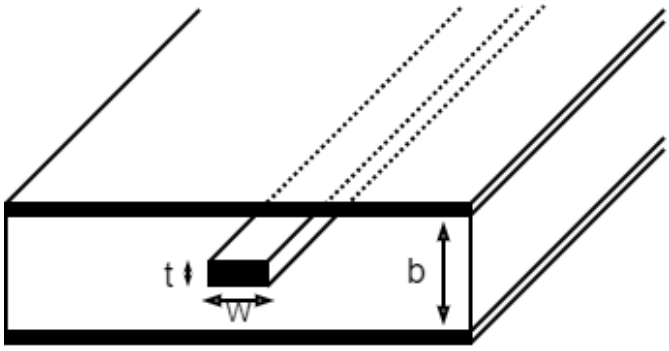

Figure 2.5: Stripline

Dielectric structure leads to a natural shielding effect on the circuit since it is completely enclosed with metal both on top and bottom. Impedance in striplines can be defined by equation 2.19,

$$Z_0[\Omega] = \frac{30\pi}{\sqrt{\epsilon_r}}\left(\frac{b}{W_e + 0.441b}\right), \tag{2.19}$$

where b is the dielectric thickness and W_e is the center strip effective width, given by,

$$\frac{W_e}{b} = \frac{W}{b} - \begin{cases} 0, & \text{if } \frac{W}{b} > 0.35, \\ (0.35 - \frac{W}{b})^2, & \text{if } \frac{W}{b} < 0.35. \end{cases} \tag{2.20}$$

According to equation 2.20, characteristic impedance decreases as the strip width increases.

Stripline is one of the transmission lines currently used when the interconnect density must be high,

such as in integrated circuit packages and high speed digital circuits.

Main disadvantage in stripline is its complex structure. This structure origins high costs and makes it difficult to deal with troubleshooting due to its entire structure being in the middle. The packages sometimes are laminated and sealed with epoxy which worsens the previous situation.

Microstrip is one of the developed solutions that allow to solve the disadvantages of stripline.

2.3 Microstrip transmission line

Grieg and Engelmann in 1952 offered a solution to adjust some problems of the transmission line stripline, as referred in [7]. They developed microstrip while removing one of stripline's ground planes. This microwave transmission line has become one of the most important base for printed microwave circuits, Radio Frequency Integrated Circuits (RFICs) and Microwave Monolithically Integrated Circuits (MMICs).

Unlike stripline the substrate discontinuity makes the dominant mode to be quasi-TEM not TEM, resulting in the phase velocity and characteristic impedance varying with the frequency.

Microstrip line is a transmission-line geometry with a single conductor trace on one side of the dielectric substrate and a ground plane on the opposite side.

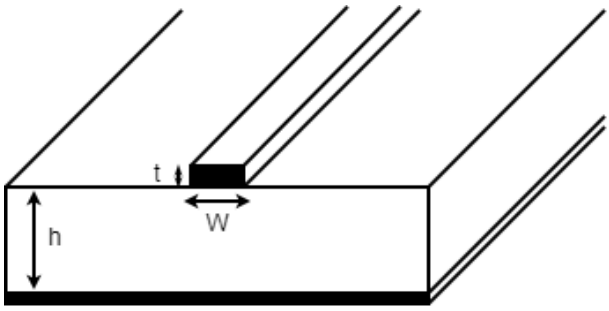

Figure 2.6: Microstrip transmission, as presented in [8].

The wavelength observed in the microstrip line is obtained from

$$\lambda_{eff} = \frac{\lambda}{\epsilon_{eff}^{0.5}}, \tag{2.21}$$

where λ is the free-space wavelength and ϵ_{eff} the effective dielectric constant which takes into account that most electric field is contained in the substrate, even so, some runs above the board, as demonstrated in [9].

$$\epsilon_{eff} = \frac{\epsilon + 1}{2} + \frac{\epsilon - 1}{2} \frac{1}{\sqrt{1 + \frac{12h}{W}}}, \tag{2.22}$$

Some of the field lines in the dielectric region are in air, therefore, the dielectric constant depends on the conductor width, frequency, substrate thickness and subtract dielectric constant.

According to [5], an accurate equation for microstrip characteristic impedance is:

$$Z_0[\Omega] = \begin{cases} \frac{60}{\sqrt{\epsilon}} ln(\frac{8h}{W} + \frac{W}{4h}), & \text{if } \frac{W}{h} \leq 1, \\ \frac{120\pi}{\sqrt{\epsilon}[\frac{W}{h} + 1.393 + 0.667 ln(\frac{W}{h} + 1.444)]}, & \text{if } \frac{W}{h} \geq 1. \end{cases} \tag{2.23}$$

The characteristic impedance changes lightly with frequency. The limitation in frequency is given mainly by the lowest order transverse resonance, which occurs when the width of the line is closer to half-wavelength in the dielectric.

Some of the of the conductor losses increase with the characteristic impedance due to the greater resistance of narrow strips and it follows a trend that is opposite to the radiation loss. To reduce radiation losses in a feed network at a very high frequency, the width of the microstrip line should be less than $\frac{\lambda}{8}$.

In microstrip lines, small width strips lead to higher losses and the thickness of the metal microstrip lines affect the insertion loss.

An increase in temperature and dielectric losses limits the Average Power - the heat that the circuit is able to generate and how it is delivered to the environment [10] - of the microstrip line.

Microstrip devices fabrication process creates some roughness, scratches and bumps on the metal surfaces to promote adhesion to the dielectric material. Electrical impact of conductor roughness increases with frequency, increasing the group delay and its capacitance while decreases the characteristic impedance over a wide bandwidth.

Most metal finishes used in Printed Circuit Board (PCB) fabric are less conductive than copper and a lower conductivity cause higher conductor losses, which increases insertion losses.

Microstrip benefits are the low cost, compact size and lighter in weight. The tendency to be more lossy than coaxial cable and stripline it is still present. This type of line is difficult to mount chip in shunt mode but easy in series mode.

In section 2.4, is presented a solution for the problem of easiness of mounting in shunt mode.

2.4 Coplanar transmission line

The alternative for stripline and microstrip transmission lines is the Coplanar Waveguide (CPW) which places both signal and ground currents on the same layer. This type of line was created by Cheng P. Wen in 1968, presented primarily in [11].

The conductors form a center strip that is detached by a narrow gap from two ground planes on each side. The gap is usually very small and supports electric fields primarily concentrated in the dielectric. In order to concentrate the fields in the area for the substrate and minimize radiations, the substrate of the dielectric thickness is about twice the gap width.

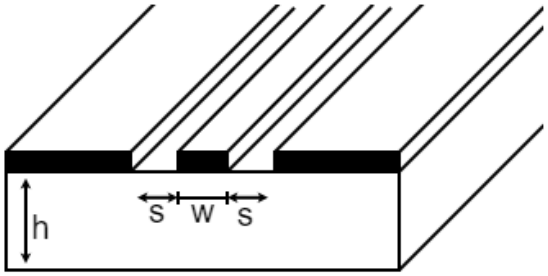

Figure 2.7: Coplanar transmission line [8]

CPW is suitable for wideband and zero cutoff frequency, however, the propagation mode of CPW is quasi-TEM which enables, at high frequencies, the field mode to become more TE and less TEM.

The characteristic impedance of CPW can be described by,

$$Z_0[\Omega] = \frac{30\pi}{\sqrt{\epsilon_{eff}}} \frac{K(k')}{K(k)}, \tag{2.24}$$

where $K(k)$ is the elliptical integral of the first degree, as referred in [8], and ϵ_{eff}, k_1' and k' are given by,

$$\epsilon_{eff} = 1 + \frac{(\epsilon_r - 1)K(k_1')K(k')}{2K(k_1)K(k)}, \tag{2.25}$$

$$k_1' = \sqrt{1 - k_1^2} = \frac{sinh[\pi W/(4h)]}{sinh[\pi d/(4h)]}, \tag{2.26}$$

$$k' = \sqrt{1 - k^2} = \sqrt{1 - (W/d)^2}. \tag{2.27}$$

$$d = 2s + W, \tag{2.28}$$

Complementing CPW, there is also Grounded Coplanar Waveguide (GCPW) that is used in printed circuit boards as alternative to microstrip line, as illustrated in [8] and [12].

$$Z_0[\Omega] = \frac{60\pi}{\sqrt{\epsilon_{eff}}} \frac{1}{\frac{K(k)}{K(k')} + \frac{K(k_1)}{K(k_1')}}, \tag{2.29}$$

$$\epsilon_{eff} = 1 + \frac{(\epsilon_r - 1)K(k_1')K(k')}{2K(k_1)K(k)}, \tag{2.30}$$

$$k' = \sqrt{1 - k^2}, \tag{2.31}$$

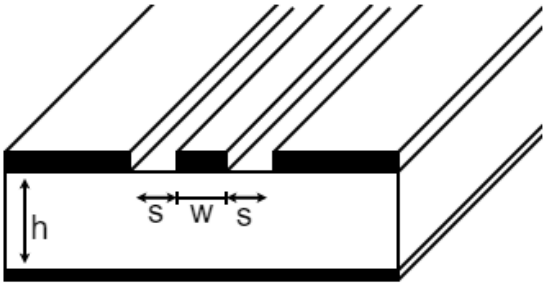

Figure 2.8: Grounded coplanar transmission line [8]

$$k_1' = \sqrt{1 - k_1^2}, \tag{2.32}$$

$$k_1 = \frac{tanh[\pi W/(4h)]}{tanh[\pi d/(4h)]}, \tag{2.33}$$

$$k = \frac{W}{d}, \tag{2.34}$$

$$d = 2s + W, \tag{2.35}$$

The gap, s, between the strip and the ground is larger than h thus allowing the field to be concentrated between the strip and the ground, behaving like microstrip lines.

The losses in CPW are commonly attributed to conductor loss, presence of dielectric conductivity, substrate magnetic loss (ferromagnetic material), radiation loss [5] or even size (considering characteristic impedance is mostly defined by the ratio between the center strip width and the gap, size reduction can originate higher losses).

As referred, in CPW, characteristic impedance is largely determined by the dependence of the ratio of between the center strip width with the gap width, thus, the design of a CPW line with a particular characteristic impedance is non-unique because an infinite range of W and s values will result in a specific characteristic impedance requirement. For a given characteristic impedance, to maintain the same capacities to the ground, the strip width will be minor that the one obtained for microstrip in the same conditions. It can be seen that the resistive loss for CPW line and GCPW can exceed the corresponding microstrip line, as demonstrated in [8].

The symmetrical structure in coplanar waveguides leads to a relative frequency independence of the effective permittivity that originates to a almost total lack of dispersion in the signal transmission, as portrayed in [8].

2.5 Attenuation in transmission lines

Attenuation in transmission lines can come from conductor losses (skin effect), dielectric losses and hysteresis losses, which are absorptive losses by nature and dissipate energy. Can also come from mismatch losses or even losses due to radiation which reflect and guide the energy away from the transmission line.

2.5.1 Conductor losses (Skin effect)

Skin effect attenuations are caused by the conducting medium series.

Skin depth is the layer thickness. In the referred layer, current decreases to $1/\epsilon$ of the value at the surface, as exhibited at [13].

Skin depth can be defined by equation 2.36.

$$\delta[cm] = \frac{1}{2\pi}\sqrt{\frac{\rho}{f\mu_r}}. \tag{2.36}$$

ρ is the specific resistivity of the conductor, μ_r is the conductor relative permeability - only considered when the material is ferromagnetic and has a relative permeability different from non-ferrous materials (these considerations were expressed in [13]).

Analysing equation 2.36, a thicker conductor is more limited by the skin effect at a lower frequency than a thinner conductor and as frequency increases this effect becomes more critical, restricting the current to travel only on the surface layer of the conductor.

2.5.2 Dielectric losses

Dielectric loss measures the electromagnetic energy dissipation. For an uniform filled transmission line the dielectric losses may be written as (2.37), as described in [14],

$$\alpha = 27.3\frac{\epsilon_r}{\sqrt{\epsilon_{eff}}}\frac{\epsilon_{eff}-1}{\epsilon_r-1}\frac{tan(\delta)}{\lambda_0}, \tag{2.37}$$

where tan(δ) is the loss tangent for the substrate material, λ_g represents microstrip wavelength and is given by

$$\lambda_g = \frac{\lambda_0}{\sqrt{\epsilon_{eff}}}. \tag{2.38}$$

As the substrate thickness decreases, dielectric losses become more severe, reducing efficiency. On the other hand, when substrate thickness increases, the surface wave power also increases which limits efficiency. Conductor losses exceed dielectric losses for most microstrip lines on alumina, sapphire

substrates or similar low-loss substrates. Especially when using silicon or gallium arsenide substrates, the outcome is bigger dielectric losses, as described in [8].

2.5.3 Hysteresis losses

When the magnetizing force (current) increase, the magnetic flux increases but when the magnetic force decrease, the magnetic flux does not decrease at the same rate. Therefore, flux density was still a positive value when the magnetic force reaches zero.

As defined in [8], hysteresis loss exist because of "friction-like effects when the magnetic moments of the domains rotate. Thus loss increases linearly with frequency."

One example of theoretical curves of losses for hysteresis is illustrated in Figure 2.9, as referenced in [8]. In this figure, two curves are represented, as well as a line. The small curve represents small levels of magnetic fields.

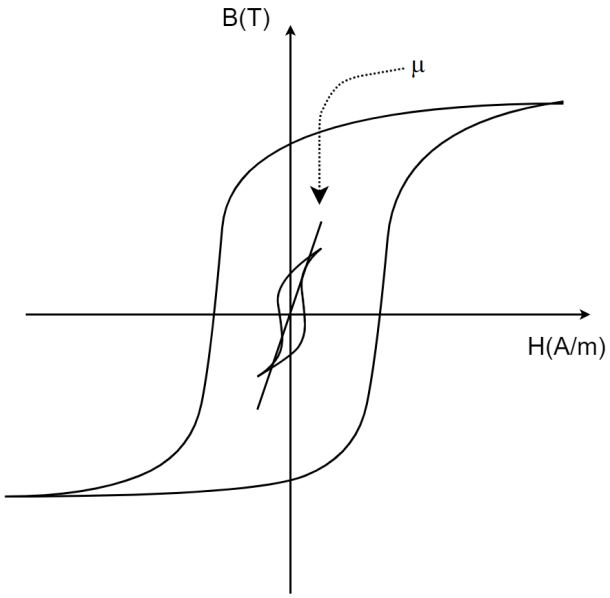

Figure 2.9: Hysteresis losses example, B is the flux density and H is the magnetic field [8]

In 2.9 the relation B-H is represented by an ellipse that results from hysteresis. The slope is the permeability of the material, μ. Ideally the ellipse that is represented in 2.9 must collapse into a line.

2.5.4 Mismatch losses

Mismatch losses occur when a discontinuity appears on a transmission line or when a termination of the transmission line is not equal to the characteristic impedance, as described in [13]. Thus, in those discontinuities, not all power is propagated, some is reflected. Considering the transmission line and the load, not all energy is transferred to the load.

2.5.5 Losses due to radiation

Discontinuities , like abrupt open-circuits, steps and bends will have losses due to radiation. Some of these losses cannot be eliminated to its full extension. Because radiation loss from an open ended waveguide can be extreme, they are usually short circuited at both ends forming a cavity. In high microwave frequencies, to reduce losses due to radiation, some cables are double and triple shielded. In addition, the passage of high frequency currents through an open wire increases the electromagnetic field around it. The RF power is radiated to free space or close circuits.

2.6 Comparison between transmission lines

For the present work purpose, the closest to ”perfect” type of transmission line must be chosen. To achieve this goal, some characteristics of the previously mentioned transmission lines are assembled in the following tables. In tables 2.1, 2.2, 2.3 and 2.4 are presented values that are neither consistent or coherent among literature, as showed bellow in the respective tables. In table 2.5 is an aggregate of compromises between consulted papers and books.

Table 2.1: Characteristic impedances

Transmission lines	[8]	[15]	[16]
Stripline	-	20-120	5-150
Microstrip	10-110	20-120	20-125
CPW	40-110	40-150	40-150

Table 2.2: Q factors

Transmission lines	[8]	[15]	[16]
Stripline	-	High (500)	High
Microstrip	250	Medium (250)	Medium
CPW	200	Low	Low

Table 2.3: Dispersion

Transmission lines	[5]	[15]	[16]
Stripline	None	None	Small
Microstrip	Low	Small	Medium
CPW	Medium	Medium	High

Table 2.4: Relative circuit size

Transmission lines	[5]	[16]
Stripline	Largest	Largest
Microstrip	Medium	Intermediate
CPW	Largest	Smallest

Table 2.5: Comparison transmission lines

Transmission line	**Characteristic impedance range** $[\Omega]$	**Q factor**	**Relative Dispersion**	**Relative circuit size**	**Relative Power handling capability**
Stripline	20-120	450	None	Large	Medium
Microstrip	20-120	250	Low	Small	High
Coplanar	40-110	175	Medium	Medium	Medium

In table 2.6 are resumed advantages and disadvantages of the three transmission lines.

Table 2.6: Advantages and disadvantages of transmission lines

Transmission lines	Advantages	Disadvantages
Stripline	The centered metal structure allows a good shield therefore there is a good isolation and lower attenuation loss. It has wider bandwidth.	The structure is complex turning fabrication expensive and troubleshooting hard.
Microstrip	Generally has rugged structures which handles higher voltage and power. It is compact size and light weight due to wavelength reduces to a third of its free space on account of the substrate fields.	Temperature variances must be accounted for because it limits the Average Power. Although being an advantage, small circuit dimensions might lead to problems in fabrication. The conductor losses increase with frequency. The quality factor is greatly reduced as thinner the substrate becomes.
CPW	Good for dense circuits due to crosstalk being limited by its geometry. CPW is less very sensitive to substrate thickness and allows a wide range of characteristic impedance values on thick substrates. It resists discontinuities on the ground plane. Good for high frequencies.	Thicker substrates are needed therefore the size will be bigger and the fabrication more expensive. There is the possibility of transference of heat between close devices.

This study is comparative, not conclusive. For this work, microstrip, CPW or even GCPW could be chosen.

The chosen transmission line is microstrip line. This choice was made based on the manufacturing influencers, that in microstrip line include conductor width, substrate thickness, copper surface roughness and substrate dielectric constant and the others had, for example, coplanar spacing, as referred to in [14].

3

De-embedding Techniques

4

S-parameters

In electronics, especially in microwave frequency range, it is hard to directly measure voltages and currents, since requires open or short connections. An ideal open connection is not easy to create due to parasitic capacitance and radiation. In the case of shorts the problem would be finite inductance. Nevertheless, it is still necessary to describe the network's parameters.

In order to solve this problem, the scattering matrix S was introduced in 1967 on the HP Journal Cover [17], where they were called S-parameters.

S-parameters in microwave frequencies are important considering they are easier than other parameters to measure at higher frequencies. Simpler, analytically convenient and direct, S-parameters are a measure of relative quantities.

S-parameters are reflection and transmission coefficients between incident and reflected waves and are a way to describe n-port networks.

Considering that two networks are connected, once the parameters in one network are measured, it is easier to predict the parameters on the other network and characterize RF and microwave components. RF and microwave components must operate together, for example in amplifiers, in transmission lines or even on free space.

Figure 4.1 is a 2-port network [18],

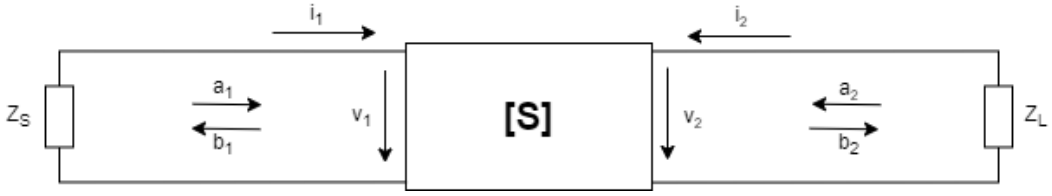

Figure 4.1: Two-port S-parameter network

Considering a 2-port network, S can be written as a 2x2 matrix:

$$\begin{bmatrix} b_1 \\ b_2 \end{bmatrix} = \begin{bmatrix} S_{11} S_{12} \\ S_{21} S_{22} \end{bmatrix} \begin{bmatrix} a_1 \\ a_2 \end{bmatrix} \tag{4.1}$$

The linear equations that describe two-port equations are:

$$b_1 = S_{11} a_1 + S_{12} a_2, \tag{4.2}$$

$$b_2 = S_{21} a_1 + S_{22} a_2. \tag{4.3}$$

where a_1 and a_2 are independent and normalized incident waves while b_1 and b_2 are dependent and normalized reflected waves [18], as follows:

$$a_1 = \frac{V_1 + I_1 Z_0}{2\sqrt{Z_0}}, \tag{4.4}$$

$$a_2 = \frac{V_2 + I_2 Z_0}{2\sqrt{Z_0}}, \tag{4.5}$$

$$b_1 = \frac{V_1 - I_1 Z_0}{2\sqrt{Z_0}}, \tag{4.6}$$

$$b_2 = \frac{V_2 - I_2 Z_0}{2\sqrt{Z_0}}. \tag{4.7}$$

Z_0 in the previous equations is the characteristic impedance of the material [18].

S-parameters S_{11}, S_{12}, S_{21} and S_{22} can be described with the help of a_1, a_2, b_1 and b_2, as follows:

$$S_{11} = \frac{b_1}{a_1} \tag{4.8}$$

, when $a_2 = 0$

$$S_{22} = \frac{b_2}{a_2}\Big| \tag{4.9}$$

, when $a_1 = 0$

$$S_{21} = \frac{b_2}{a_1}\Big| \tag{4.10}$$

, when $a_2 = 0$

$$S_{12} = \frac{b_1}{a_2}\Big| \tag{4.11}$$

, when $a_1 = 0$.

Each parameter has its own significance.

S_{11} is the input reflection coefficient with the output port terminated by a matched load. S_{22} is the output reflection coefficient with the input terminated by a matched load. S_{21} is the forward insertion (transmission) gain with the output port terminated in a matched load. S_{12} is the reverse insertion (transmission) gain with the input port terminated in a matched load. In other words, S_{11} and S_{22} are the optical reflection coefficients, S_{12} and S_{21} are the optical transmission coefficients.

As is known, input characteristic impedance at port 1 is measured with the following equation.

$$Z_1 = \frac{V_1}{I_1} \tag{4.12}$$

Notice that

$$S_{11} = \frac{\frac{V_1}{I_1} - Z_0}{\frac{V_1}{I_1} + Z_0} = \frac{Z_1 - Z_0}{Z_1 + Z_0} \tag{4.13}$$

Even if they are not being used in this work, it is important to mention the parameters that can be deducted from the S-parameters. The parameters are the Transducer Power Gain (GT), the Power Gain (G_P), the Reflection Coefficient, the Available Gain (G_A), the Maximum Available Gain (MAG), the Maximum Stable Gain (MSG) and the Stability Factor (K).

GT is defined as the ratio between the power delivered to the load P_L, and the available power from the source P_{avs}.

Assuming sinusoidal steady-state and that the source has a real resistance Z_0, when looking at a 1-port circuit, P_{avs} is defined as:

$$P_{avs} = \frac{V_s^2}{8Z_0}. \tag{4.14}$$

$$G_T = \frac{1-|\Gamma_s|^2}{|1-\Gamma_{\text{in}}\,\Gamma_s|^2}\,|S_{21}|^2\,\frac{1-\left|\Gamma_L^2\right|^2}{|1-S_{22}\Gamma_L|^2} \tag{4.15}$$

where Γ_{in} is given by:

$$\Gamma_{\text{in}} = S_{11} + \frac{S_{12}S_{21}\Gamma_L}{1-S_{22}\Gamma_L}. \tag{4.16}$$

G_P is defined as the ratio between the power delivered to the load and the input power at the network,

$$G_P = \frac{1}{1-|\Gamma_{\text{in}}|^2}\,|S_{21}|^2\,\frac{1-|\Gamma_L|^2}{|1-S_{22}\Gamma_L|^2}. \tag{4.17}$$

G_A is defined as the ratio between available power from the network P_0, and the available power from source P_{avs},

$$G_A = \frac{1-|\Gamma_s|^2}{|1-S_{11}\Gamma_s|^2}\,|S_{21}|^2\,\frac{1}{1-|\Gamma_{\text{out}}|^2}, \tag{4.18}$$

where Γ_{out} is given by

$$\Gamma_{\text{out}} = S_{22} + \frac{S_{12}S_{21}\Gamma_s}{1-S_{11}\Gamma_s} \tag{4.19}$$

The equations from 4.15 to 4.19 were withdrawn from [19].

5

Calibration

The common equipment used to characterize RF and microwave devices is the Vector Network Analyzer (VNA). Besides VNA, there is also the Spectrum analyzer. Both these equipments are needed for RF accurate measures and their differences will be addressed in the following section 5.1.

5.1 Network analyzer vs Spectrum analyzer

A spectrum analyzer is a device that measures the magnitude of the input signal in its entire range of frequency bandwidth. It is helpful to look at spectrums of a signal to have a closer look on the spurious signals, noise, modulation bandwidth, etc. These calculations are not essential to the goal of this thesis but to better understand the theme in question, it will be addressed.

A network analyzer allows the user to observe specific network parameters in an electrical network. It is helpful to look at a network analysis to obtain Y-parameters, Z-parameters, H-parameters and more commonly, S-parameters. S-parameters are used on this thesis since they are more suitable for measurements at higher frequencies.

5.1.1 When and where should network analysis and spectrum analysis be used?

Table 5.1: Differences between network and spectrum analyzers and when to use them [20]

Test equipment	When to use	Where to use
RF Spectrum analyzer - Measures unknown signals	When measuring signal amplitude characteristics (carrier level, sidebands, harmonics, etc.). The sophisticated ones can demodulate (and measure) complex signals. For scalar component test (no phase) with the help of a generator.	Primarily to display the spectrum of a radio frequency signal. Can also be used to make power and frequency measurements, although not as accurately as dedicated instruments.
RF Network analyzer - Measures known signals	When measuring components, devices, circuits, subassemblies. Offer advanced error correction. Contains source and receiver, can display amplitude and phase (frequency or power sweeps).	To measure the properties of the RF devices, they look at the various ports on the device and provide information about each characteristic impedance and transmission through the device. Can be used as generator (if that option is available).

5.1.2 Why is network analysis needed?

There are several types of RF network analyzers such as the Vector Network Analyzer (VNA), the Scalar Network Analyzer (SNA) (no longer used), the Large Signal Network Analyzer (LSNA) (VNA with capacity to measure large signals), among others.

VNA is a test instrument that measures the response of a network as a vector. It acquires real and imaginary parameters and evaluates the performance of the network. This makes the device a vital item of the RF design laboratories as in many manufacturing areas.

SNA is a form of a RF network that measures the amplitude properties of the Device Under Test (DUT) - scalar properties.

LSNA is a specific network analyzer that only assesses large signals.

SNA is the cheapest one but also the least thorough. It is a combination of a spectrum analyzer with a generator. It is useful (and limited) to measure the magnitude response of different components.

LSNA measures voltages and currents in time and frequency domain.

For the purpose of the current work, only the VNA will be used.

5.2 Vector Network analyzer

”A modern vector network analyzer can measure a component’s magnitude, phase, and group delay, show port characteristic impedances on a Smith Chart, and, with time-domain capability, show the distance from a test port to an characteristic impedance mismatch or circuit fault. Understanding a network analyzer’s capabilities and operation can help an operator derive optimum performance from the instrument.”

The previous citation was drawn from [20], and it will be the main purpose of this work - to achieve the best performance possible.

As stated in chapter 2, one of the fundamental concepts in high-frequency is the know-how of waves travelling in a transmission line. In network analysis, this concept had become the study of the ratios between reflected and transmitted signals on the DUT. Components are tested for several reasons. The main reason is to verify simulation models and proper functioning of hardware - compulsory when selling to a consumer and there is need to prove proper behavior.

5.2.1 Four stages of a network analyzer

The subjects discussed in chapter 4 are necessary to characterize the performance of the DUT.

In order to measure incident, reflected and transmitted signals there are four blocks in the network analyzer.

In the majority of situations, measuring magnitude would be sufficient, however, in this work and on other specific cases, measuring phase is imperative. Combining magnitude and phase leads to a complete characterization of the devices’ networks.

1. Source of stimulus;
2. Signal separation devices;
3. Receivers that detect the signals;
4. Processor/display for calculation and viewing results.

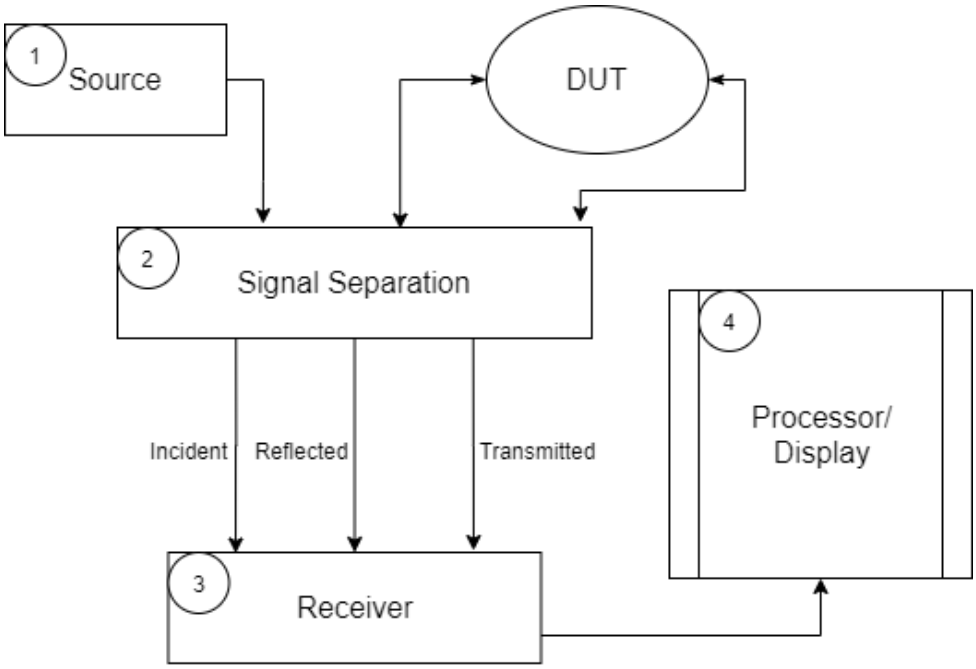

Figure 5.1: The 4 blocks - Network Analyzer

The first block is the signal source which gives stimulus to the system.

The second block is the signal separation device and has two functions. The first function is the measurement of a sample of the incident signal - done with splitters or directional couplers. Splitters are non-directional devices. Directional couplers[1] have low insertion loss, good isolation and directivity (accurately addressed on 5.2.2). The second function is the separation of forward and reverse waves at the output of the DUT.

The third block is the receiver block. There are two ways to detect a signal in network analyzers: Diode detectors and tuned receivers. The diode detector block converts the RF signal level to the correspondent DC level. The use of the diode allows the analysis of a range of frequency ($>$10 MHz to $<$26.5 GHz), its use is less expensive compared with using a tuned receiver. The diodes are also capable of measuring signals below -60 dBm and have a dynamic range around 60-75 dB. The problem about the diode is its frequency coverage limitation of sensitivity, making them susceptible to source harmonics and artificial signals. Tuned receivers use a local oscillator to mix RF into an intermediate frequency. Tuned receivers have better sensitivity and dynamic range, and contrary to diodes, reject harmonic and artificial signals - this comes from the narrowband of the tuned receivers. Furthermore, the dynamic range is improved when increasing power and, as mentioned before, decreasing frequency.

The fourth block of the network analyzer is the processor/display. In this block lays the process

[1] Considering the difficulty to make true broadband couplers, it is common to install bridges instead. Even though bridges have more losses and are unable to work in DC (the operation is similar to the Wheatstone bridge but with a unbalanced bridge - measuring both magnitude and phase through the bridge one can deduct the complex characteristic impedance).

of changing and displaying information to the user in a more readable and easy way. Results can be presented in linear/logarithmic sweeps and formats like Smith charts, polar plots, etc.

5.2.2 Errors in network analyzers

In network analyzers three types of errors can occur: systematic, random and drift.

The systematic errors are due to a faulty equipment or bad experiment design. They are usually derived from incorrect calibration or improper use. They are predictable and removed mathematically during measurements.

The following 6 figures help to better understand systematic errors and how they behave. In these images, 'A' is the reflected receiver channel, 'B' is the transmitted receiver channel and 'R' is the receiver's reference channel. The green line represents the expected behaviour and the red line is the error signal behavior.

Two major systematic errors are directivity and crosstalk.

Crosstalk is an isolation error. Isolation errors arise from signals, other than the transmission signal, leaking to the test receiver.

There are standard loads placed at Port 1 and Port 2 to measure isolation. The signal at 'B' is leakage that goes through different paths.

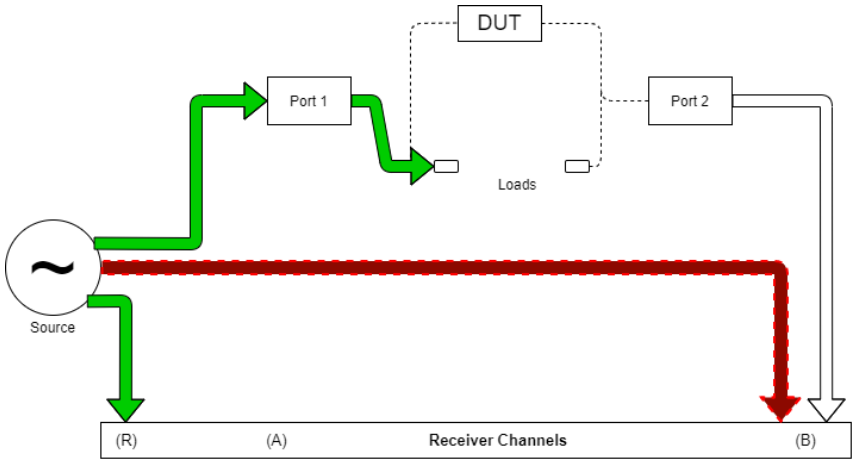

Figure 5.2: Isolation error draw

Furthermore, when installing a directional coupler it is important to know its directivity. Directivity is the analysis of how well a coupler can separate signals moving in opposite directions. It can be defined as

$$\text{Directivity}(dB) = \text{Isolation}(dB) - \text{Forward Coupling Factor}(dB) - \text{Loss through arm}(dB), \quad (5.1)$$

as it is shown in Figure 5.3.

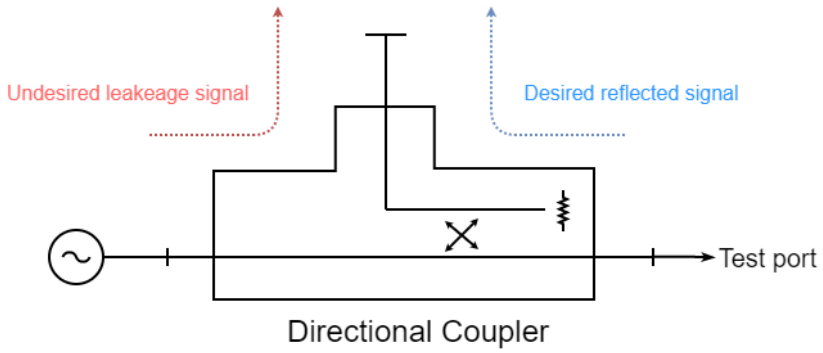

Figure 5.3: Directivity in a directional coupler as described in [21]

Considering Figure 5.4, real port separations do not exist. Directivity is the main reason why a large ripple pattern is seen in several measurements of return losses. In their ripple peaks, directivity is adding in phase with reflection from the DUT.

A matched load is connected in Port 1 (no reflections are accounted for) to measure directivity. The signal at 'A' is the incident signal's leakage that goes through the coupler and/or other paths.

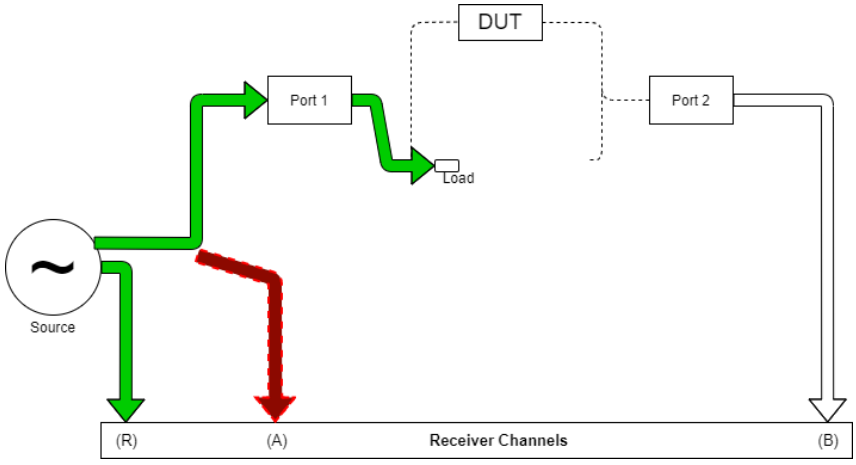

Figure 5.4: Directivity draw

Adding to isolation and directivity errors, there are also source and load match errors.

The source match error comes from the reflection signal of the DUT. It is reflected at the signal source and goes back to the DUT.

Considering Figure 5.5, all reflection standards are connected to Port 1 to measure the source match error. The reflection standards are measured in 'A'.

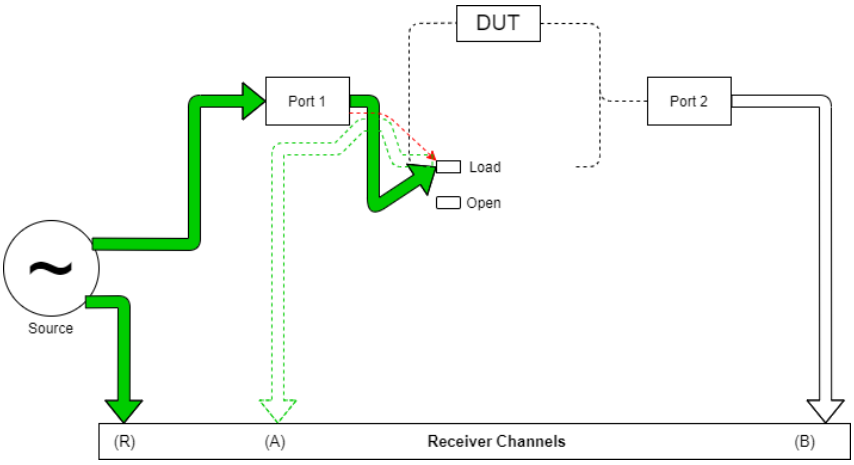

Figure 5.5: Source match error draw

Considering Figure 5.6, the load match error is equivalent to the source match error. The error appears when a part of the transmitted signal is reflected at the response port and the measured signal is not the total of the sent signal.

To measure the load match error, Port 1 and Port 2 are connected forming a perfect zero-length thru connection - if this perfect zero-length cannot be achieved, a characterized thru adapter is placed. In consequence, a known signal is granted at Port 2 and a reflection signal is placed 'A'.

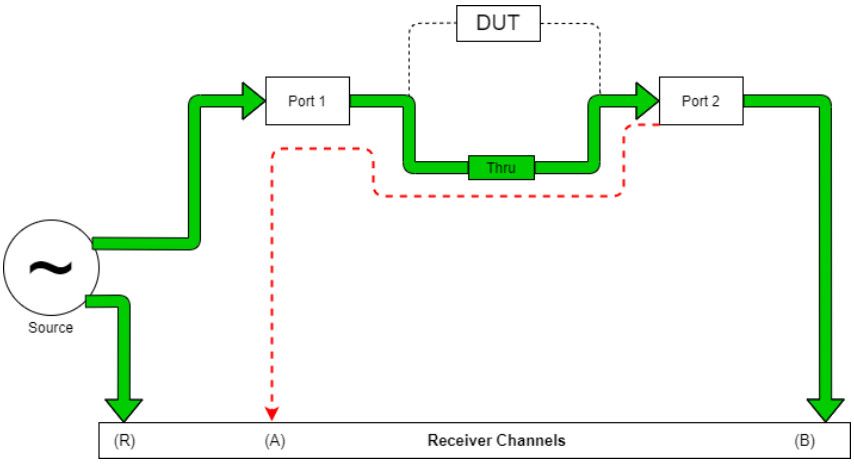

Figure 5.6: Load match error draw

The last two systematic errors (Figures 5.7 and 5.8) are called reflection and transmission tracking error and are related to frequency.

The reflection tracking error is caused by differences in frequency response between incident and reflected signal at the receiver.

All reflection standards are used to measure the reflection tracking error. The response received on 'A' is compared with the response received on Port 1.

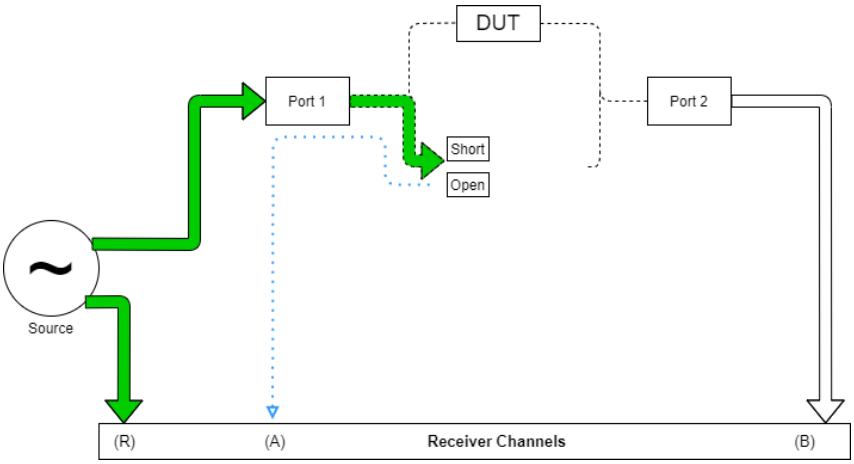

Figure 5.7: Frequency response reflection tracking error draw

The transmission tracking error, Figure 5.8, is caused by the difference in frequency response between the incident and the transmitted signal at the receiver.

To measure the transmission tracking error, ports are connected to form a ”perfect zero-length” thru connection - if this kind of perfection cannot be reached, a characterized thru adapter is placed, as was done for measuring the load match error. This allows a known signal to arrive at Port 2, then the values obtained at ’B’ and at Port 1 are compared.

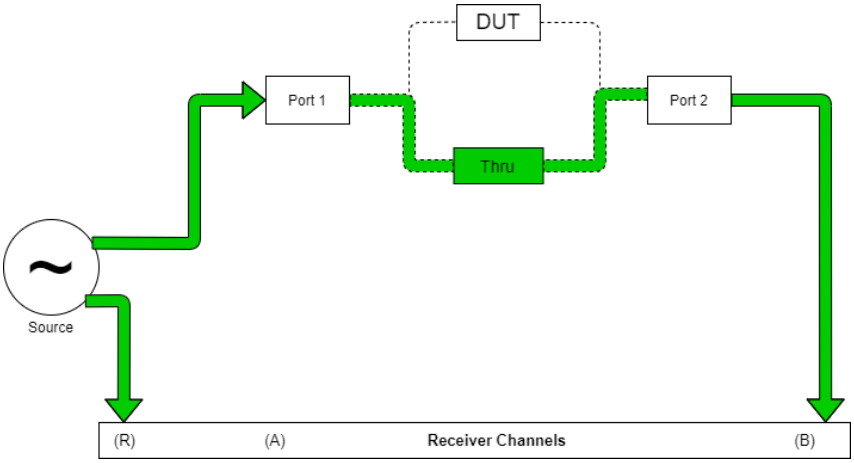

Figure 5.8: Frequency response transmission tracking error draw

Altogether there are 6 sources of systematic errors. When observed in the opposite signal direction, one can gather the 12 sources of systematic errors.

These errors will be applied in the 12-Term Error Correction calculations presented and explained in the next subsection.

Random errors (also called unsystematic) do not have a pattern, therefore they are unpredictable and cannot be removed by calibration. Usually this type of errors come from instrument noise.

Drift errors are caused by deviations in the performance of the instrument after calibration. Usually these types of errors come from temperature - expansion of connecting cables, etc. These errors can be removed with frequent calibrations whilst measuring.

5.2.3 Error corrections

There are two types of error correction - response error correction and vector error correction.

In response error correction a reference trace is stored in memory and is divided by its measurement traces. It is simple to perform, but only effective in some of the errors pointed before - the tracking ones.

In vector error correction it is required an analyzer that can measure magnitude and phase. Measurements are more accurate and the majority of errors can be disclosed. These errors can vary from simple vector normalization to a 12-term error correction.

Vector error correction allows the characterization of the systematic error terms. This process is performed by measuring known standards, calculating and storing the errors in the analyzer's memory and removing them from the next measurements.

There are two main vector error corrections, one-port and two-port calibrations.

One-port calibration only works with reflection and can remove three systematic errors - directivity, source match and reflection tracking.

The used technique for these three errors is 3-Term Error Model represented next on the diagram of signal flow 5.9.

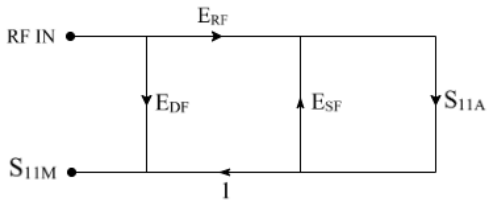

Figure 5.9: 3-Term Error Model [22]

In Figure 5.9, E_{DF} is the directivity error, E_{SF} is the port match error and E_{RF} is the tracking error. With 3-Term Error Model the relation between actual and measured reflection coefficients can be obtained.

Theoretical equations gives S_{11M} (S_{11} measured) and S_{11A} (S_{11} de-embedded) as follows,

$$S_{11M} = E_{DF} + \frac{S_{11A}(E_{RF})}{1 - E_{SF}S_{11A}}. \tag{5.2}$$

$$S_{11A} = \frac{S_{11M} - E_{DF}}{(S_{11M} - E_{DF})E_{SF} + E_{RF}} \tag{5.3}$$

Errors enforced in the previous equations are obtained by measuring the system using three independent standards where S_{11A} is known in all tested frequencies.

First standard is achieved when a ”perfect load” is applied (hard to get by its own, good broadband is usually available in calibration kits to help achieve this), which makes S_{11A} = 0. Directivity is measured and E_{DF} is derived from equation 5.2. Only if S_{11A} is perfect can E_{DF} be measured directly. If it is not the case, it is a system of 3 equations for three unknown parameters.

As referred, there is no perfect load so there is always reflection, therefore any reflection from termination represents an error called match error.

An open circuit is enforced to establish the final standard. It is called tracking error.

Thus the values of the three errors, E_{DF} (directivity), E_{SF} (source match) and E_{RF} (reflection frequency response) are known and stored.

Two-port calibration works both with reflection and transmission measurements. Therefore 12 errors can be measured. This calibration is the most accurate, owning six forward and six reverse sources of systematic errors. These errors can be used in known equations (presented moreover) to obtain the S-parameters.

This corrections removes directivity errors of test setup, source match errors, load match errors, isolation errors and frequency response in both forward and reverse directions.

The diagram of signal flow of the 12-Term Error Model is represented on 5.10.

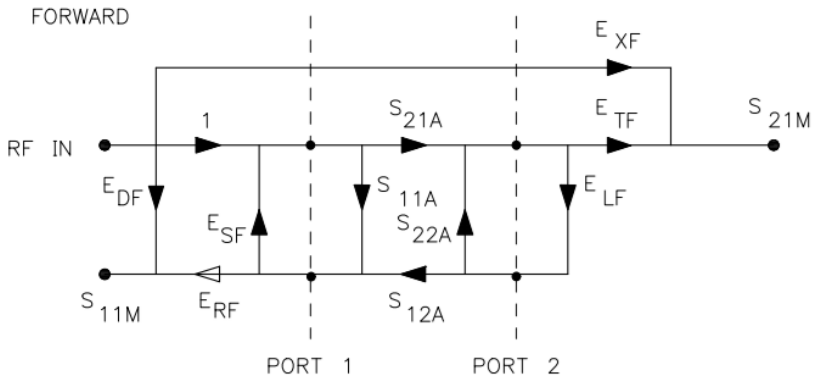

Figure 5.10: Forward 12-Term Error Model [23]

In Figure 5.10, E_{DF} is the directivity error, E_{SF} is the source match error, E_{RF} is the reflection tracking error, E_{TF} is the transmission tracking error, E_{LF} is the load match error and E_{XF} is the isolation error. These error are obtained from the forward diagram of the 12-Term Error Model signal flow.

With the same type of analysis done for one-port calibration (solving the flow graph), the equations reached in the forward 12-Term error model are equation 5.4 and equation 5.5.

$$S_{11A} = \frac{\left[\left(\frac{\mathrm{S_{11M}-E_{DF}}}{\mathrm{E_{RF}}}\right)\left[1+\left(\frac{\mathrm{S_{22M}-E_{DR}}}{\mathrm{E_{RR}}}\right)\mathrm{E_{SR}}\right]\right]-\left[\left(\frac{\mathrm{S_{21M}-E_{XF}}}{\mathrm{E_{TF}}}\right)\left(\frac{\mathrm{S_{12M}-E_{XR}}}{\mathrm{E_{TR}}}\right)\mathrm{E_{LF}}\right]}{\left[1+\left(\frac{S_{11M}-E_{DF}}{E_{RF}}\right)E_{SF}\right]\left[1+\left(\frac{S_{22M}-E_{DR}}{E_{RR}}\right)E_{SR}\right]-\left[\left(\frac{S_{21M}-E_{XF}}{E_{TF}}\right)\left(\frac{S_{12M}-E_{XR}}{E_{TR}}\right)E_{LF}E_{LR}\right]} \tag{5.4}$$

$$S_{21A} = \frac{\left[]1+\left(\frac{S_{22M}-E_{DR}}{E_{RR}}\right)(E_{SR}-E_{LF})\right]\left(\frac{S_{21M}-E_{XF}}{E_{TF}}\right)}{\left[1+\left(\frac{S_{11M}-E_{DF}}{E_{RF}}\right)E_{SF}\right]\left[1+\left(\frac{S_{22M}-E_{DR}}{E_{RR}}\right)E_{SR}\right]-\left[\left(\frac{S_{21M}-E_{XF}}{E_{TF}}\right)\left(\frac{S_{12M}-E_{XR}}{E_{TR}}\right)E_{LF}E_{LR}\right]} \tag{5.5}$$

The missing six error coefficients are gathered in the reverse flow graph.

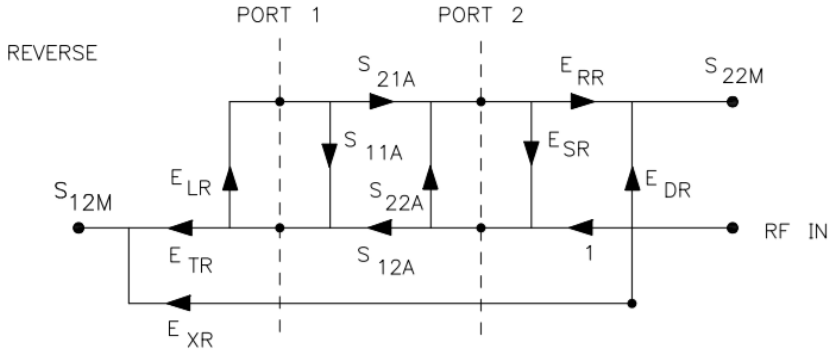

Figure 5.11: Reverse 12-Term Error Model [23]

In Figure 5.11, E_{DR} is the directivity error, E_{LR} is the source match error, E_{RR} is the reflection tracking error, E_{TR} is the transmission tracking error, E_{SR} is the load match error and E_{XR} is the isolation error. These error are obtained from the reverse diagram of the 12-Term Error Model signal flow.

Similarly to the previous two equations, equation 5.6 and equation 5.7 are obtained when the flow graph is resolved.

$$S_{12A} = \frac{\left[1+\left(\frac{\mathrm{S_{11M}-E_{DF}}}{\mathrm{E_{RF}}}\right)(\mathrm{E_{SF}}-\mathrm{E_{LR}})\right]\left(\frac{\mathrm{S_{12M}-E_{XR}}}{\mathrm{E_{TR}}}\right)}{\left[1+\left(\frac{\mathrm{S_{11M}-E_{DF}}}{\mathrm{E_{RF}}}\right)\mathrm{E_{SF}}\right]\left[1+\left(\frac{\mathrm{S_{22M}-E_{DR}}}{\mathrm{E_{RR}}}\right)E_{\mathrm{SR}}\right]-\left[\left(\frac{\mathrm{S_{21M}-E_{XF}}}{\mathrm{E_{TF}}}\right)\left(\frac{\mathrm{S_{12M}-E_{XR}}}{\mathrm{E_{TR}}}\right)\mathrm{E_{LF}E_{LR}}\right]} \tag{5.6}$$

$$S_{22A} = \frac{\left[\left(\frac{\mathrm{S_{22M}-E_{DR}}}{\mathrm{E_{RR}}}\right)\left[1+\left(\frac{\mathrm{S_{11M}-E_{DF}}}{\mathrm{E_{RF}}}\right)\mathrm{E_{SF}}\right]\right]-\left[\left(\frac{\mathrm{S_{21M}-E_{XF}}}{\mathrm{E_{TF}}}\right)\left(\frac{\mathrm{S_{12M}-E_{XR}}}{\mathrm{E_{TR}}}\right)\mathrm{E_{LR}}\right]}{\left[1+\left(\frac{\mathrm{S_{11M}-E_{DF}}}{\mathrm{E_{RF}}}\right)\mathrm{E_{SF}}\right]\left[1+\left(\frac{\mathrm{S_{22M}-E_{DR}}}{\mathrm{E_{RR}}}\right)\mathrm{E_{SR}}\right]-\left[\left(\frac{\mathrm{S_{21M}-E_{XF}}}{\mathrm{E_{TF}}}\right)\left(\frac{\mathrm{S_{12M}-E_{XR}}}{\mathrm{E_{TR}}}\right)\mathrm{E_{LF}E_{LR}}\right]} \tag{5.7}$$

There are three steps that must be followed to obtain the unknown parameters presented in equations

5.4, 5.5, 5.6 and 5.7. The first step is coincident to one-port calibration. This step determines the directivity, the match error and the reflection tracking error. In step two, leakage and the crosstalk error are obtained from both ports by placing loads on each. In the last step, ports are connected. Port-2 match is measured directly with the calibrated port-1 reflectometer. With the two ports connected, the transmitted signal is derived and the transmission tracking is determined. These methods are applied in both forward and reverse models.

De-embedding and Embedding S-parameters

As referred to before, it is mandatory to mind the accuracy and precision of the measurements when increasing frequencies. It can no longer be assumed that the transmitter output meets the eye-diagram [2].

The possibility to develop an equipment that erases all effects from fixtures is not possible considering the amount of different printed circuit transmission lines, connections to the exterior, etc.

As detailed before, the common equipment used to characterize RF and microwave devices is the VNA. As explained in [25], *the test equipment is calibrated at the coaxial interface defined as the "measurement plane," and the required measurements are at the point where the surface-mount device attaches to the printed circuit board, or the "device plane". When the VNA is calibrated at the coaxial interface using any standard calibration kit, the DUT measurements include the test fixture effects*.

The SMA connector from the test fixture must be removed from the measured results to accurately characterize the DUT.

The Figure 5.12 is a representation of a test fixture configuration and the measurement planes.

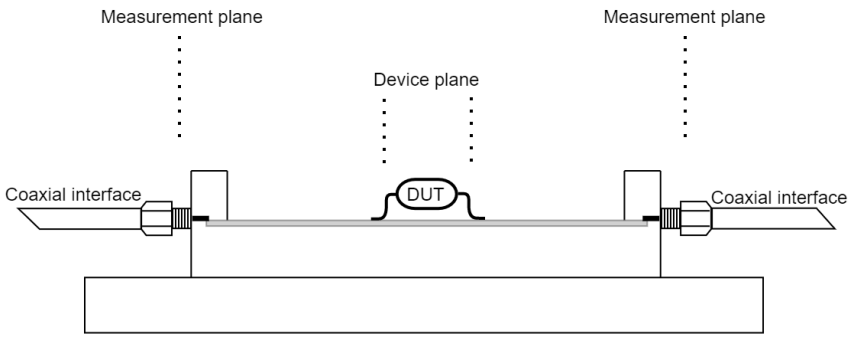

Figure 5.12: Text fixture configuration

[2] The communications industry uses eye diagrams to observe and analyze the performance of circuits that drive the transfer of digital data streams. In its simplest form, the eye-diagram is generated on the screen of a storage oscilloscope (analog or digital) by overlaying sweeps of different segments of a long data stream driven by a master clock [24].

The VNA has to be calibrated at the coaxial interface to enable measuring results. When this happens, measurements still include the SMA connector from the test fixture. There are two options to solve this matter, direct measures and de-embedding.

In order to solve through the direct measures, the calibration standards need to be placed in the DUT. In most cases, accessing the DUT is difficult. The chosen standards must be precisely characterized. The quality of the standards affect directly the measurements of the DUT.

In the de-embedding case, a model for the test fixture is obtained and the effects can be removed.

Applying the theory described in chapter 4, the representations of the test fixtures and the DUT are shown in the Figure 5.13.

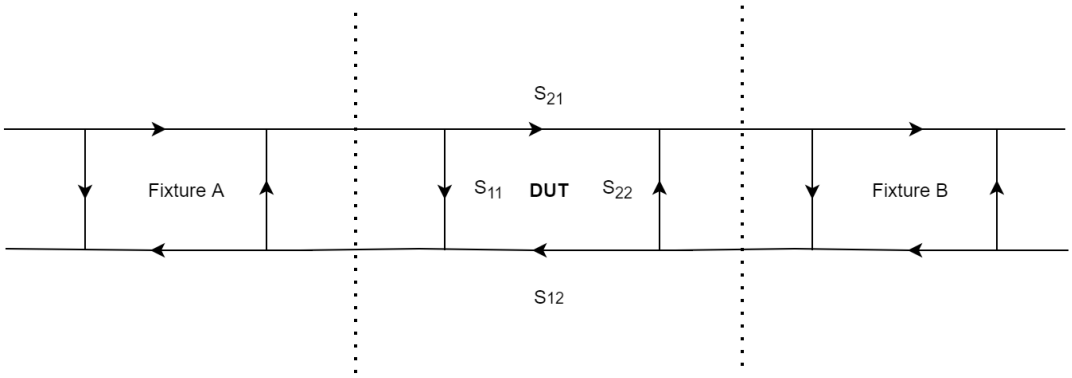

Figure 5.13: Signal flow representing test fixture and DUT

The Figure 5.13 will only be applied into calculations when bridges to the DUT are not directly bonded with coaxial connections.

There are various methods to turn experimental measurements into a close approximation of ideal measures.

The following methods that can be applied are ordered by increase in easiness and decrease in accuracy: TRL, Short-Open-Load-Thru (SOLT), Port rotation and Time domain gating.

In time domain gating, frequency domain is converted into a Time Domain Response (TDR). A small part of the response is selected and converted into frequency domain to be interpreted as return loss from a region of the DUT. It is a very easy but limited approach. However, this method only takes into consideration return loss.

Port rotation is present in all network analyzers and compensates return and insertion loss. Accuracy decreases as the length of the transmission line increases.

The following two calibration techniques are not forthright. They need to take into account standards.

Thru-Reflect-Line (TRL) is used for de-embedding S-parameter data and has lower frequency limitation. Thru is a transmission line with twice the length of the transmission line of the test fixture. Reflect has the same length of the transmission line of the test fixture but with an open or short circuit at the

end. Line is the same as thru but with a bigger length.

The usual error model used in TRL calibration is the 7-Term Error Model. In this model, like in the 12- Term Error Model, a virtual network is placed between the reference plane and the physical port.

The standards for the TRL algorithm have different categories, Thru is known, Reflect is unknown and Line is partially known, as referred to in [26] and [27].

TRL algorithm is introduced in Apendix A, with credits to T. Reveyrand from University of Colorado that presented this matter in a more comprehensible way [28].

TRL has certain disadvantages, which were described in [29]. It is time consuming, needs assumptions and is not cost efficient.

SOLT calibration model requires accurate knowledge of the behavior of 4 standards (short, open, load, thru) to solve the four error coefficients of the 10 error term model (or 12 if isolation error is included).

In [29], drawbacks of the SOLT were described. They include poor low-frequency behaviors, low accuracy at high frequencies, uncontrollable parasitics for manufacturing standards and expensive calibration kits.

6

Development

7

Development

In the development of this work, two experiments were performed. One based on Advanced Design System (ADS), a software from Keysight, and the other on the developed PCB. This PCB was tested on a VNA.

The first step of these experiments was the development of a PCB with seven lines with different widths, in ADS. These lines had characteristic impedances close to 50Ω. These width variations were made to evaluate the characteristic impedance variations between the lines. Considering the aspects mentioned in chapter 2, microstrip was the chosen transmission line to develop the PCB.

7.1 Prototype design

In the next figures are presented the schematic and the respective testbench of a simple microstrip line.

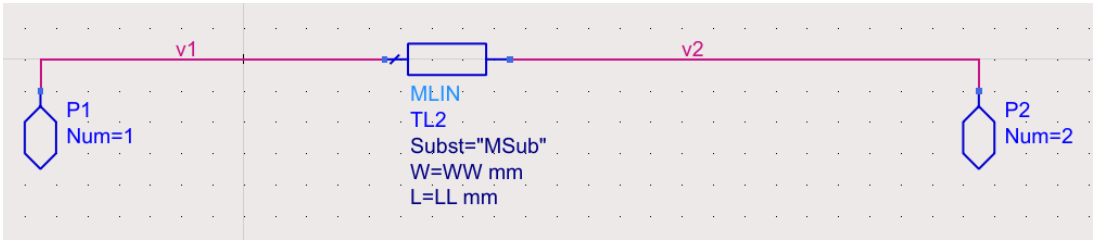

(a) Microstrip schematic

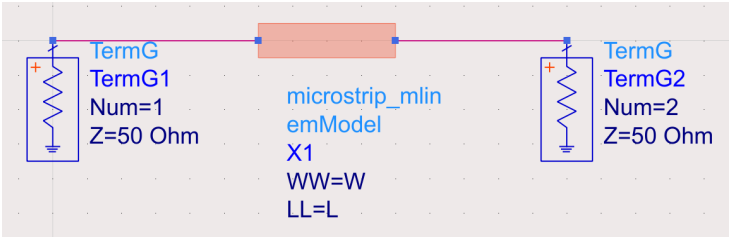

(b) Microstrip testbench

Figure 7.1: Schematic and testbench of microstrip line

The characteristics of the substrate used in the microstrip line are presented in the table 7.1 and its characteristics can be observed in detail in the Figure 7.2 [30].

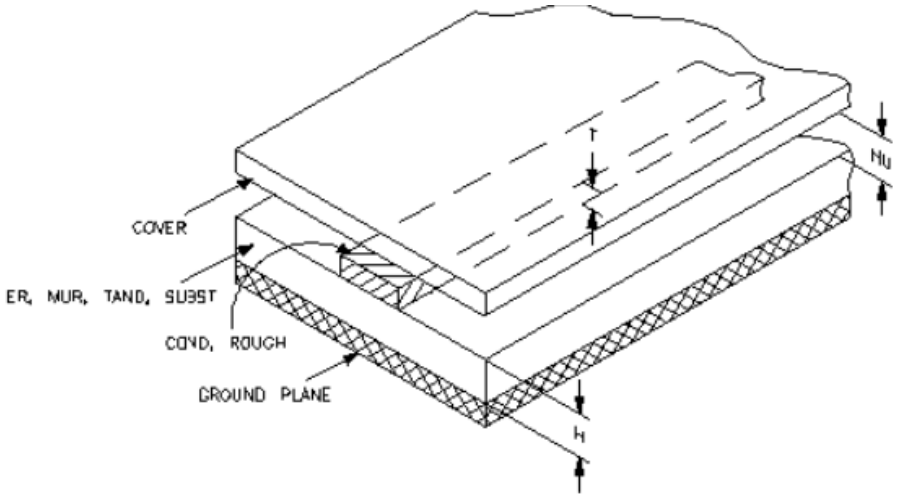

Figure 7.2: Detail of the substrate

Table 7.1: Characteristics of the substrate

Characteristic	Value
Substrate thickness (H)	1 mm
Relative dielectric constant (E_r)	4.37
Relative permeability (Mur)	1
Conductor conductivity (Cond)	5.7E+7
Cover height (Hu)	1.0e+33 mm
Conductor thickness (T)	35 μm
Dielectric loss tangent (TanD)	0.018
Conductor surface roughness (Rough)	0 mm

The line was implemented in a PCB with 7 different widths chosen with 2.45GHz of frequency. The length of the lines is the same since it does not affect the measures of the characteristic impedance. This can be confirmed with equation 2.23 in chapter 2.

After analysing the microstrip line, the Figure 7.3 presents the curve of the characteristic impedance when the width is altered, the Figure 7.4 presents the curve of the characteristic impedance when the frequency is altered, the Figure 7.5 presents the attenuation, the Figure 7.6 presents the delay and the Figure 7.7 presents the Effective Dielectric sweeps, both in function of the width. This characteristics were obtained when the width changed from 1.2mm to 2.6mm and the length was fixed at 7cm.

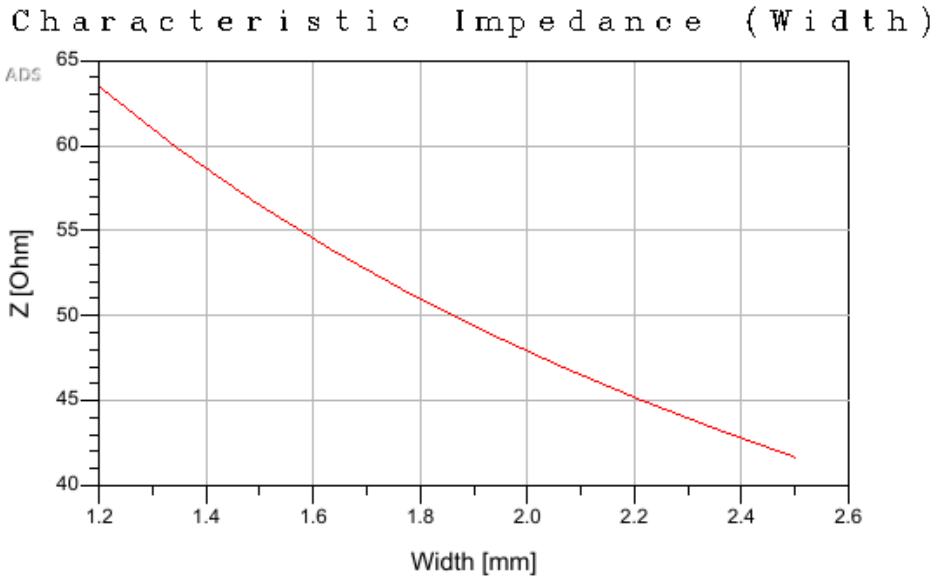

Figure 7.3: Impedance characteristic - width sweep

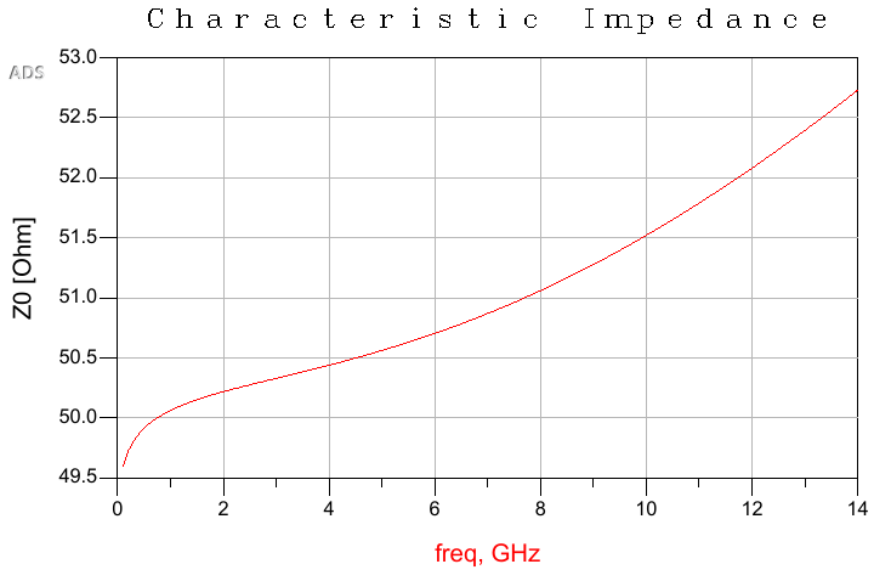

Figure 7.4: Impedance characteristic - frequency sweep

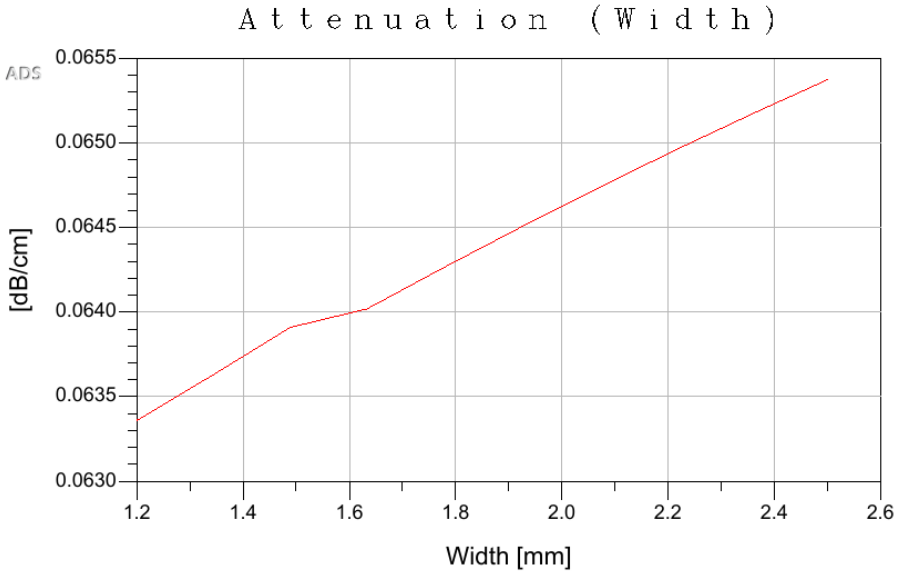

Figure 7.5: Attenuation sweep

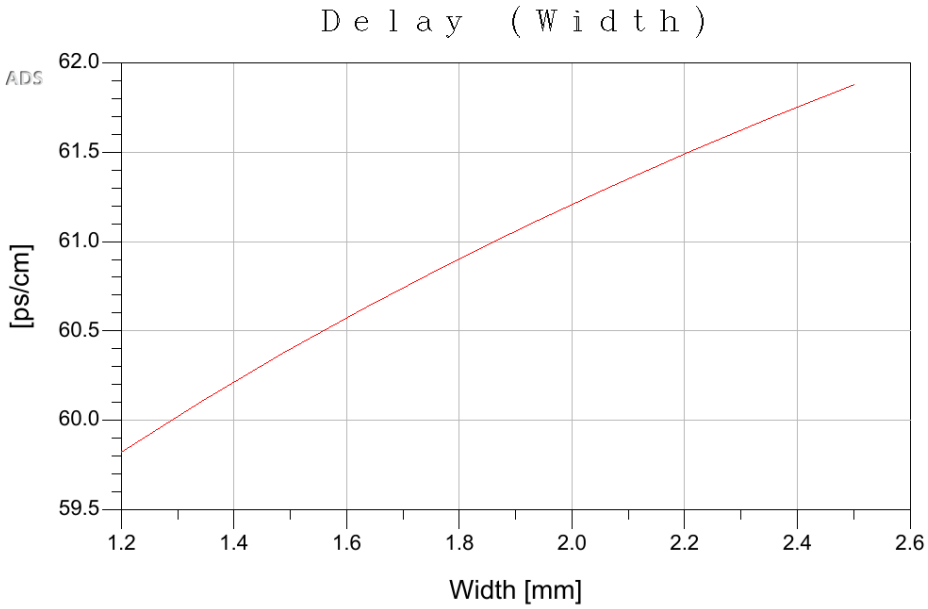

Figure 7.6: Delay sweep

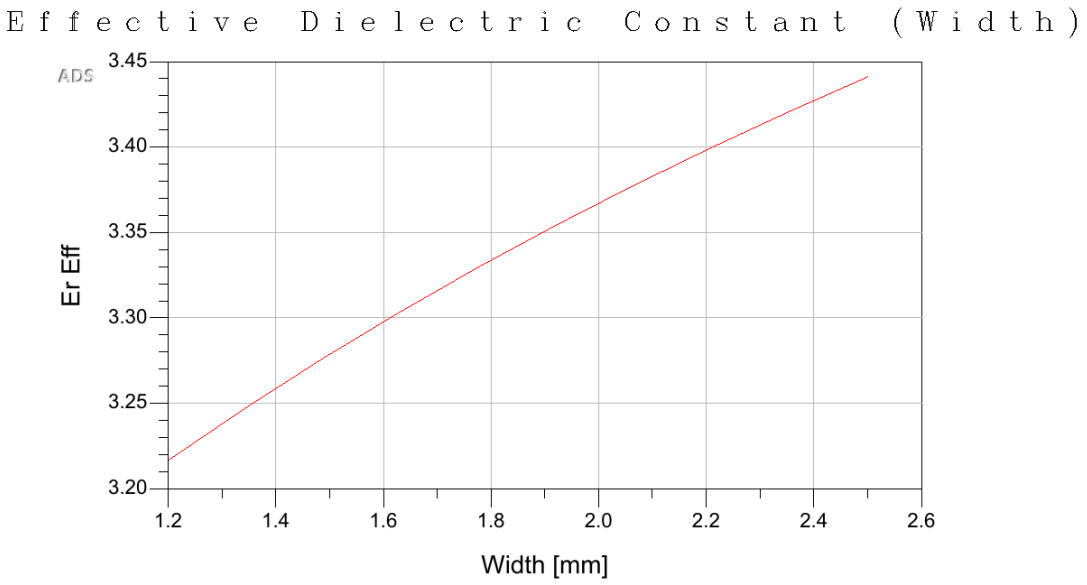

Figure 7.7: Effective Dielectric constant sweep

The range of the values of the width (1.2mm to 2.6mm) was chosen accordingly to the characteristic impedance, allowing it to vary from approximately 42Ω to approximately 61.5Ω. It enables the test of the transmission lines. It also enables the study of the difference between the modeled line in ADS and the line in a PCB. The purpose of the chosen range of the characteristic impedance was to obtain values of the characteristic impedance that neared 50Ω.

The values of the characteristic impedances, the attenuation and the delay are displayed in the tables 7.2 and 7.3.

Table 7.2: Characteristics (1)

Width (mm)	Impedance (real) Ω	Impedance (imag)Ω
1.28	61.42	0.39
1.58	54.89	0.36
1.78	51.30	0.34
1.88	49.69	0.33
1.98	48.18	0.32
2.18	45.44	0.30
2.48	41.89	0.28

Table 7.3: Characteristics (2)

Width (mm)	Attenuation (dB/cm)	Delay (ns/cm)
1.28	0.0635	0.0599
1.58	0.0640	0.0605
1.78	0.0643	0.0608
1.88	0.0644	0.06102
1.98	0.0646	0.0611
2.18	0.0650	0.0615
2.48	0.0653	0.0618

Considering the optimum case (the optimum case is an utopia, it is impossible to achieve in a real context), S-parameters are equal when considering S_{11} and S_{22}, and considering S_{12} and S_{21}.

In Figure 7.8, S_{11} and S_{22} are represented in blue and S_{12} and S_{21} are represented in red (as referred before, S_{11} and S_{22}, and S_{12} and S_{21} are coincident .

The remaining figures of S_{11} and S_{22}, and of S_{12} and S_{21}, with different widths, are represented in the appendix E.

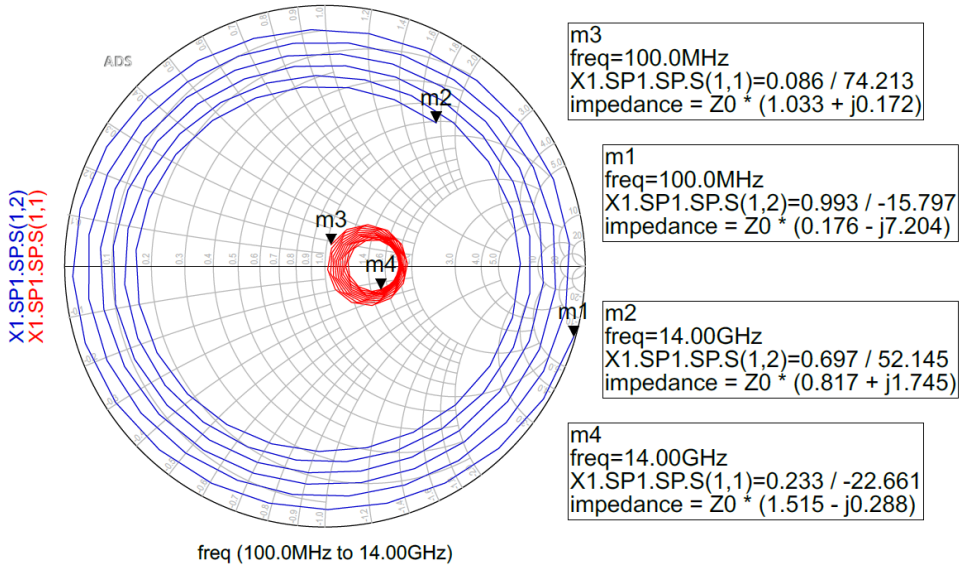

Figure 7.8: S-parameters S_{11} and S_{12} described with Smith Chart from ADS - line of 1.88mm of width

The schematic of the PCB in ADS is presented in Figure 7.9 and the respective layout is in Figure 7.10a.

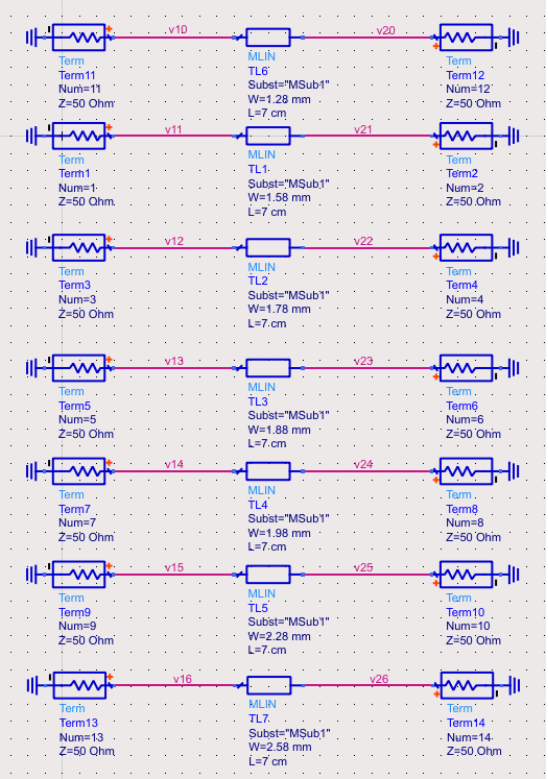

Figure 7.9: Schematics PCB

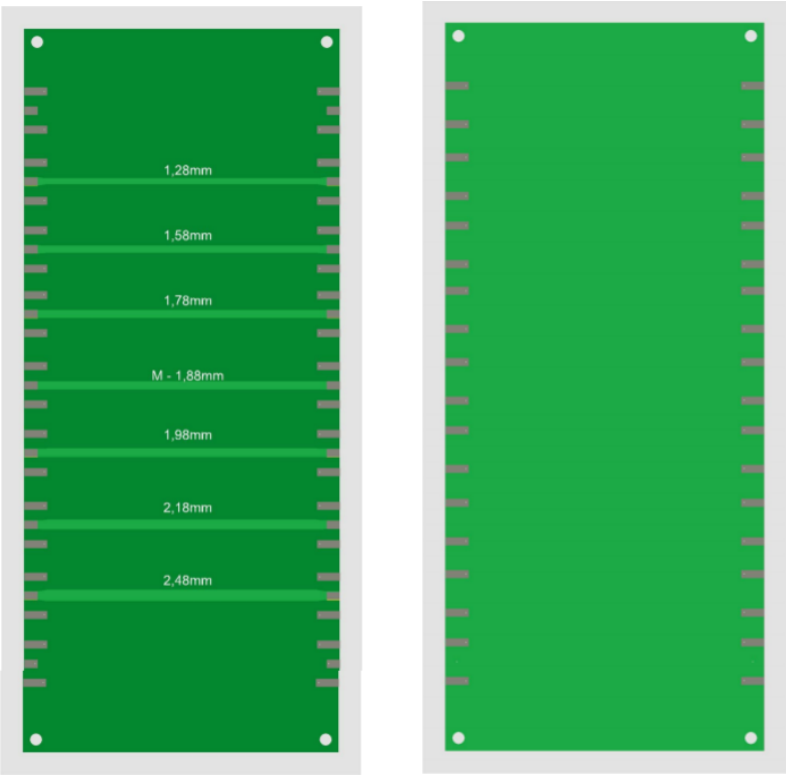

(a) Top View PCB **(b)** Bottom View PCB

Figure 7.10: PCB in ADS - top and bottom views

It is important to refer that the prints on the bottom view of the PCB are the same size of the ones on the top view.

As mentioned before, to test the PCB, connections to the exterior had to be made.

Several kinds of connectors are used to connect the exterior to the devices. Usually, the Sub-Miniature version A (SMA) connectors are used to connect coaxial lines and traces to the PCB.

The SMA connectors were invented in 1960 as connectors for coaxial cables. This type of connector presents good performance from DC up to 26,5GHz, as described in [31]. This component, when used with microstrip lines, offers excellent coupling characteristics and few undesirable properties.

A direct model for a coaxial to microstrip transition is presented in Figure 7.11. It is a model accepted by current scholars and listed in [25]. This model is not sustained by all authors, that presented, for example, a T-model.

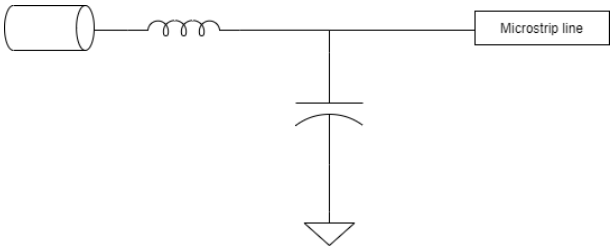

Figure 7.11: Simplified model of a coax to microstrip transition

In the beginning of this experiment, this model was considered the correct one and the connections in the developed PCB are exemplified in Figure 7.12.

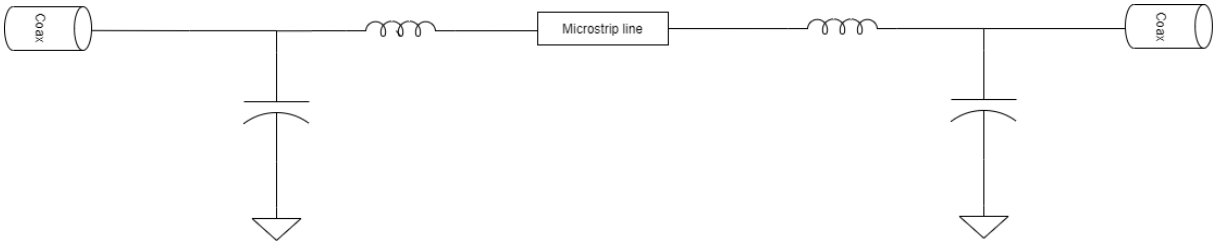

Figure 7.12: Model of coax to microstrip transition applied in developed PCB

The objective of this part of the work was to demonstrate the effectiveness of the model presented in 7.11.

The SMA connectors can be divided according to their connection to the PCB. They can be divided in Connector Straight Jack, Right Angle, Edge-Mount and others. The PCB connectors used in this work are Edge-Mount. An Edge-Mount connector allows to diminish the area between the connector and the center pin of the microstrip. This areas' length is the same as the length of the connector's pin.

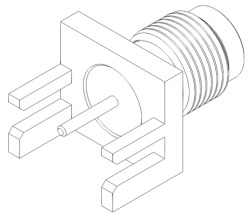

Figure 7.13: Edge-Mount coaxial connector 3D drawing

In literature some authors prefer to evaluate, not only the SMA connectors connected to the microstrip line (or other types of line), but also the small gap that can rest between them, as portrayed in [32]. In the current work, this condition will be ignored based on its scarce relevance [32].

The equivalent circuit model of the SMA connectors is represented in Figure 7.14 [32].

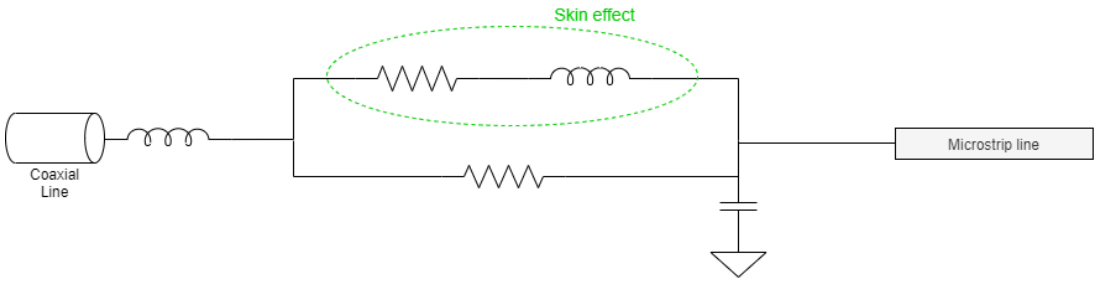

Figure 7.14: Circuit model of a coaxial connector

The superior branch in Figure 7.14, with inductor and resistance in series, represents the skin effect.

As indicated in chapter 2, skin effect has more impact at higher frequencies. At lower frequencies, the current in coaxial cables usually travels on the curved surface area of the conductor.

Even with the considered frequencies in this work being high-frequencies (frequencies where skin effect is more pronounced), skin effect was not accounted for. This approximation leads to a simplified model presented in Figure 7.15 and it tends to agree with the Figure 7.11. The resistance in this Figure will be ignored.

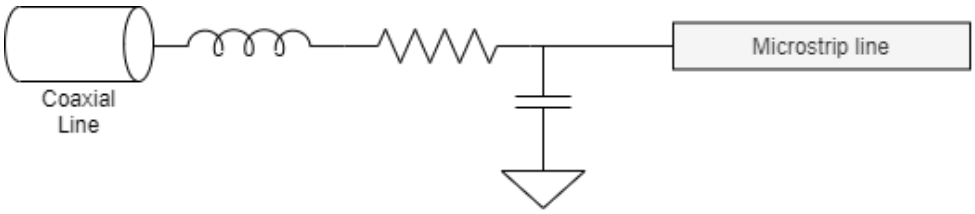

Figure 7.15: Approximated circuit model of coaxial connector

In this work, the true physical representation of the SMA connector was derived from the results of the modulations obtained in section 7.2.

7.2 Experimental results

The next phase in the current work was to weld the SMA connectors to the PCB. The PCB is shown in Figure 7.16. This PCB was used to perform tests of the SMA connectors to derive the SMA connectors' model and to test the miscrostrip lines' model accuracy.

The same PCB, without the SMA connectors welded, was placed on a test fixture (Argumen's test fixture) and was used to model the test fixture.

The picture of the test fixture, with and without the SMA connectors, is in Figure 7.17a.

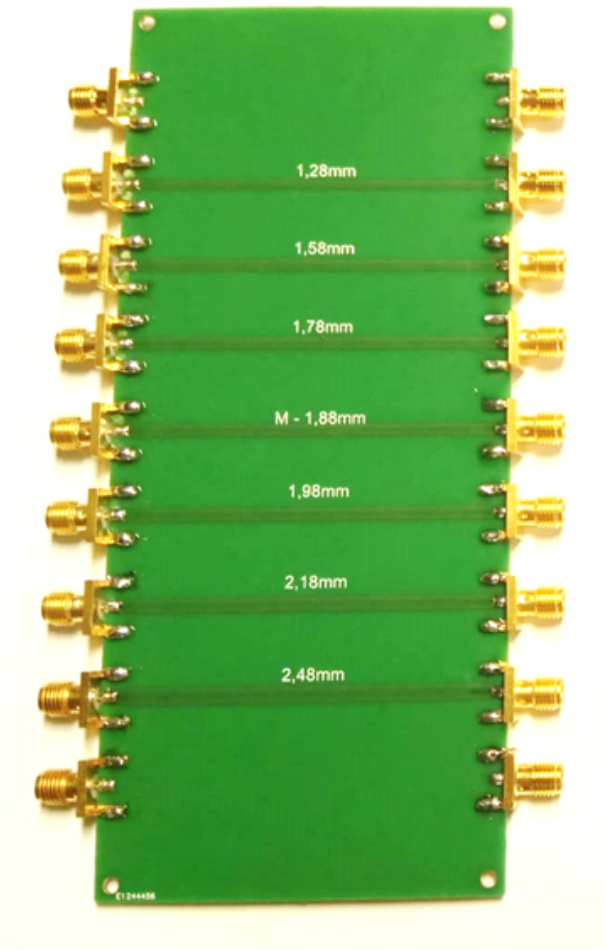

Figure 7.16: PCB with SMA connectors photo

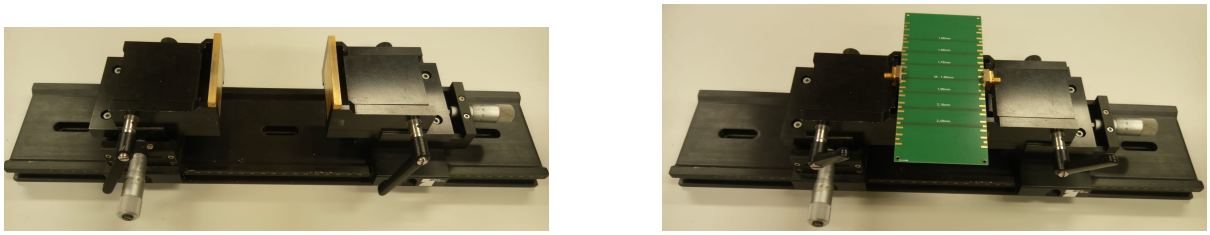

(a) Test fixture - ground plane detail

(b) Test fixture - With PCB detail

Figure 7.17: Test fixture

With the ADS schematic in Figure 7.18, the S-parameters taken from the VNA can be evaluated. These results from the VNA, regarding the PCB and the test fixture, are presented in appendix B.

The network parameters were included in the 2-port block and placed on a schematic with both input and output port's characteristic impedance equal to 50 Ω, as presented in Figure 7.18.

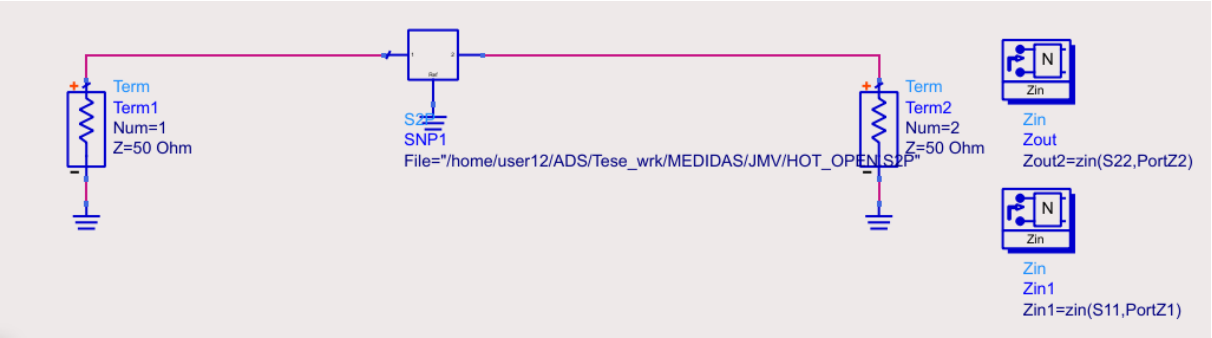

Figure 7.18: Schematic with network parameters

This section is divided in two subsections: experiments with the SMA connectors and with the test fixture's SMA connectors.

7.2.1 Experiments with SMA connectors

The input and output reflection coefficients were obtained with the VNA, presented in Figure B.3 and zoomed into Figure 7.19.

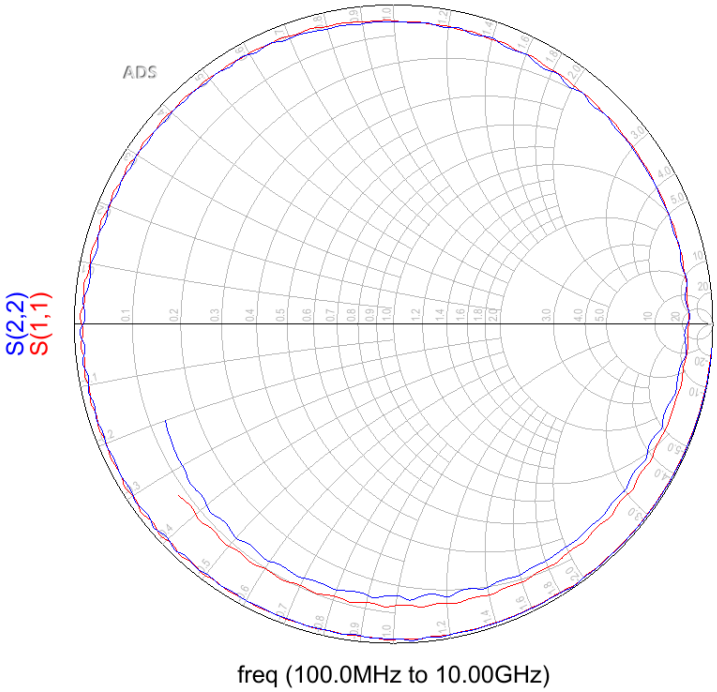

Figure 7.19: S_{11} and S_{22} representation in Smith Chart with open transmission line

The line in the Smith Chart of the Figure 7.19 starts from the open point (right side of the Smith Chart) and, if a lossless line was present, the line would run along the exterior side of the chart until it reached the short point (left side of Smith Chart). This characteristic would describe a perfect capacitive

behaviour.

With some basic knowledge of the characteristics of the Smith Chart, it is possible to deduce from Figure 7.19 that there is influence from a capacitor, but also from an inductor. The inductive influence can be seen when the line crosses the short point, around 4GHz. This frequency is called resonance frequency.

The stated characteristics are even more visible in the Figure 7.20 where until 4GHz, C11 has a positive value and after 4GHz, C11 has a negative value until roughly 8GHz, which means it has an inductive behaviour.

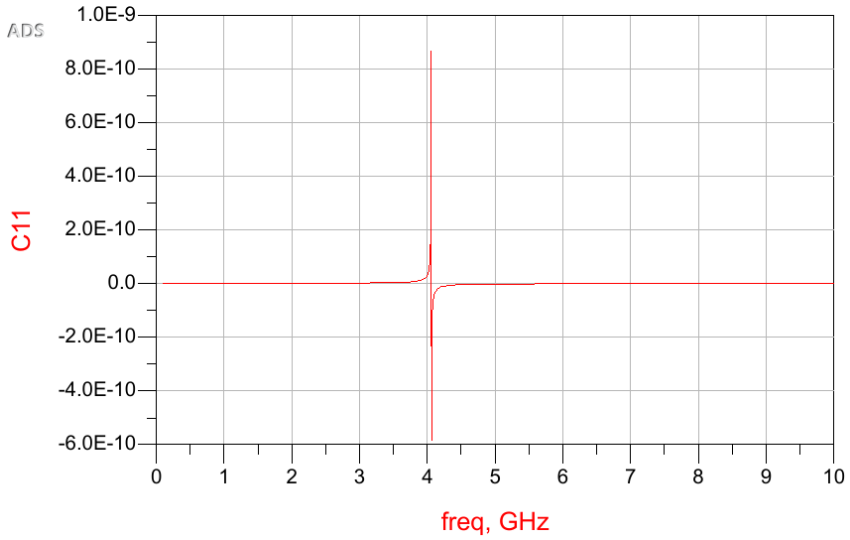

Figure 7.20: C's equation graph

The Figure 7.20 results from equation 7.1.

$$Im(Z_C) = -\frac{1}{2\pi f C} \tag{7.1}$$

where f stands for frequency.

The initial value C does not make sense on its own if taken into account its (pF). This value can be explained by the capacitance in parallel planes.

As referred to in [33], capacitance can be described in the following equation where ϵ is the dielectric constant $(4, 37)$, A is the area at issue of the PCB $(1.88 * 3mm = 5, 64mm^2)$ and d is the distance between plates (PCB's thickness).

$$C = \epsilon \frac{A}{d} \tag{7.2}$$

The result of the equation 7.2 is 0,218 pF.

Area A corresponds to the square in the PCB where the conductor of the SMA connector is welded.

The result obtained helps justify the unreasonable value of C.

As stated before, resonance starts around 4GHz (Figure 7.20) and, until then, the capacitor describes an almost linear behaviour. Similar results were obtained with the short line, as presented in Figure 7.21.

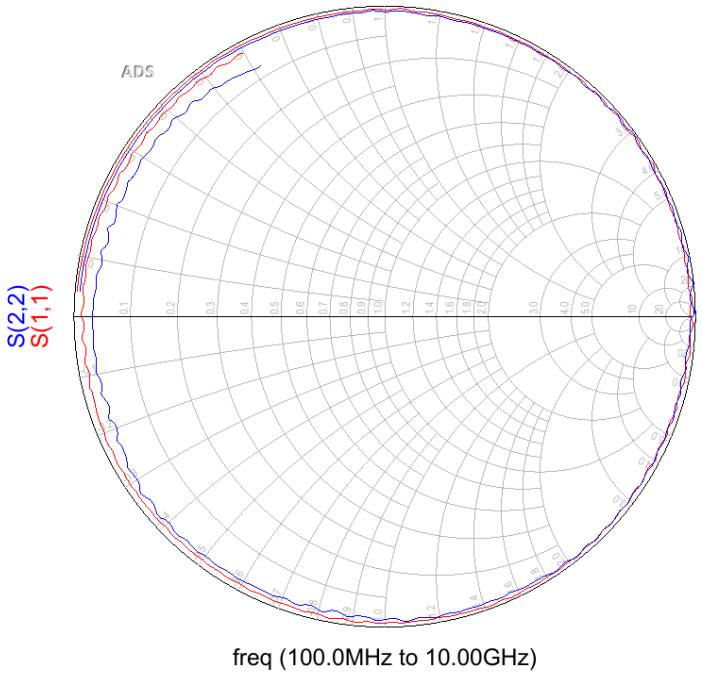

Figure 7.21: S_{11} and S_{22} representation in Smith Chart with short transmission line

The graph from Figure 7.22, similarly to the graph from Figure 7.20, can be derived when using the following equations.

$$Im(Z_L) = 2\pi f L \tag{7.3}$$

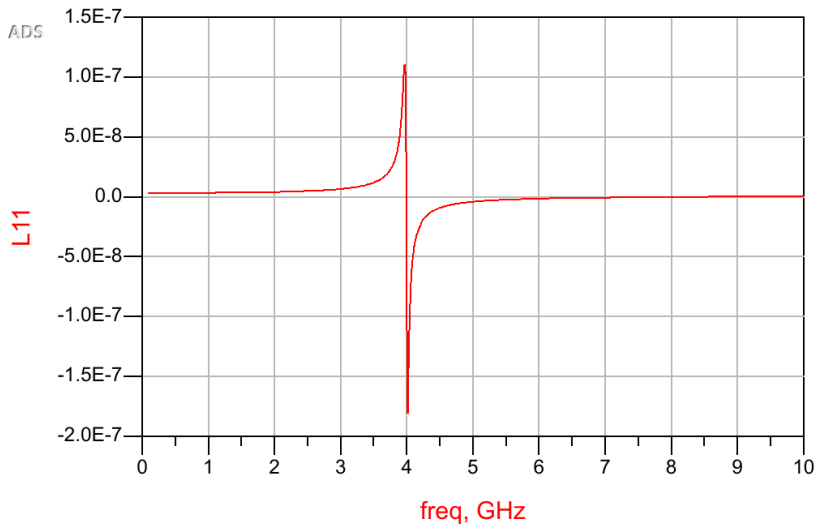

Figure 7.22: L's equation graph

A model similar to the one on Figure 7.15 was attempted but its results were not adequate. The model was altered to obtain results close to the experimental ones, in order to describe a model of a SMA connector.

Using a tuning tool included in ADS, the information presented in Figure 7.19 and the model of the Figure 7.15, it was possible to obtain a close model of SMA connectors.

The first step to achieve the SMA connector model is applying the model introduced before.

Considering the known characteristics of the Smith Chart (7.19), the resistance is not considered, as already mentioned. The series resistance alters the line in the Smith Chart, shrinking it or enlarging it, moving the line from the edges of the Smith Chart.

The second step comes more logically. Considering that the line in the Smith Chart passes by the open point at roughly 8GHz and by the short point at 4GHz, the model must have two ladders, as introduced in Figure 7.23.

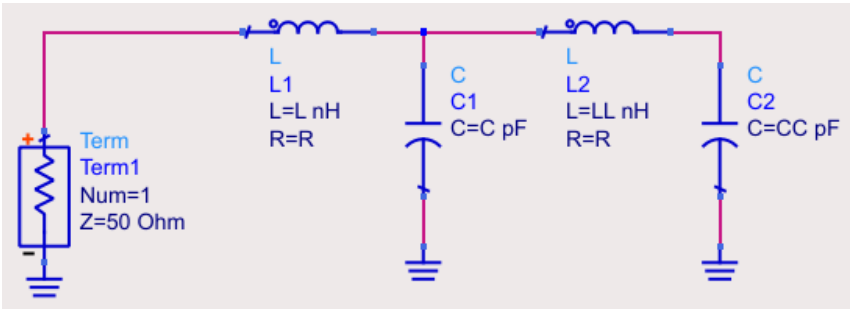

Figure 7.23: Incomplete SMA schematic

The tuning tool from ADS is used to obtain the values of L and C.

In practice, the presented line did not approach the experimental line - it did not move away from the unitary circle of the Smitch Chart.

In order to create some losses in the model, resistances had to be included, as can be seen in Figure 7.24.

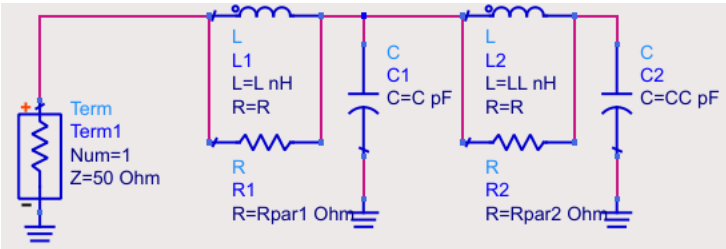

Figure 7.24: Complete SMA schematic

The tuning tool was used after the placement of the resistances. To use the tuning tool, some kind of comparison had to be made. The Smith Chart's and phase's graphs used to approximate the simulated and the experimental lines are displayed in Figure 7.25. The schematic with the values obtained from the tuning tool is also shown. The final schematic is presented in 7.24.

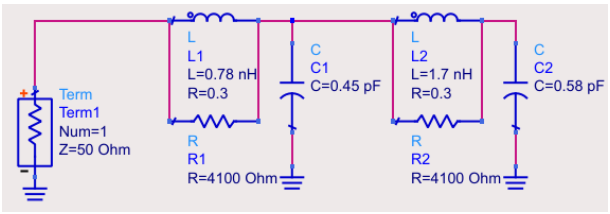

(a) Complete SMA connector's model schematic with values

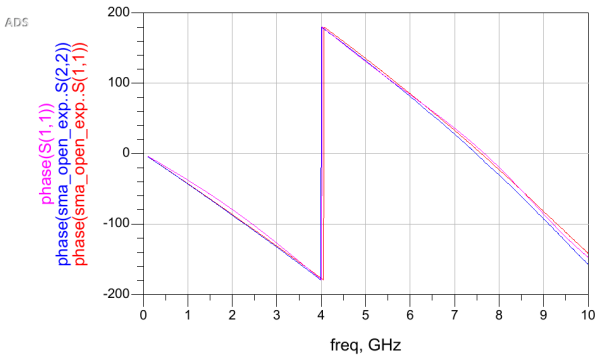

(b) Phase graph used for tune - red and blue line refer to the experimental data, pink line refers to results of the SMA connector's model applied

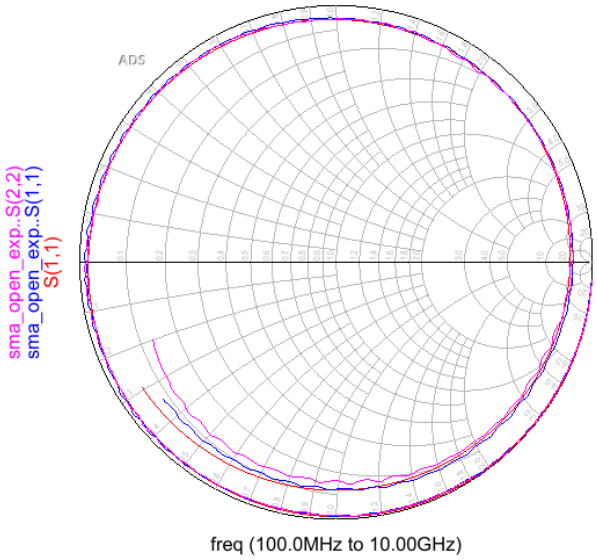

(c) Smith Chart open transmission line for SMA connector model - pink and blue line refer to the experimental data, red line refers to results of the SMA connector's model applied

Figure 7.25: Graphs of steps followed to obtain SMA model

It is possible to see that the red line in Figure 7.25c at higher frequencies, does not accurately follow the other two lines. This inaccuracy could not be solved.

The Figure 7.25a regards only the SMA connector in port 1. The complete model used for testing has both the schematic for port 1 and its symmetric for port 2, as presented in Figure 7.26

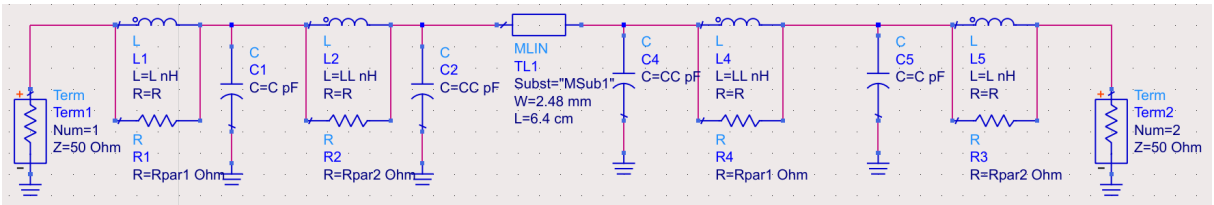

Figure 7.26: SMA's Schematic for tests

This model validity was also tested using short experimental measures.

Figure 7.27's green and orange lines corresponds to the SMA connector's model. Blue and red lines corresponds to the experimental results.

Figure 7.27: Phase in SMA model vs. experimental short line

The schematic used for the test of the short line was built according to the schematic previously built (Figure 7.25a). The schematic from Figure 7.26 cannot be directly used. Some slight changes in the schematic were made to enable short line testing, as presented in Figure 7.28. The introduced inductors represent the vias of the PCB ans its values were obtained with the tuning tool from ADS.

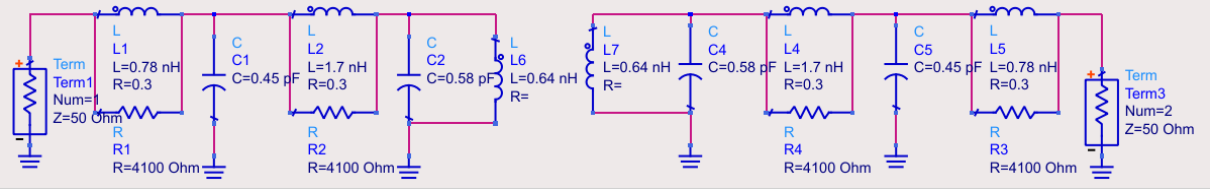

Figure 7.28: SMA connector model in short to verify assumptions

Applying the proposed model with the microstrip line from ADS, the results should be close to the results obtained experimentally.

Figure 7.30 is an example of the SMA connectors model applied to a line of 1.88mm (the remaining lines with different widths are presented in appendix C). In this Figure the green and the black lines correspond to the experimental results and the blue line to the model results.

Figure 7.30, also shows in pink the line with 1.88mm of width of the MLIN component from ADS. It is possible to observe that the behaviour of this line has the same progression as the experimental and the simulated lines.

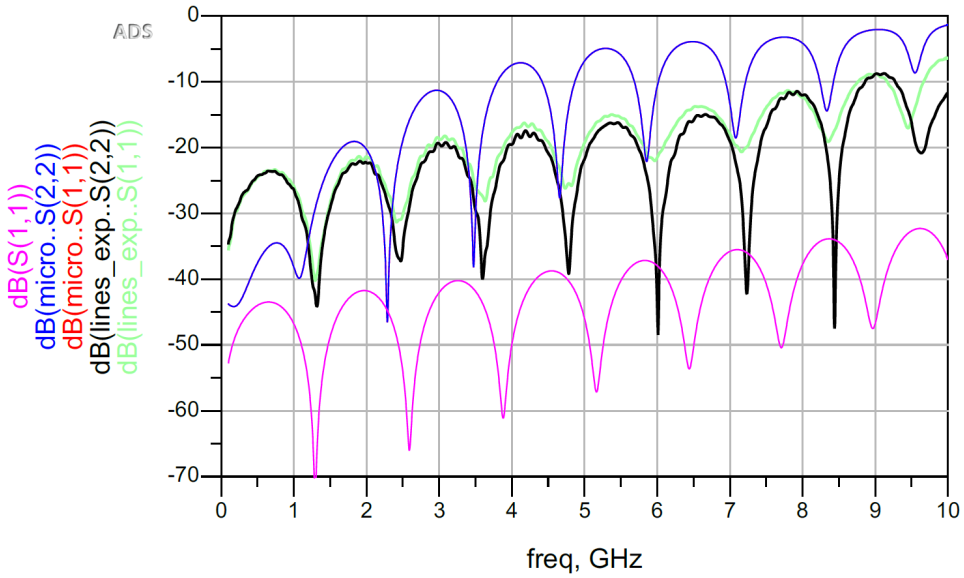

Figure 7.29: SMA model applied to MLIN of 1.88mm

It is important to refer that in the Figure C.2 (line with 1.28mm of width) the behaviour of the line comes close to a short line behaviour (as it is possible to observe better in Figure B.5). It is fair to assume that this behaviour is not the correct one, the real behaviour must have been deleted while measuring by mistake.

It is visible from the previous picture that the model is not totally reliable. The minimums of the tests with the model of the SMA connector are not exactly in the same frequency as the experimental ones and neither are the values of magnitude. Nevertheless, it is a close model for the SMA connector considering that the behaviour of the simulated line follows the same behaviour as the experimental one.

In the figures of appendix B, the frequency varies from 100MHz to 14GHz. In the current work, the used frequencies vary from 100MHz to 10GHz. After 10GHz and before 100MHz, the data is not reliable enough to enable valid conclusions.

In the same appendix are presented the graphs of the insertion loss. Figure 7.30 presented the line with 1.88mm of width.

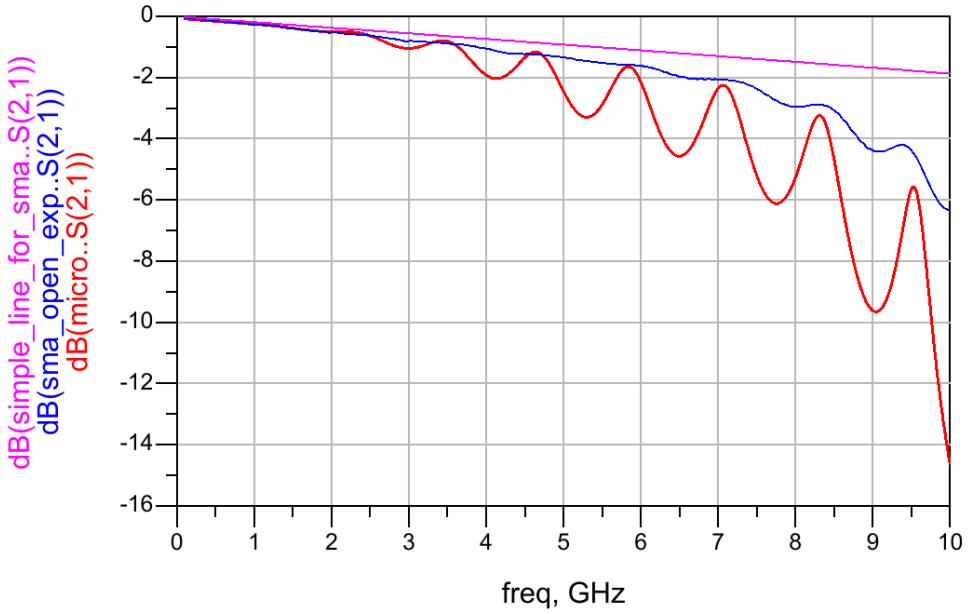

Figure 7.30: SMA model applied to MLIN of 1.88mm - Insertion loss

The blue line in Figure 7.30 depicts the results obtained experimentally and the red line depicts the results obtained with the MLIN of the ADS with the SMA connector's model applied.

The values of S_{11}, S_{12}, S_{21} and S_{22} of the graphs presented in the appendix C, were obtained in two phases: with the first welding and after applying a flow of hot air to reattach the PCB to the SMA connector. The reason for this two experiments was the poor quality of the connection between the SMA connector and the ground plane welding. The welding quality had to be ensured because of this. In consequence, a hot air flow had to be applied twice.

These considerations had to be included when looking at simulation vs. experimental results. The model of the SMA connector comes from the Figure 7.19 that was obtained in the same conditions as the previous measures.

In the graphs of insertion loss, it is possible to observe that between the experimental and the simulated results, until the frequency of resonance, the insertion loss differences are not very pronounced. Whereas when the frequency increases, the difference between them tends to grow. Until 8GHz, in experimental line, insertion loss is cut 3dB - signal strength is reduced 50 percent. This behaviour can be observed in all the lines when the width is changed. These lines are presented in appendix C.

In the simulated line, the behaviour of the lines' insertion loss, can be compared with the pink line of Figure 7.29. The downward peaks in both lines are linked. The same behaviour is also present in the experimental line, but it is not so noticeable.

The previous observations about the line of 1.28mm, are more assertive in Figure C.8.

Even with not so trustworthy results, the model of the SMA connector can be accepted to be a

general model of this component, especially at lower frequencies.

Choosing the most adapted line, was an important decision. This decision was made considering the figures presented in appendix B.1 and the same figures with more detail in appendix B.2.

Considering that the lines are under -20dB until at least 5GHz, the line with 1.58mm of width and the line with 1.78mm could be an option. This contradicts the theoretical obvious line choice, width of 1.88mm. This result proves that, even in the most simple component, mismatch has a great effect.

Even if both lines could be selected, considering the ripple in the line of 1.58mm, the line with 1.78mm of width was a better option, as presented in Figure 7.31. In this figure, red and blue lines represent the experimental results.

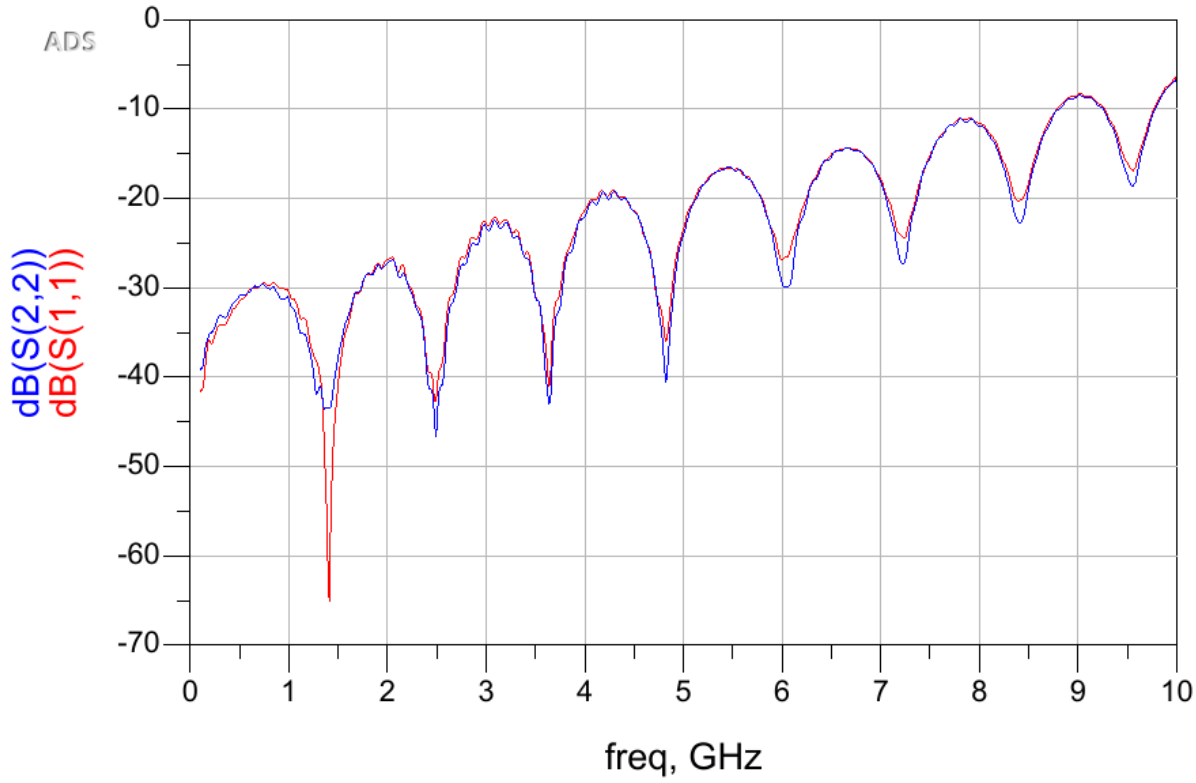

Figure 7.31: S11 S22 graphs from experiment for matching analyse - 1.78mm

A schematic was developed to test the model of the SMA connector, as presented in Figure 7.32.

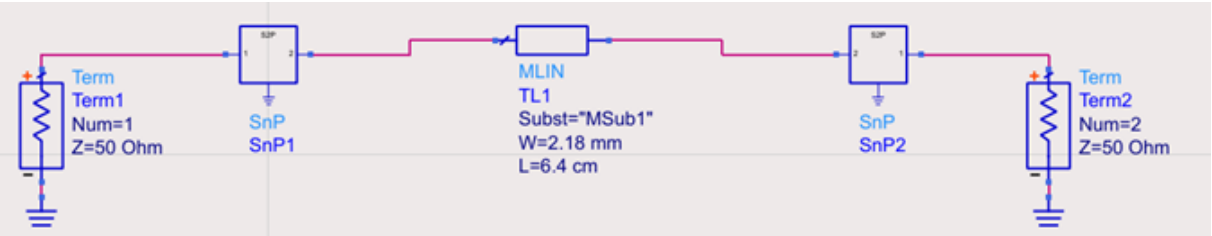

Figure 7.32: Schematic to test SMA connector model

SnP1 block and SnP2 block in Figure 7.32 have S-parameters simulated from the SMA connector's model, both from Port 1 and Port 2. The widths were altered and the results are available in the appendix C. These results only reinforce the previous conclusions, the SMA connector model can be applied until 5GHz with minimum mistakes.

7.2.2 Experiments with test fixture

When the input and output reflection coefficients of the PCB are observed in the test fixture, the model presented in section 7.2.1 has to be adjusted to include the test fixture.

Figures 7.33 and 7.34 present Argumen's test fixture, one with PCB and the other with a detailed connection to the test fixture. The SMA connectors belong to the test fixture and their positions are adjusted to the PCB's size. The SMA connector makes electrical contact to the PCB lines by mechanical pressure.

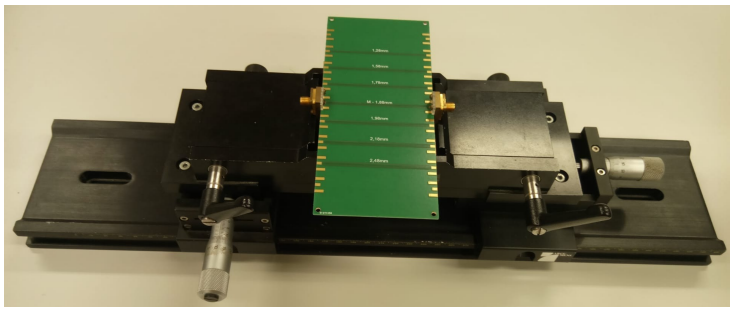

Figure 7.33: Test fixture with PCB

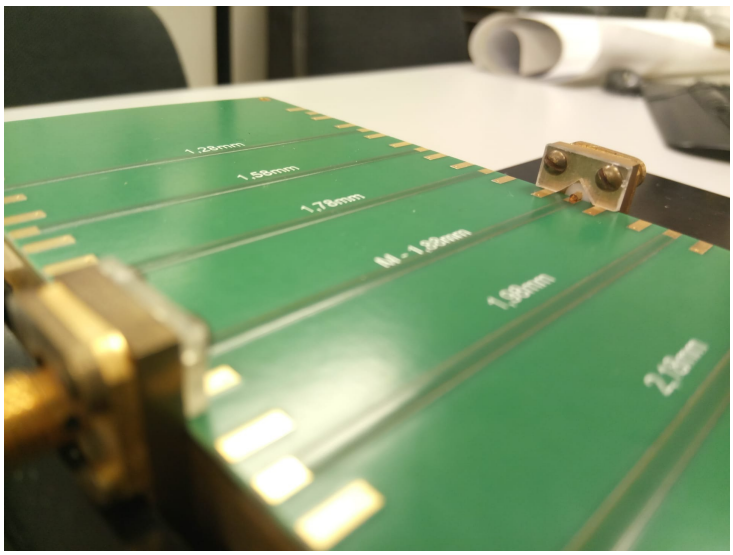

Figure 7.34: Test fixture detail

The input and the output reflection coefficients are presented in Figures 7.35 and 7.36. In Figure

7.35, the red line represents the applied model, remaining lines represent the experimental results. In Figure 7.36, green and pink lines represent the experimental results.

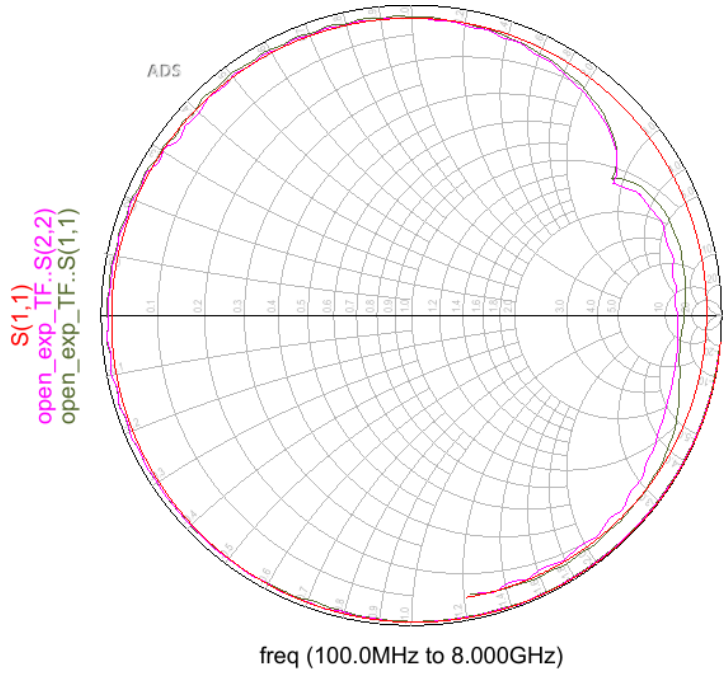

Figure 7.35: S_{11} and S_{22} representation in smith chart with an open transmission line on test fixture

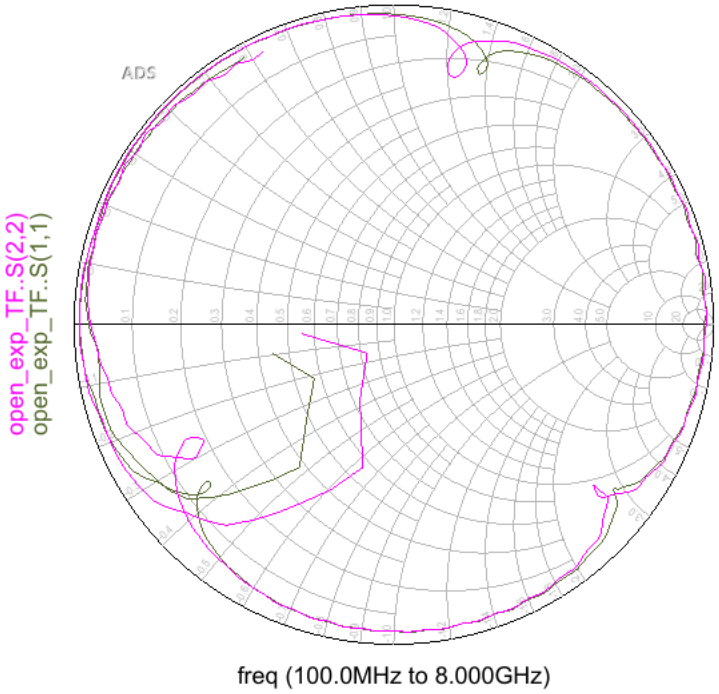

Figure 7.36: S_{11} and S_{22} representation in smith chart with a short transmission line on test fixture

C and L can also be described in graphs (Figures 7.37 and 7.38), similarly to the results obtained with the SMA connector.

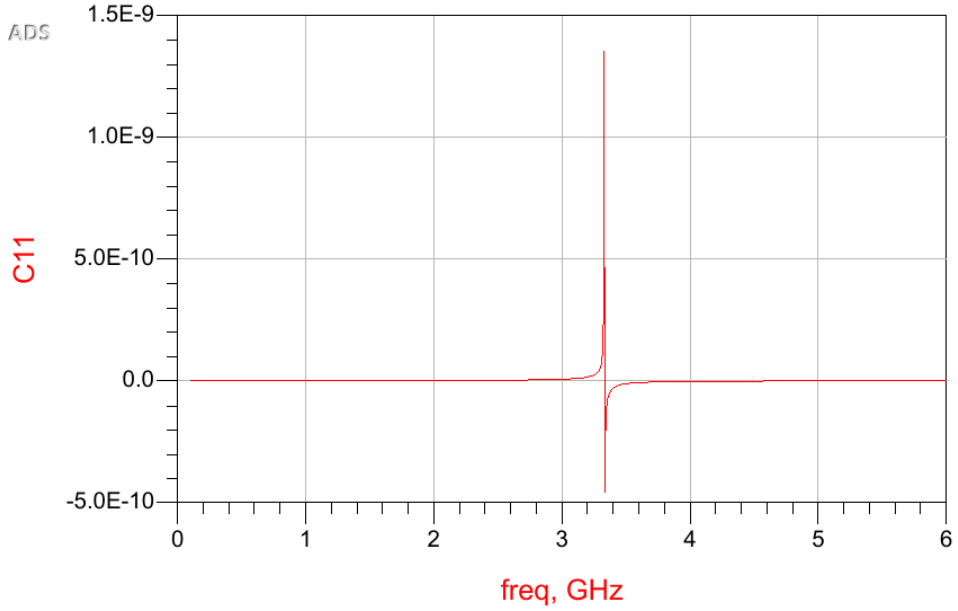

Figure 7.37: C's equation graph with test fixture

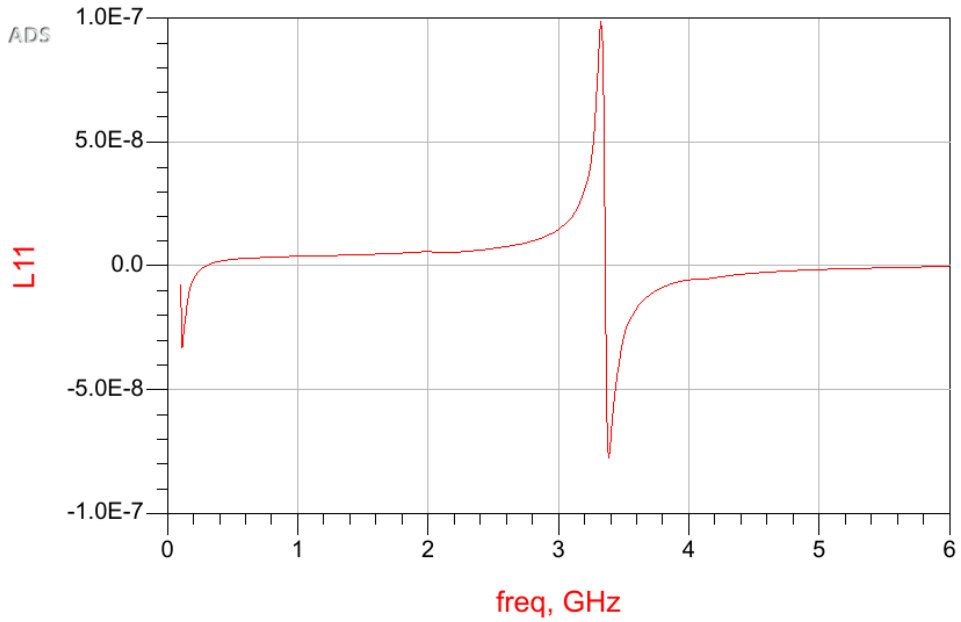

Figure 7.38: L's equation graph with test fixture

It is noticeable that the previous graphs are very similar to the previous experiment (with SMA connectors), distinguishing themselves by the resonance's frequency. In the test fixture's case, the resonance frequency is 3.32GHz, and therefore, C, R and L are different. Considering this aspect, the

approximations and considerations are the same as the SMA connector's experiment.

It is possible to claim that the previous experiment model can be implemented in this case, taking into account its capacitive behaviour at low frequencies and inductive behaviour in higher frequencies - similar to previous experiment.

Similarly to the previous experiment, with the help of Figure 7.35, Figure 7.39 and the ADS tuning tool it should be possible to obtain a model for the test fixture's SMA connector.

It is important to mention that unlike the previous experiment, the lines of the Figures 7.35 and 7.36 do not have a favorable behaviour. In the case of the SMA connectors, the lines described a close to unitary circle and had a constant evolution with frequency.

Even with this considerations, and for the sake of this experiment, the steps followed in the SMA connector experiment were repeated in the test fixture's case and are shown in Figure 7.39.

In Figure 7.39, the red line represents the experimental results and the blue line the model applied.

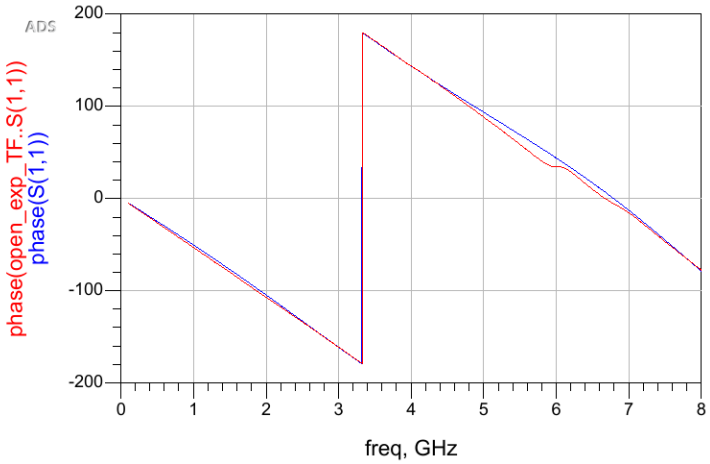

Figure 7.39: Phase graph used for tune - test fixture

The obtained model is presented in Figure 7.40.

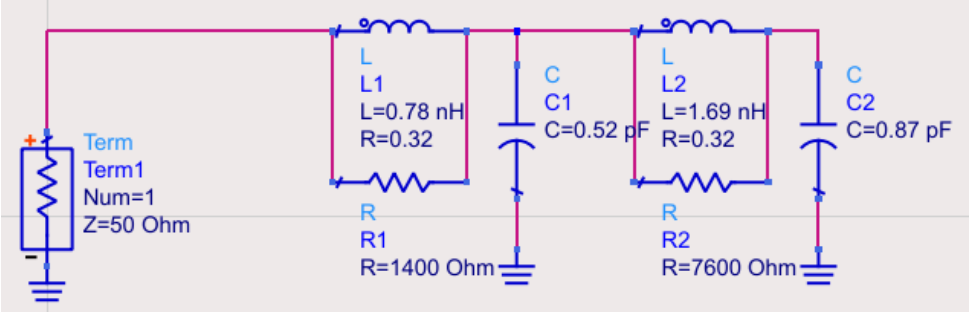

Figure 7.40: Schematic test fixture complete with values

Figure 7.40 is applied to a schematic used for tests which is presented in Figure 7.41.

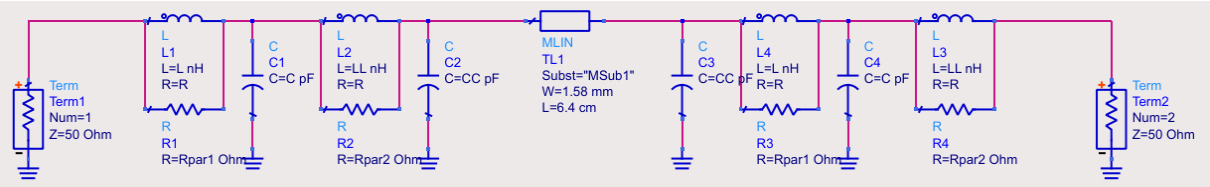

Figure 7.41: Schematic with test fixture designed to test R's, L's and C's values

The results were not close to what was expected, as can be noticed in Figure 7.42. In this figures, red line represents the model applied and the blue ones the experimental results. The remaining graphs of the model SMA connector of the test fixture applied are presented in appendix D.

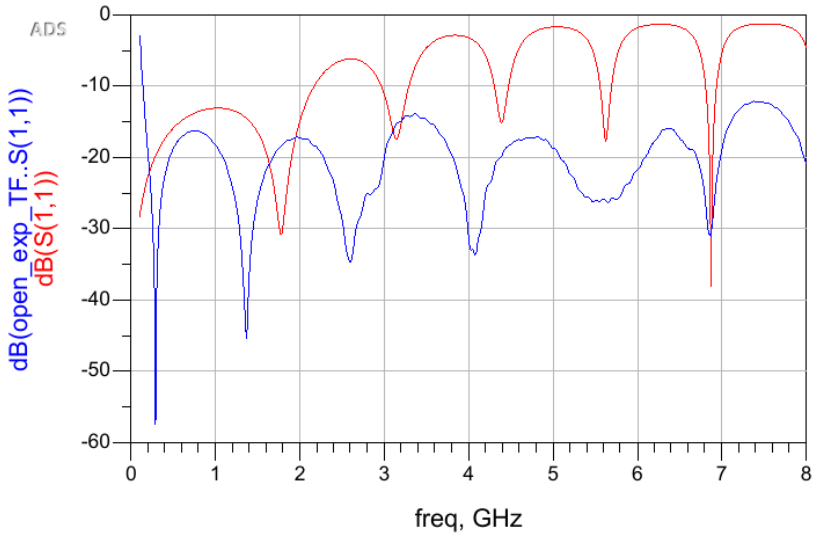

Figure 7.42: TF model applied to MLIN of 1.28mm

As mentioned before, in Figure 7.35 it is possible to notice a deviation of the line from what should be expected. This deviation can derive from the lack of ground existing in these connections.

In Figure 7.34, it can be seen that the connections between the PCB and the test fixture (on the upper side) only exist through mechanical pressure and there is no ground plane on the top.

The existence of a green layer on the PCB is also visible, it protects the metal from erosion. In the test fixture's case, this green layer was hampering the measures. On the backside ground plane, where the ground plane between the test fixture and the PCB should have been made, this green layer prevented the ground connectors from touching the ground plane of the test fixture, cutting its electrical contact. If a wave passes through the connector and the way back is blocked, or a path to return does not exist, the return of the wave becomes unknown and the correct results cannot be ensured.

The ground connections problems are the origin of the input reflection coefficient and insertion loss behaviour in the figures presented in appendix D.

These problems could be solved if a small quantity of weld was placed on the connectors on the backside of the PCB, in order to lift the ground plane.

With the previous considerations in mind, the model of the test fixture's SMA connector cannot be considered as a good model, nor can the values obtained be considered correct.

To obtain a proper test fixture's SMA connector model, an adequate ground plane must be assured. The steps followed in this work, both for the experiment with the SMA connector and for the experiment with the test fixture, can be followed.

8

Conclusions and Future Work

Conclusions and Future Work

The goal of this work was the development of a SMA connector to microstrip transition model for welded and test fixture situations. In order to attain this objective, a PCB prototype was designed using the software ADS. This PCB included seven transmission lines as well as an open and a short line to be able to produce the models.

After manufacturing the PCB, its thickness was a concern. The PCB was fabricated with 1mm of thickness. This allowed the PCB to bend which could jeopardize the welds.

During PCB design the SMA connector dimensions for the PCB ground mask provided by the manufacturer were used. Later it was observed that there was not enough size for a reliable bottom ground plane welding. As a consequence this translated into incorrect results which were described throughout this work.

Even with some bad experimental results, it was still possible to obtain a model for the SMA connector to microstrip transition model for the welded case. The model is valid until 5GHz. For higher frequencies, the comparison between experimental and simulated results were significantly different. Developing a model for the test fixture was not possible. The obtained experimental data that was not reliable.

The test fixture's ground metallic parts touched the bottom of the PCB. The metal's protection layer of the PCB did not allow for a connection to be realized between the ground planes. Subsequently, collecting satisfactory results was not possible. Unfortunately there was no time, neither VNA availability, to repeat test fixture measurements after placing a superficial amount of solder in the bottom ground plate uncovered regions, that would allow a much better connection to ground.

This work's objectives also included the selection of the best line in terms of 50 Ohms characteristic impedance. It was concluded that 1.78mm was the most matched line considering its first four S_{11} magnitude lobes. These lobes were under -20dB which indicated lower mismatch. Its frequencies assumed values up to 5GHz. Exceeding this frequency value, mismatch is beyond acceptable.

Based on these conclusions, future studies should consider increasing the thickness of the PCB and enlarging the soldering area. When using the test fixture, the ground plane connection must be ensured.

Repeating this work with a more suitable ground plane is highly recommended in order to confirm if the results and conclusions presented can be applied on higher frequencies.

Bibliography

[1] J. Paleček, M. Vestenický, P. Vestenický, and J. Spalek, “Examination of sma connector parameters,” in *2012 IEEE 16th International Conference on Intelligent Engineering Systems (INES)*, 2012, pp. 259–263.

[2] T. Hirano, J. Hirokawa, and M. Ando, “Influence of the sma connector and its modeling on electromagnetic simulation,” *Microwave and Optical Technology Letters*, vol. 57, 09 2015.

[3] H. Meng, S. Chen, Y. L. Guan, C. L. Law, P. L. So, E. Gunawan, and T. T. Lie, “A transmission line model for high-frequency power line communication channel,” in *Proceedings. International Conference on Power System Technology*, vol. 2, Oct 2002, pp. 1290–1295 vol.2.

[4] T. Rozzi and M. Farinai, “Fundamentals of electromagnetics,” pp. 23–74, 2011.

[5] D. M. Pozar, *Microwave engineering; 3rd ed.* Hoboken, NJ: Wiley, 2005. [Online]. Available: https://cds.cern.ch/record/882338

[6] M. LAverghetta, Eroglu S., Toprak S., Urgan O, MD, Ozge E. Onur, MD, Arzu Denizbasi, MD, Haldun Akoglu, MD, Cigdem Ozpolat, MD, Ebru Akoglu, “Microwave and Wireless simplified,” pp. 3–8, 2012.

[7] D. D. Grieg and H. F. Engelmann, “Microstrip-a new transmission technique for the klilomegacycle range,” *Proceedings of the IRE*, vol. 40, no. 12, pp. 1644–1650, 1952.

[8] M. F. Flow, C. Spinners, F. Bore, F. Meters, D. F. Meters, L. Format, C. Speed, S. Conventions, F. F. Principles, R. T. Tools, O. A. Logging, O. Activation, L. Example, S. Water, F. Log, O. Principles, S. Oxygen, A. Example, S. Oxygen, and A. Example, “Foundation For Microstrip Circuit Design,” pp. 1–12, 2002.

[9] L. G. Maloratsky, “Reviewing the basics of suspended striplines,” *Microwave Journal*, vol. 45, no. 10, 2002.

[10] Y. Quer and V. L. Saux, “Peak and Average Power Handling Capability of Microstrip Filters,” pp. 1–14.

[11] C. P. Wen, “Coplanar waveguide: A surface strip transmission line suitable for nonreciprocal gyromagnetic device applications,” *IEEE Transactions on Microwave Theory and Techniques*, vol. 17, no. 12, pp. 1087–1090, December 1969.

[12] B. C. Wadell, “Transmission line design handbook,” p. 513, 1991. [Online]. Available: http://www.lavoisier.fr/livre/notice.asp?id=OS6WOOAXK2XOWK

[13] J. A. Bland and D. R. Bland, “Wave Theory and Applications,” p. 126, 1991.

[14] Ramesh Garg; I J Bahl; Maurizio Bozzi, “Microstrip lines and slotlines,” 1996.

[15] Several, “Microwave Materials,” 1994.

[16] R. Mongia, I. Bahl, and P. Bhartia, “RF and Microwave Coupled-Line Circuits,” Norwood, p. 521, 1999.

[17] R. W. Anderson and O. T. Dennison, “An Advanced New Network Analyzer for Sweep-Measuring Amplitude and Phase from 0.1 to 12.4 GHz,” *Hewlett-Packard Journal*, no. February 1967, pp. 2–9, 1967. [Online]. Available: http://scholar.google.com/scholar?hl=en{&}btnG=Search{&}q=intitle:S-Parameter+Techniques+for+Faster,+More+Accurate+Network+Design{#}0

[18] F. Caspers, “Rf engineering basic concepts: S-parameters,” 01 2012.

[19] E. C. Flow, C. Logging, N. R. Magnetization, C. Testing, I. W. Chemistry, and W. R. Elements, “Measurement Catalog,” pp. 1–28.

[20] A. Technologies, “Agilent AN 1287-2 Exploring the Architectures of Network Analyzers,” *Differences*, 2000.

[21] K. Technologies, “Network Analyzer Basics (slides with notes),” 2012.

[22] A. C. T.-p. Vector and N. Analyzer, “A Complete Two-Port Vector Network Analyzer.”

[23] A. Technologies and N. Analyzer, “User ’ s Guide,” *Differences*, no. April, 2012.

[24] M. Lauterbach, “Getting more out of eye diagrams [circuit testing],” *IEEE Spectrum*, vol. 34, no. 3, pp. 60–63, 1997.

[25] A. Note, “Agilent De-embedding and Embedding S-Parameter Networks Using a Vector Network Analyzer,” *Test*, pp. 1–24, 2008.

[26] B. Chen, X. Ye, B. Samaras, and J. Fan, “A novel de-embedding method suitable for transmission-line measurement,” in *2015 Asia-Pacific Symposium on Electromagnetic Compatibility (APEMC)*, 2015, pp. 1–4.

[27] G. F. Engen and C. A. Hoer, “Thru-reflect-line: An improved technique for calibrating the dual six-port automatic network analyzer,” *IEEE Transactions on Microwave Theory and Techniques*, vol. 27, no. 12, pp. 987–993, 1979.

[28] T. Reveyrand, “TRL algorithm to de-embed a RF test fixture,” no. July, 2013. [Online]. Available: http://www.microwave.fr/reports/CU-boulder.pdf

[29] Y. Chen, “Scholars ’ Mine De-embedding method comparisons and physics based circuit model for high frequency D-probe,” Ph.D. dissertation, 2018.

[30] K. Technologies, “MSUB (Microstrip Substrate).”

[31] L. Technologies, “SMA Connectors,” pp. 14–30, 2012.

[32] H. Zha, D. Lu, W. Wang, and F. Lin, “Rf modeling and optimization of end-launch sma to trace transition,” in *2015 IEEE 17th Electronics Packaging and Technology Conference (EPTC)*, 2015, pp. 1–4.

[33] H. Zumbahlen, “Printed Circuit-Board Design Issues,” *Linear Circuit Design Handbook*, pp. 821–895, 2008.

Appendix A- TRL algorithm

$$\left[T_{THRU}^{Std}\right] = \begin{bmatrix} 1 & 0 \\ 0 & 1 \end{bmatrix}, \tag{A.1}$$

$$\mathrm{Sgn}\left(\Re\left\{\Gamma_{REFLECT}^{Std}\right\}\right) = \pm 1 \tag{A.2}$$

$$\left[T_{LINE}^{Std}\right] = \begin{bmatrix} e^{-\gamma l} & 0 \\ 0 & e^{+\gamma l} \end{bmatrix} \tag{A.3}$$

Equations for the thru:

$$\begin{gathered} \left[T_{THRU}^{\text{Meas}}\right] = [T_{IN}]\left[T_{THRU}^{Std}\right][T_{OUT}], \\ [T_{IN}]^{-1}\left[T_{THRU}^{Meas}\right] = \left[T_{THRU}^{Std}\right][T_{OUT}], \\ [T_{IN}]^{-1}\left[T_{THRU}^{Meas}\right] = [T_{OUT}], \\ [T_{IN}]^{-1} = \left[\overline{T_{IN}}\right], \\ \left[\overline{T_{IN}}\right]\left[T_{THRU}^{Meas}\right] = [T_{OUT}]. \end{gathered} \tag{A.4}$$

Equations for the line:

$$\begin{gathered} \left[T_{LINE}^{\text{Meas}}\right] = [T_{IN}]\left[T_{LINE}^{Std}\right][T_{OUT}] \\ [T_{IN}]^{-1}\left[T_{LINE}^{Meas}\right] = \left[T_{LINE}^{Std}\right][T_{OUT}] \\ \left[\overline{T_{IN}}\right]\left[T_{LNE}^{Meas}\right] = \begin{bmatrix} e^{-\gamma l} & 0 \\ 0 & e^{+\gamma l} \end{bmatrix}[T_{OUT}] \end{gathered} \tag{A.5}$$

From the last equation of the line measurements and considering that

$$[T_{IN}] = \begin{bmatrix} T_{11} & T_{12} \\ T_{21} & T_{22} \end{bmatrix}, \tag{A.6}$$

it is logical that

$$\begin{bmatrix} \overline{T}_{11} & \overline{T}_{12} \\ \overline{T}_{21} & \overline{T}_{22} \end{bmatrix}\left[T_{LINE}^{Meas}\right] = \begin{bmatrix} T_{11}e^{-\gamma l} & T_{12}e^{-\gamma l} \\ T_{21}e^{+\gamma l} & T_{22}e^{+\gamma l} \end{bmatrix}. \tag{A.7}$$

The last line of A.4 applied in A.7 gives:

$$\begin{bmatrix} T_{11} & T_{12} \\ T_{21} & T_{22} \end{bmatrix} \begin{bmatrix} T_{THRU}^{Meas} \end{bmatrix}^{-1} \begin{bmatrix} T_{LINE}^{Meas} \end{bmatrix} = \begin{bmatrix} T_{11}e^{-\gamma l} & T_{12}e^{-\gamma l} \\ T_{21}e^{+\gamma l} & T_{22}e^{+\gamma l} \end{bmatrix}. \tag{A.8}$$

To simplify the calculations a new parameter was included:

$$[M] = \begin{bmatrix} T_{THRU}^{Meas} \end{bmatrix}^{-1} \begin{bmatrix} T_{LINE}^{Meas} \end{bmatrix}. \tag{A.9}$$

With the previous information the next equations are natural:

$$T_{11}M_{11} + T_{12}M_{21} = T_{11}e^{-\gamma l} \tag{A.10}$$

$$T_{11}M_{12} + T_{12}M_{22} = T_{12}e^{-\gamma l} \tag{A.11}$$

$$T_{21}M_{11} + T_{22}M_{21} = T_{21}e^{+\gamma l} \tag{A.12}$$

$$T_{21}M_{12} + T_{22}M_{22} = T_{22}e^{+\gamma l} \tag{A.13}$$

A.11 gives:

$$e^{-\gamma l} = \left(\frac{T_{11}}{T_{12}}\right) M_{12} + M_{22}, \tag{A.14}$$

and using it in A.10,

$$T_{11}M_{11} + T_{12}M_{21} = T_{11}\left[\left(\tfrac{T_{11}}{T_{12}}\right) M_{12} + M_{22}\right],$$

$$M_{11} + \left(\tfrac{T_{12}}{T_{11}}\right) M_{21} = \left(\tfrac{T_{11}}{T_{12}}\right) M_{12} + M_{22}, \tag{A.15}$$

$$\left(\tfrac{T_{12}}{T_{11}}\right)^2 M_{21} + \left(\tfrac{T_{12}}{T_{11}}\right)(M_{11} - M_{22}) - M_{12} = 0.$$

A.12 origins

$$e^{+\gamma l} = M_{11} + \left(\frac{T_{22}}{T_{21}}\right) M_{21}. \tag{A.16}$$

A.16 in A.13 gives

$$T_{21}M_{12} + T_{22}M_{22} = T_{22}\left[\left(\frac{T_{22}}{T_{21}}\right)M_{21} + M_{11}\right]$$

$$M_{22} + \left(\frac{T_{21}}{T_{22}}\right)M_{12} = \left(\frac{T_{22}}{T_{21}}\right)M_{21} + M_{11} \tag{A.17}$$

$$\left(\frac{T_{22}}{T_{21}}\right)^2 M_{21} + \left(\frac{T_{22}}{T_{21}}\right)(M_{11} - M_{22}) - M_{12} = 0$$

Using known maths,

$$X^2 M_{21} + X\left[M_{11} - M_{22}\right] - M_{12} \tag{A.18}$$

This polynom has two solutions, $\frac{T_{12}}{T_{11}}$ and $\frac{T_{22}}{T_{21}}$.

If the considered polynom is

$$X^2 M_{12} + X\left[M_{22} - M_{11}\right] - M_{21}, \tag{A.19}$$

then the two solutions are $\frac{T_{11}}{T_{12}}$ and $\frac{T_{21}}{T_{22}}$.

$$\begin{bmatrix} \overline{T}_{11} & \overline{T}_{12} \\ \overline{T}_{21} & \overline{T}_{22} \end{bmatrix} \left[T_{LINE}^{Meas}\right] = \begin{bmatrix} e^{-\gamma l} & 0 \\ 0 & e^{+\gamma l} \end{bmatrix} \begin{bmatrix} T_{11} & T_{12} \\ T_{21} & T_{22} \end{bmatrix} \tag{A.20}$$

As said before

$$\left[\overline{T_{IN}}\right]\left[T_{THRU}^{Meas}\right] = \left[T_{OUT}\right] \tag{A.21}$$

and combining A.20 with A.21:

$$\begin{bmatrix} \overline{T}_{11} & \overline{T}_{12} \\ \overline{T}_{21} & \overline{T}_{22} \end{bmatrix} \begin{bmatrix} T_{LINE}^{Meas} \end{bmatrix} = \begin{bmatrix} e^{-\gamma 1} & 0 \\ 0 & e^{+\gamma 1} \end{bmatrix} \begin{bmatrix} \overline{T}_{11} & \overline{T}_{12} \\ \overline{T}_{21} & \overline{T}_{22} \end{bmatrix} \left[T_{THRU}^{Meas}\right] \tag{A.22}$$

Considering

$$[N] = \left[T_{LINE}^{Meas}\right]\left[T_{THRU}^{Meas}\right]^{-1} \tag{A.23}$$

and the similarity between A.8 and the logical next steps (compared to the previous) of A.22 origins the polynom

$$X^2 N_{21} + X\left[N_{11} - N_{22}\right] - N_{12}. \tag{A.24}$$

The polynom A.24 has two solutions, $\left(\frac{\overline{T}_{12}}{\overline{T}_{11}}\right)$ and $\left(\frac{\overline{T}_{22}}{\overline{T}_{21}}\right)$.

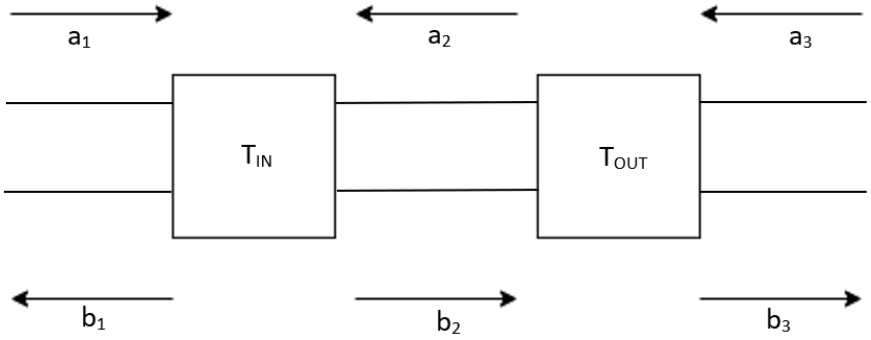

Figure A.1: THRU equality

By the same token, is the polynom is $X^2 N_{12} + X\left[N_{22} - N_{11}\right] - N_{21}$ the solutions are going to be $\left(\frac{\overline{T}_{11}}{\overline{T}_{12}}\right)$ and $\left(\frac{\overline{T}_{21}}{\overline{T}_{22}}\right)$.

$$\begin{pmatrix} b_2 \\ a_2 \end{pmatrix} = \begin{bmatrix} \overline{T}_{11} & \overline{T}_{12} \\ \overline{T}_{21} & \overline{T}_{22} \end{bmatrix} \begin{pmatrix} a_1 \\ b_1 \end{pmatrix}$$
$$\begin{pmatrix} b_2 \\ a_2 \end{pmatrix} = \begin{bmatrix} T_{11} & T_{12} \\ T_{21} & T_{22} \end{bmatrix} \begin{pmatrix} b_3 \\ a_3 \end{pmatrix} \tag{A.25}$$

b_2 equality allows the extraction $\frac{T_{11}}{\overline{T}_{11}}$. a_2 equality allows the extraction $\frac{T_{21}}{\overline{T}_{21}}$.

$$\overline{T}_{11} a_1 + \overline{T}_{12} b_1 = T_{11} b_3 + T_{12} a_3 \tag{A.26}$$

and by definition from THRU measurements,

$$S_{21}^{Meas} = \left.\frac{b_3}{a_1}\right|_{a_3=0}, S_{11}^{Meas} = \left.\frac{b_1}{a_1}\right|_{a_3=0} \tag{A.27}$$

$$a_1 \left(\overline{T}_{11} + \overline{T}_{12} \frac{b_1}{a_1}\right) = T_{11} b_3$$

$$\overline{T}_{11} \left(1 + \left(\frac{\overline{T}_{12}}{\overline{T}_{11}}\right) S_{11}^{\text{Meas}}\right) = T_{11} S_{21}^{\text{Meas}} \quad . \tag{A.28}$$

$$\left(\frac{T_{11}}{\overline{T}_{11}}\right) = \frac{\left(1 + \left(\frac{\overline{T}_{12}}{\overline{T}_{11}}\right) S_{11}^{\text{Meas}}\right)}{S_{21}^{\text{Meas}}}$$

The a_1 equality leads to

$$\overline{T}_{21} a_1 + \overline{T}_{22} b_1 = T_{21} b_3 + T_{22} a_3 \tag{A.29}$$

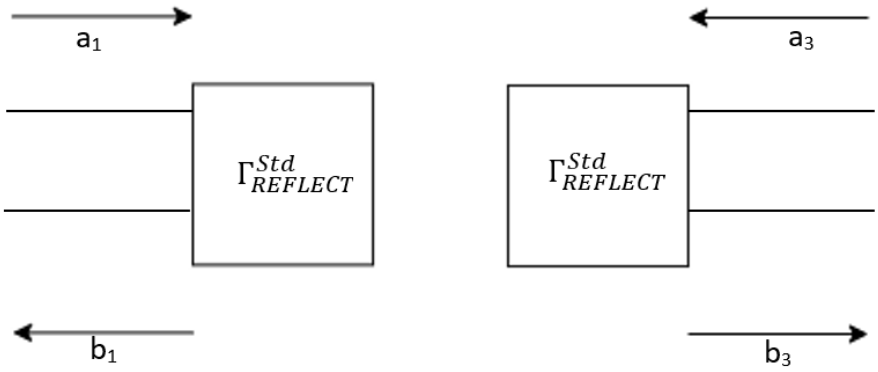

Figure A.2: REFLECT measurement

and by definition from THRU measurements,

$$S_{12}^{\text{Meas}} = \left.\frac{b_1}{a_3}\right|_{a_1=0}, S_{22}^{\text{Meas}} = \left.\frac{b_3}{a_3}\right|_{a_1=0} \tag{A.30}$$

hence,

$$b_1\overline{T}_{22} = T_{21}b_3 + T_{21}a_3 \tag{A.31}$$

leading to

$$\left(\frac{T_{21}}{\overline{T}_{22}}\right) = \frac{S_{12}^{Meas}}{S_{22}^{Meas} + \left(\frac{T_{22}}{T_{21}}\right)}. \tag{A.32}$$

From the REFLECT measurement

$$\Gamma_{REFLECT}^{Std} = \frac{b_1}{a_1} = \frac{\overline{T}_{21} + \overline{T}_{22}S_{11}^{Meas}}{\overline{T}_{11} + \overline{T}_{12}S_{11}^{Meas}} \tag{A.33}$$

$$\Gamma_{REFLECT}^{Std} = \frac{b_2}{a_2} = \frac{T_{12} + T_{11}S_{22}^{Meas}}{T_{22} + T_{21}S_{22}^{Meas}} \tag{A.34}$$

$$\frac{\overline{T}_{21} + \overline{T}_{22}S_{11}^{\text{Meas}}}{\overline{T}_{11} + \overline{T}_{12}S_{11}^{\text{Meas}}} = \frac{T_{12} + T_{11}S_{22}^{\text{Meas}}}{T_{22} + T_{21}S_{22}^{Meas}} \tag{A.35}$$

$$\frac{\overline{T}_{21}}{\overline{T}_{11}}\left(\frac{1 + \left(\frac{\overline{T}_{22}}{\overline{T}_{21}}\right)S_{11}^{\text{Meas}}}{1 + \left(\frac{\overline{T}_{12}}{\overline{T}_{11}}\right)S_{11}^{\text{Meas}}}\right) = \frac{T_{11}}{T_{21}}\left(\frac{S_{22}^{\text{Meas}} + \left(\frac{T_{12}}{T_{11}}\right)}{S_{22}^{\text{Meas}} + \left(\frac{T_{22}}{T_{21}}\right)}\right) \tag{A.36}$$

$$\left(\overline{T}_{21}\right)^2\left(\frac{T_{21}}{\overline{T}_{22}}\right)\left(\frac{\overline{T}_{22}}{\overline{T}_{21}}\right)=\left(\overline{T}_{11}\right)^2\left(\frac{T_{11}}{\overline{T}_{11}}\right)\frac{\left(\frac{s_{22}^{\text{Meas}}+\left(\frac{T_{12}}{T_{11}}\right)}{S_{22}^{\text{Mes}}+\left(\frac{T_{22}}{T_{21}}\right)}\right)}{\left(\frac{1+\left(\frac{\overline{T}_{22}}{\tau_{21}}\right)S_{11}^{\text{Meas}}}{1+\left(\frac{\overline{T}_{12}}{\overline{\tau}_{11}}\right)s_{11}^{\text{Meas}}}\right)} \tag{A.37}$$

$$\left(\frac{\overline{T}_{21}}{\overline{T}_{11}}\right)=\pm\sqrt{\frac{\left(\frac{T_{11}}{\overline{T}_{11}}\right)\left(\frac{S_{22}^{Meas}+\left(\frac{T_{12}}{T_{11}}\right)}{S_{22}^{Meas}+\left(\frac{T_{22}}{T_{21}}\right)}\right)}{\left(\frac{T_{21}}{\overline{T}_{22}}\right)\left(\frac{\overline{T}_{22}}{\overline{T}_{21}}\right)\left(\frac{1+\left(\frac{\overline{T}_{22}}{\overline{T}_{21}}\right)S_{11}^{\text{Meas}}}{1+\left(\frac{\overline{T}_{12}}{\overline{T}_{11}}\right)S_{11}^{\text{Meas}}}\right)}} \tag{A.38}$$

There are two solutions from A.38 but one of the known information from derived from A.33 the good one is selected.

The 7 terms are discovered and algorithm is complete. Ending this part the S-parameters are de-embedded:

- From [M], $\frac{T_{12}}{T_{11}}$ (T_{OUT} parameter) and $\frac{T_{22}}{T_{21}}$ (T_{OUT} parameter);
- From [N], $\frac{\overline{T_{12}}}{\overline{T_{11}}}$ ($\overline{T_{IN}}$ parameter) and $\frac{\overline{T_{22}}}{\overline{T_{21}}}$ ($\overline{T_{IN}}$ parameter);
- The THRU equality from A.28, $\frac{T_{11}}{\overline{T_{11}}}$ and from A.32, $\frac{T_{21}}{\overline{T_{22}}}$;
- The REFLECT equality from A.38, $\frac{\overline{T_{21}}}{\overline{T_{11}}}$.

Appendix B- VNA results

B.1 Experimental data

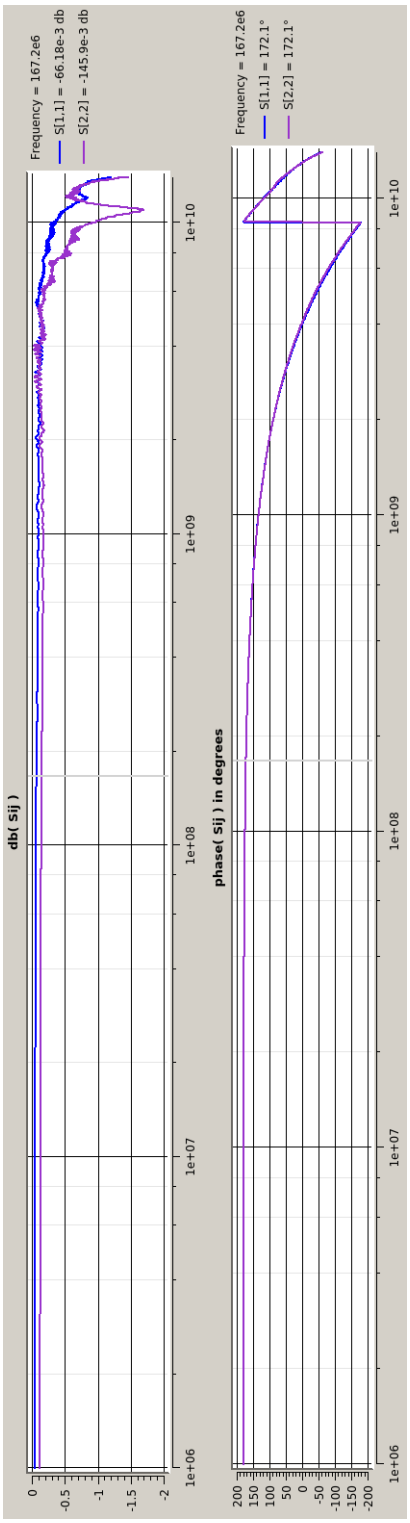

Figure B.1: Results of the VNA with short's line

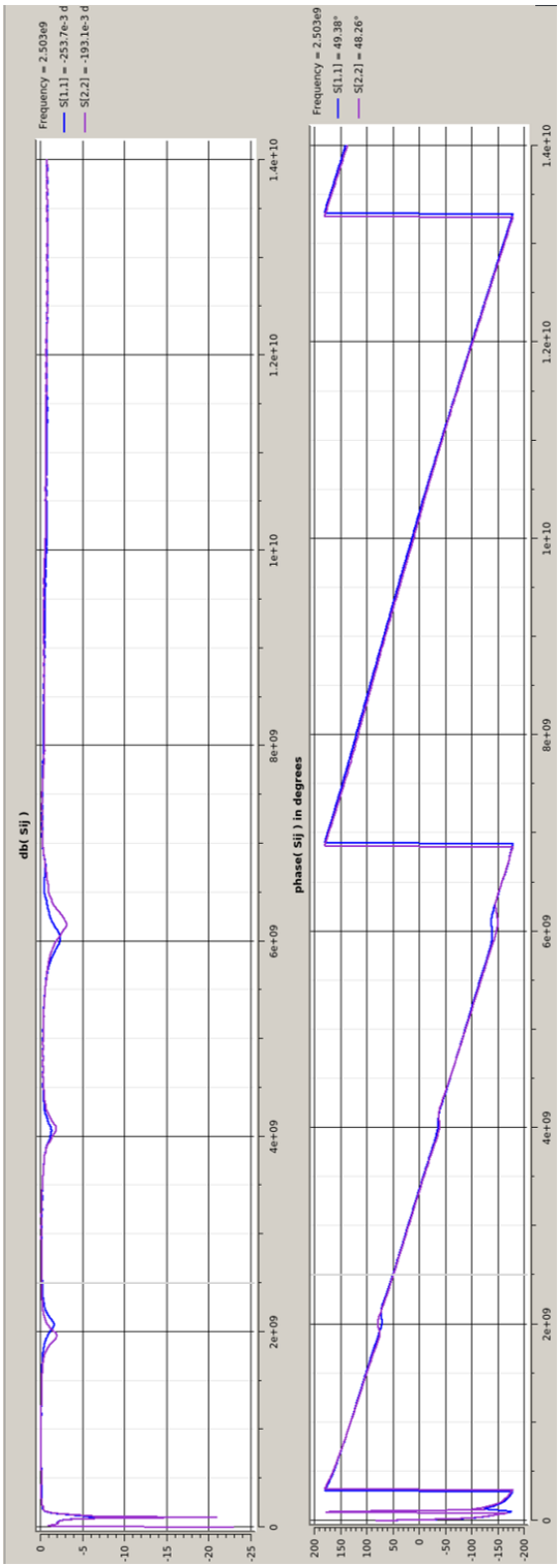

Figure B.2: Results of the VNA with short's line - test fixture

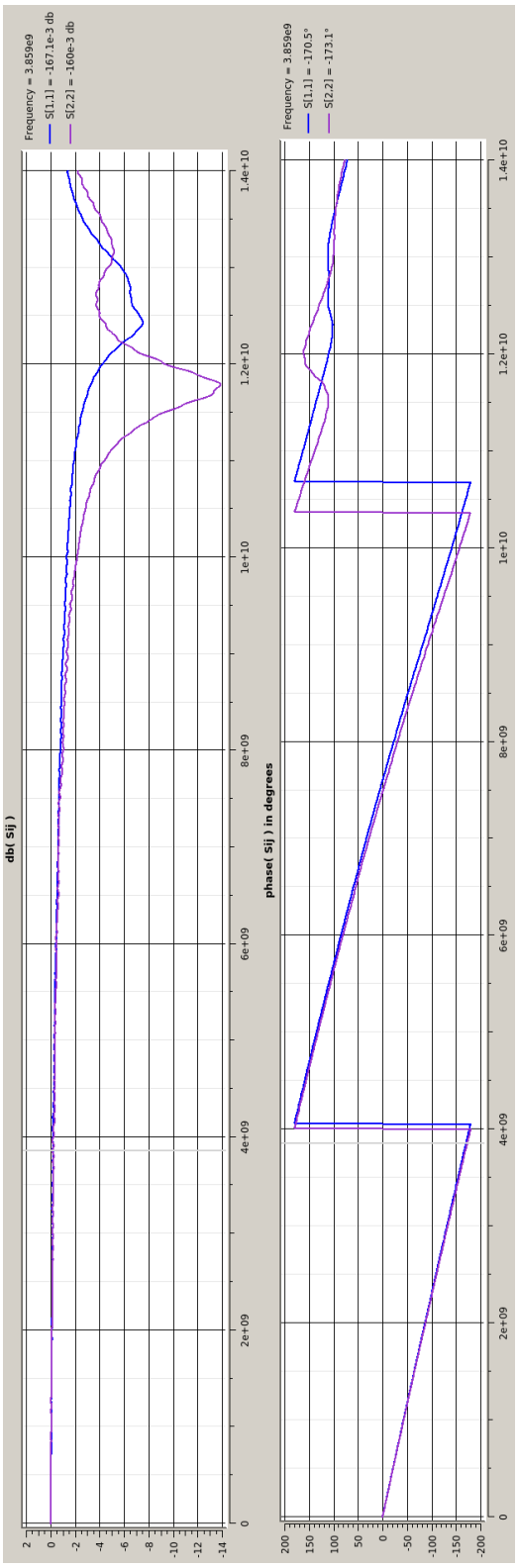

Figure B.3: Results of the VNA with open's line

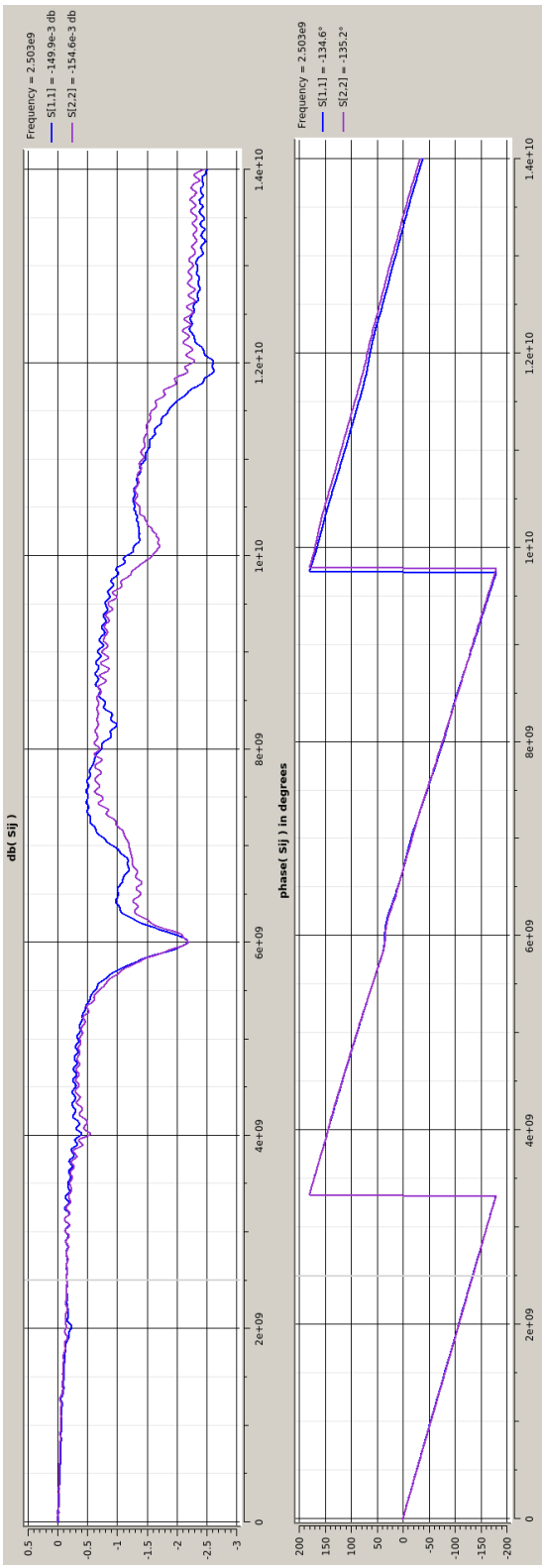

Figure B.4: Results of the VNA with open's line - test fixture

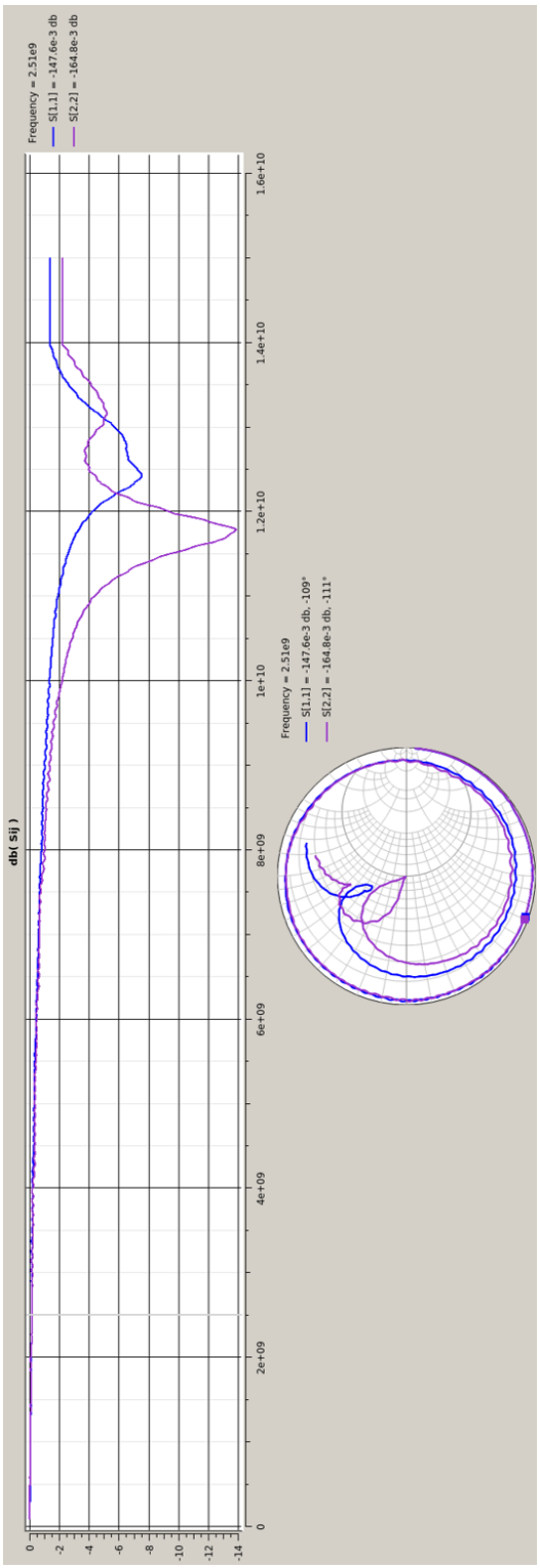

Figure B.5: Results of the VNA with 1.28mm's line

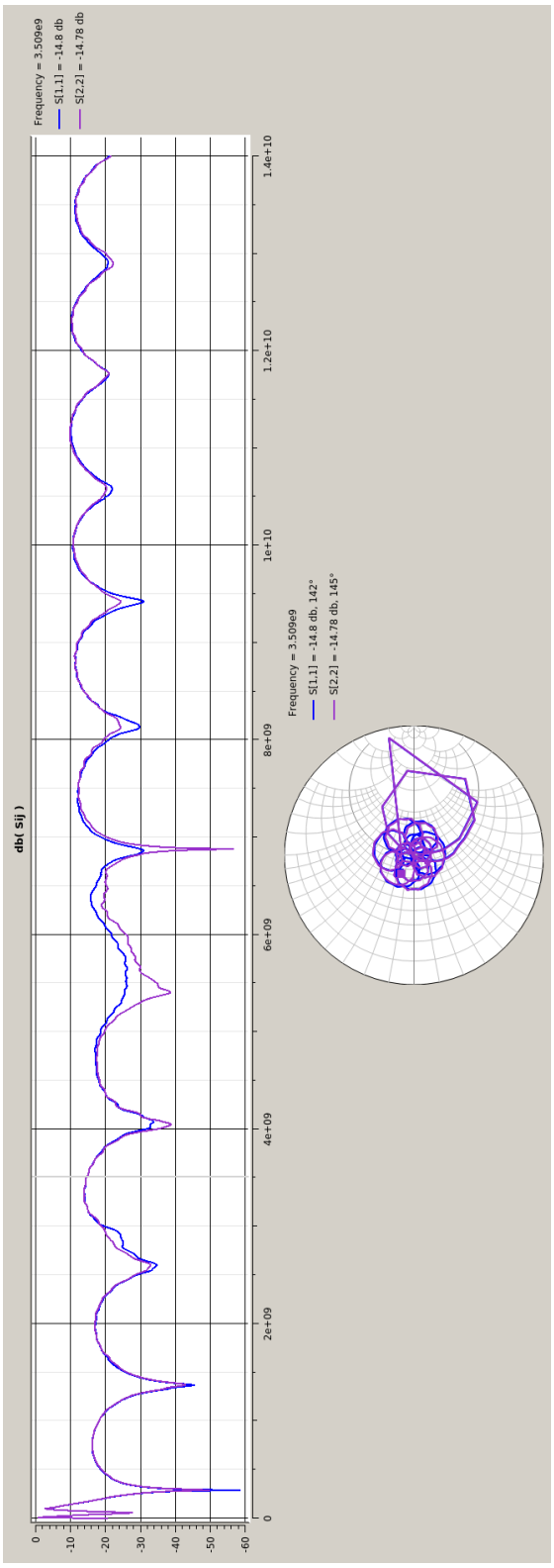

Figure B.6: Results of the VNA with 1.28mm's line - test fixture

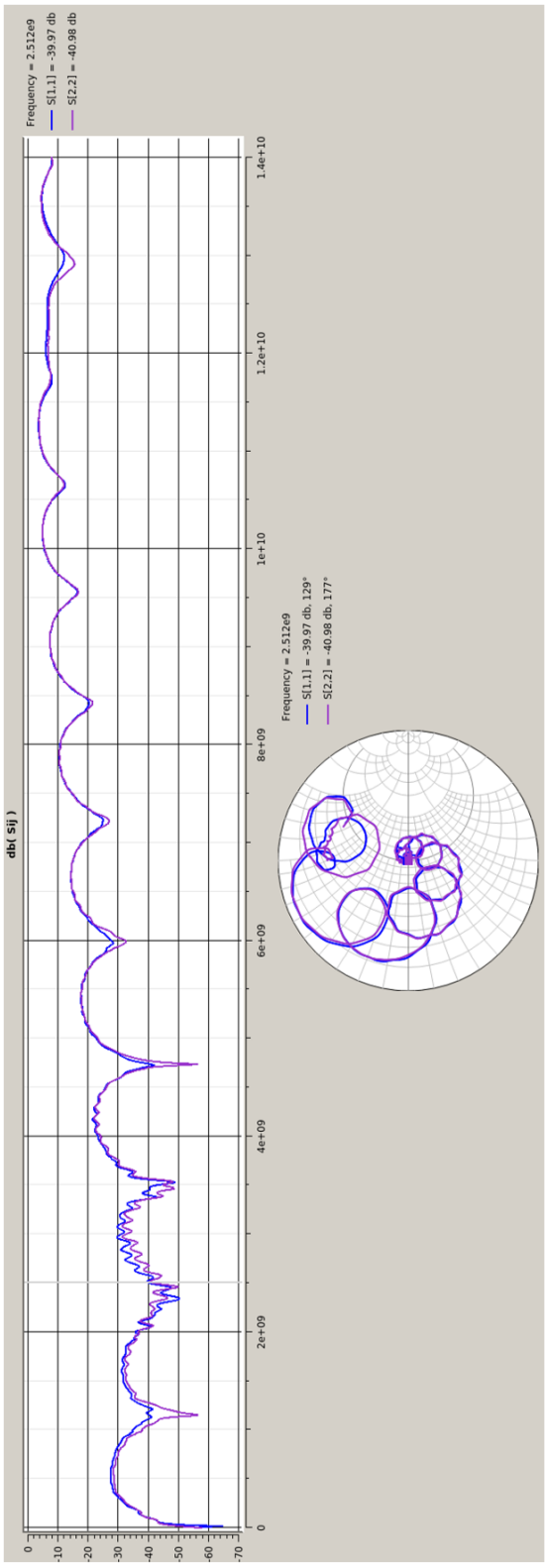

Figure B.7: Results of the VNA with 1.58mm's line

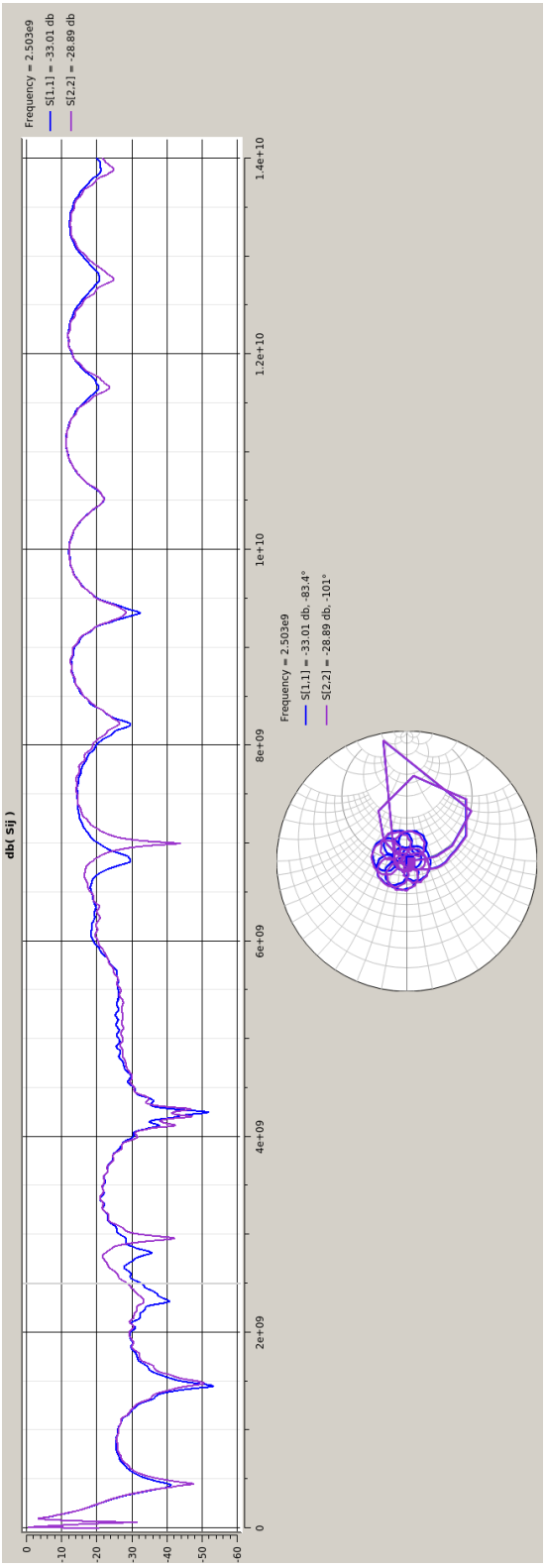

Figure B.8: Results of the VNA with 1.58mm's line - test fixture

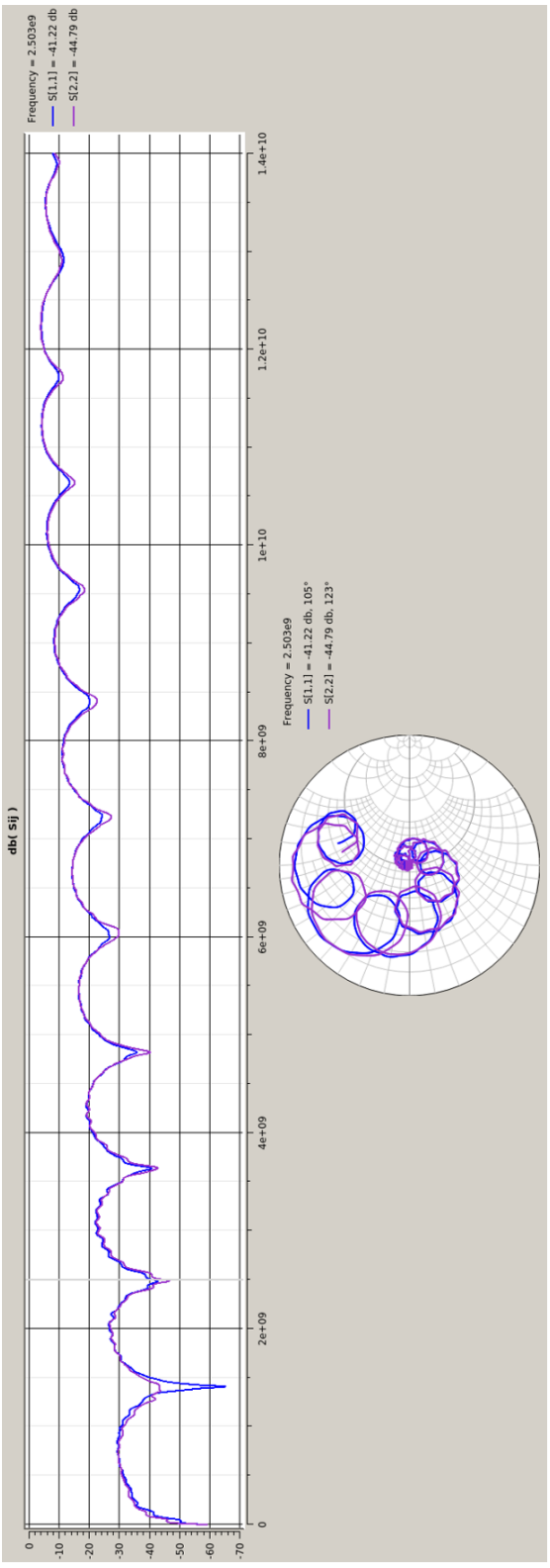

Figure B.9: Results of the VNA with 1.78mm's line

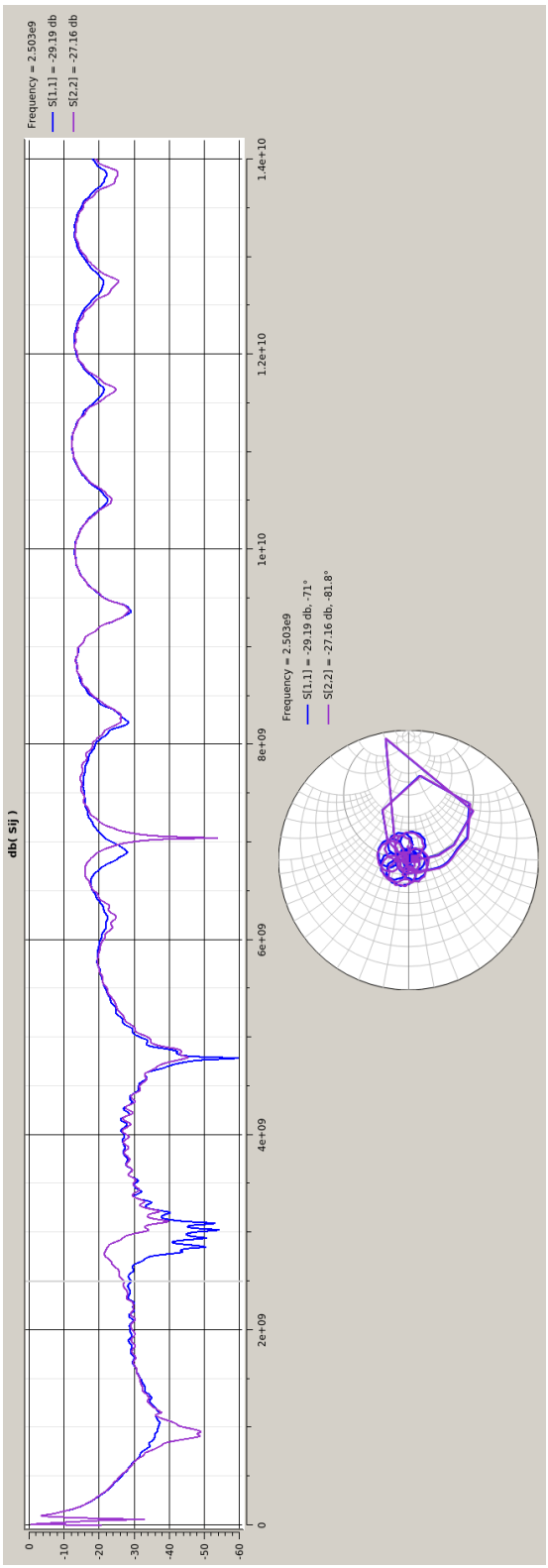

Figure B.10: Results of the VNA with 1.78mm's line - test fixture

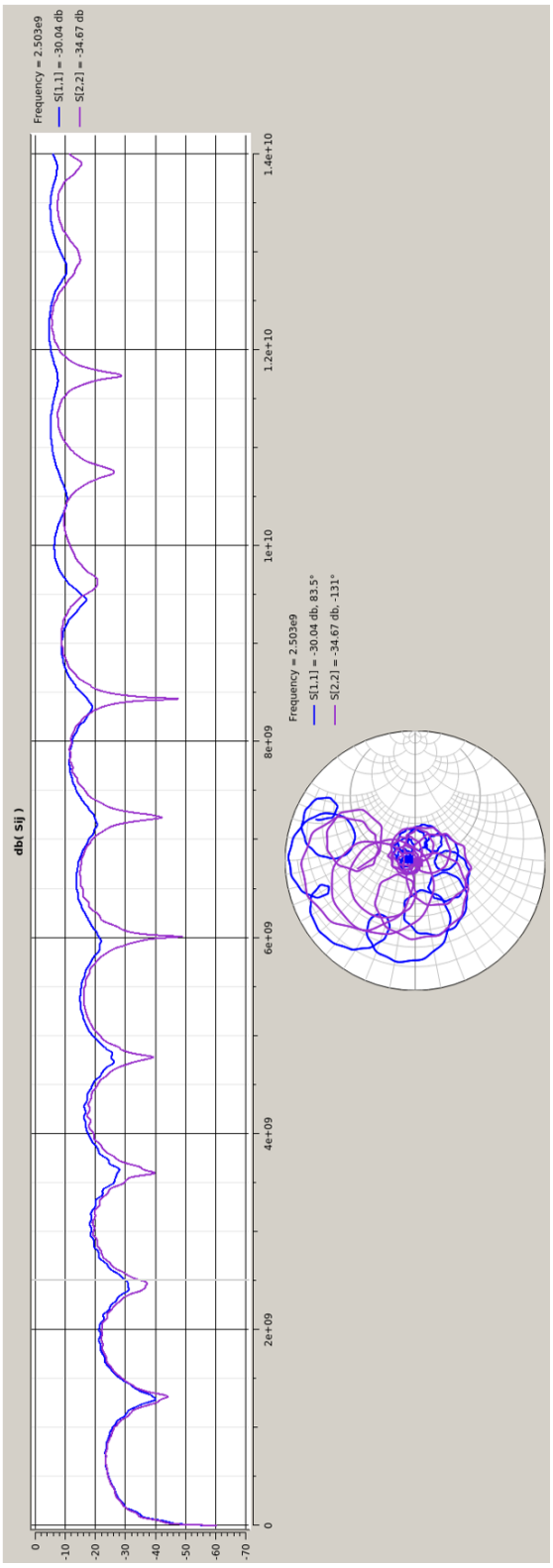

Figure B.11: Results of the VNA with 1.88mm's line

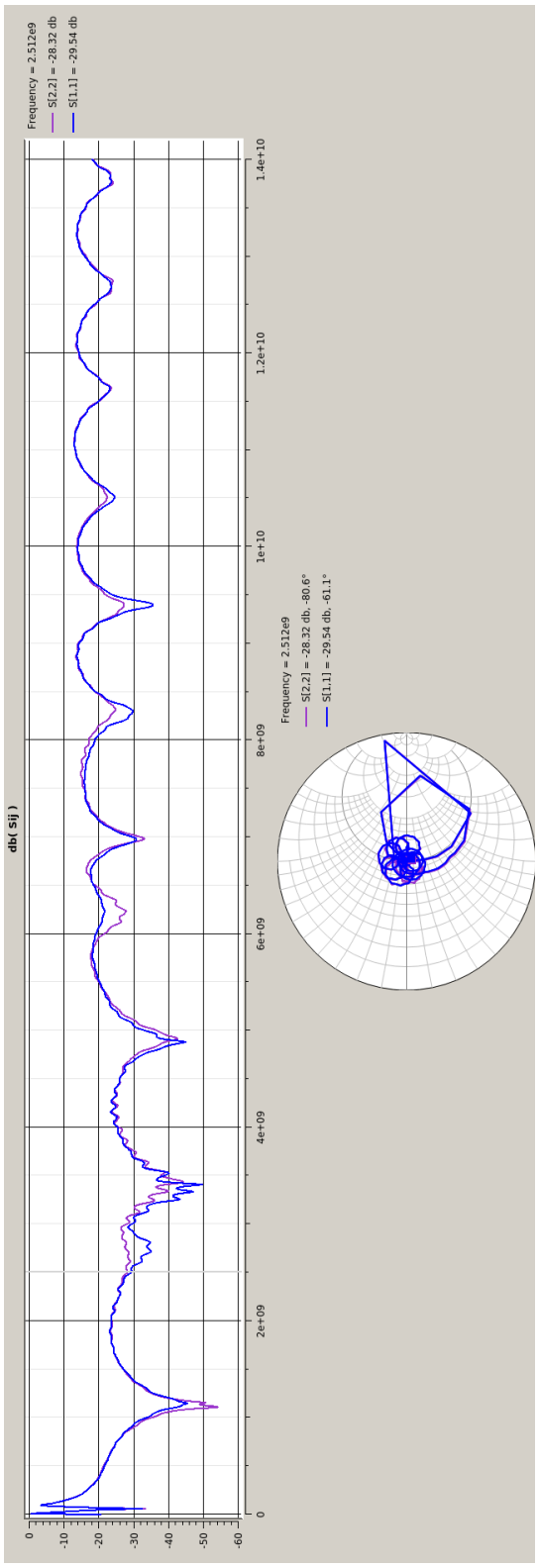

Figure B.12: Results of the VNA with 1.88mm's line - test fixture

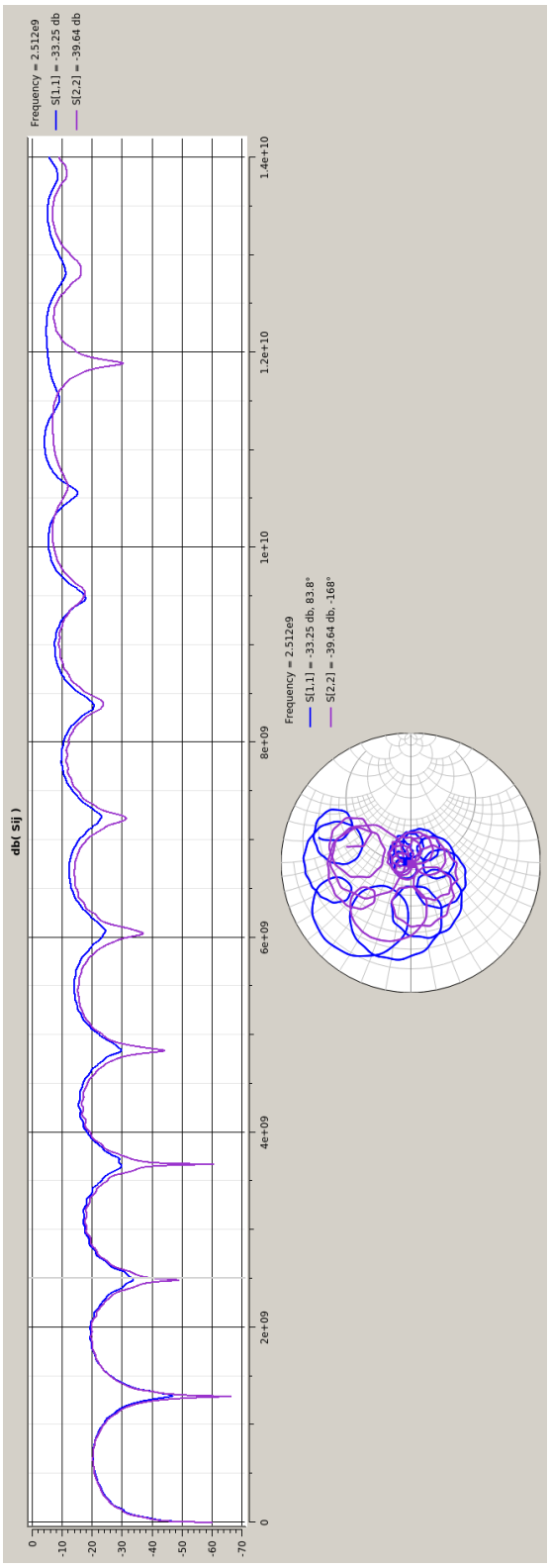

Figure B.13: Results of the VNA with 1.98mm's line

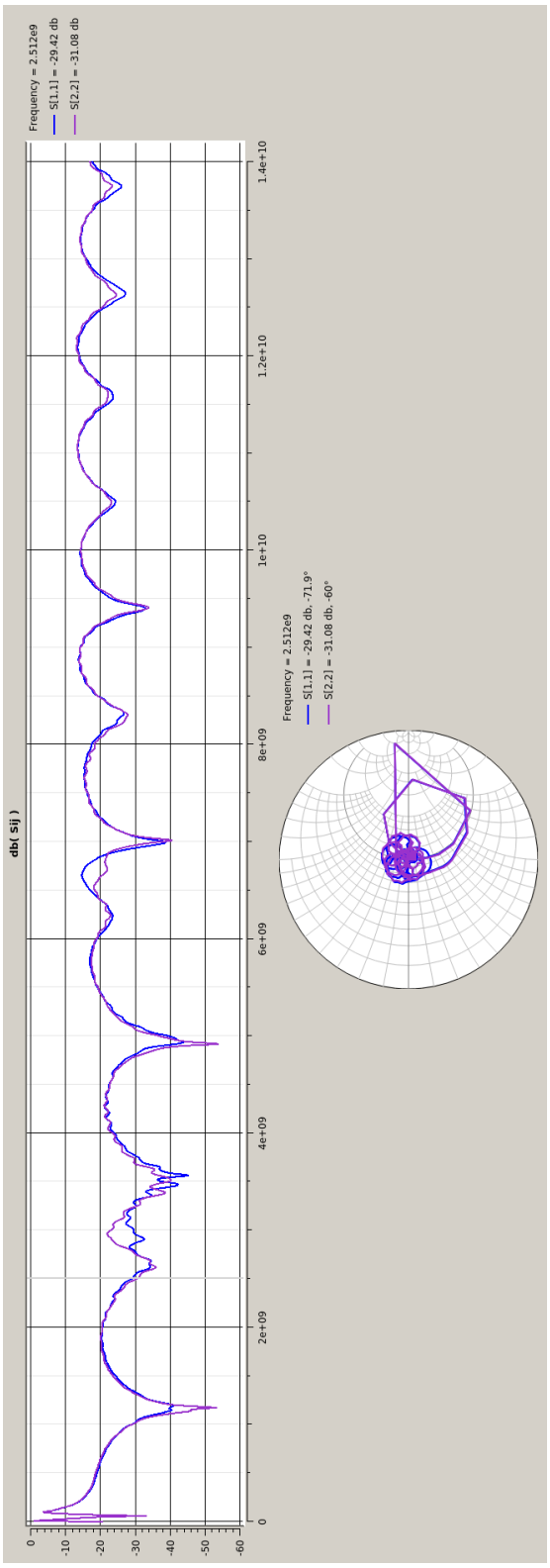

Figure B.14: Results of the VNA with 1.98mm's line - test fixture

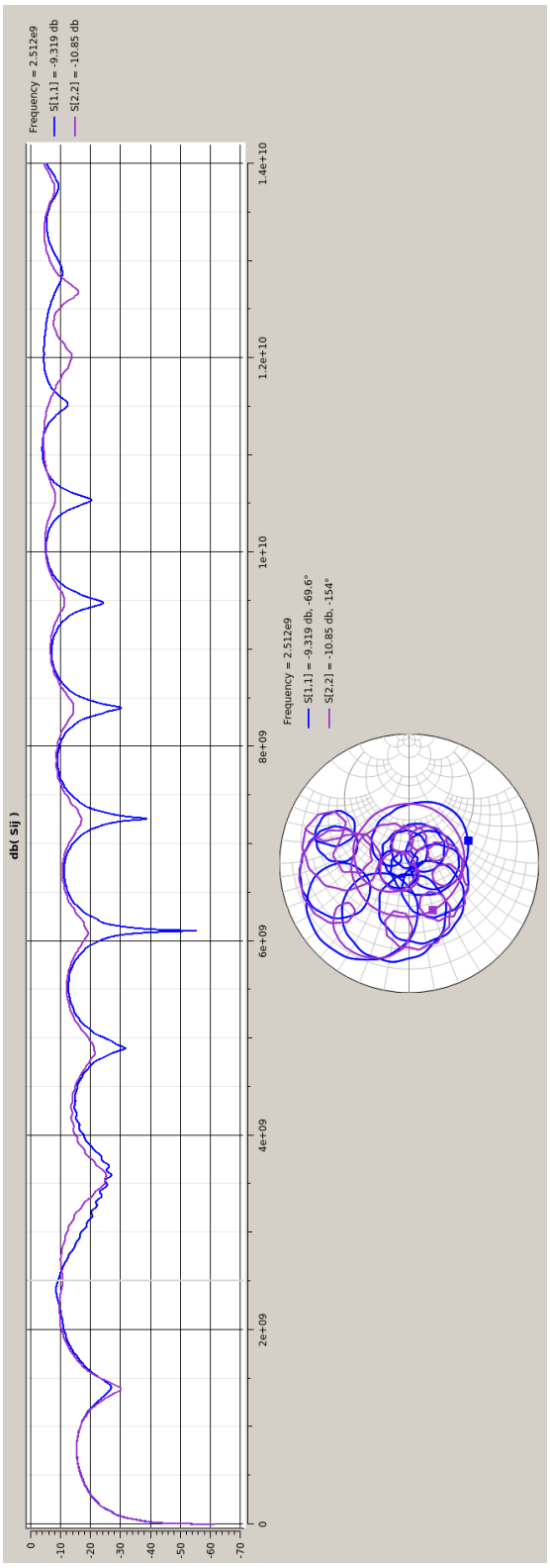

Figure B.15: Results of the VNA with 2.18mm's line

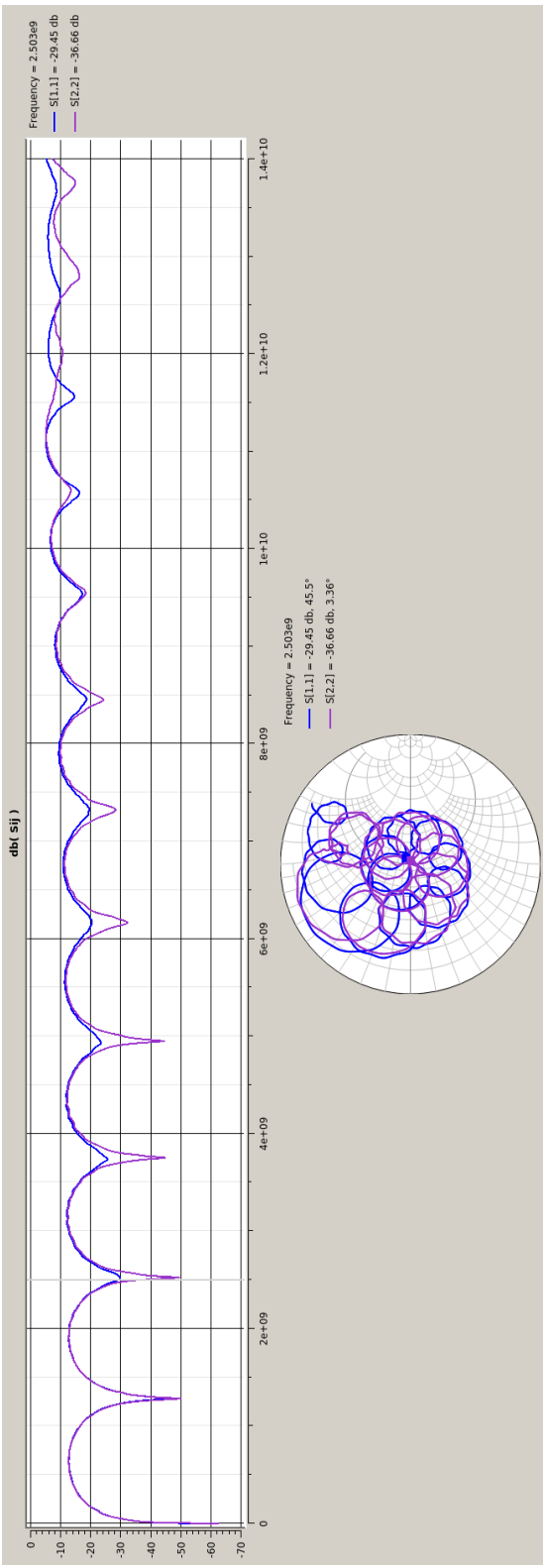

Figure B.16: Results of the VNA with 2.48mm's line

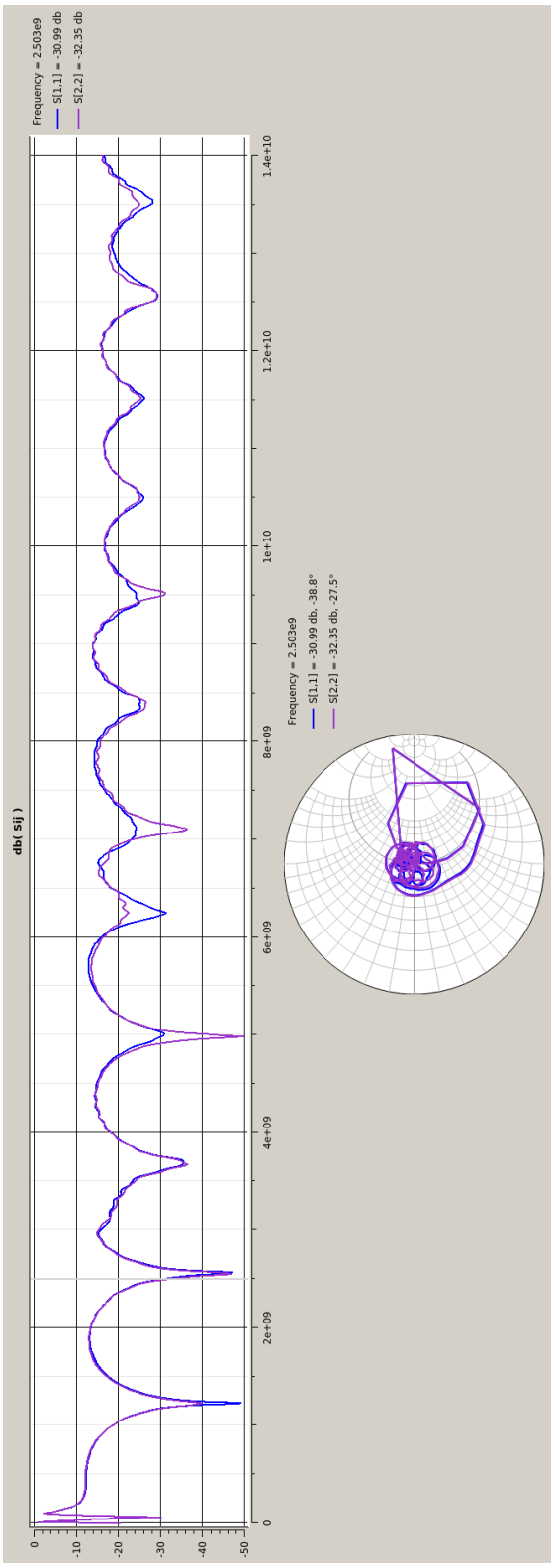

Figure B.17: Results of the VNA with 2.48mm's line - test fixture

B.2 Graphs of input reflection coefficient - experimental data

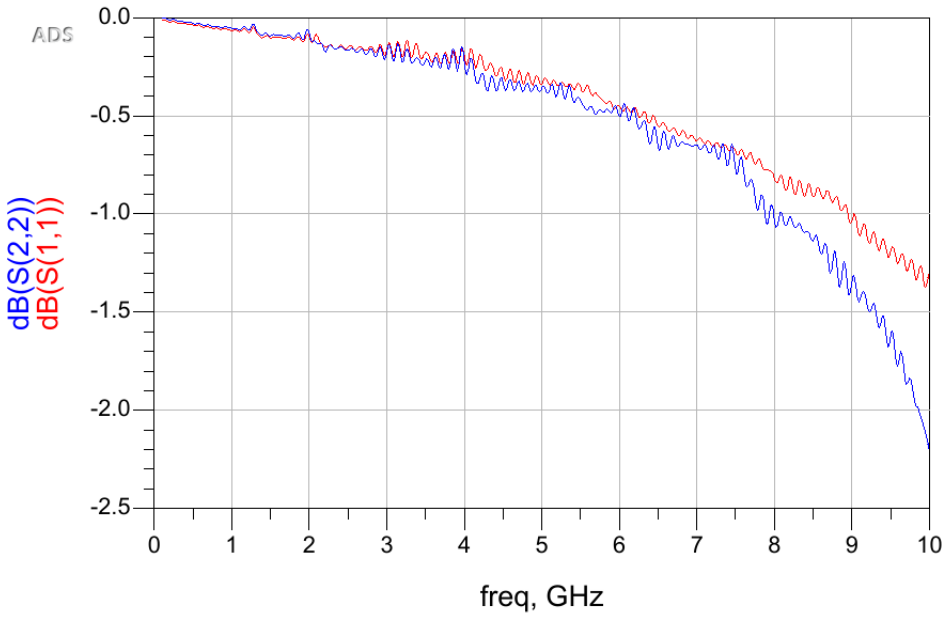

Figure B.18: S11 S22 graphs from experiment for adaptation analyse - 1.28mm (wrong data)

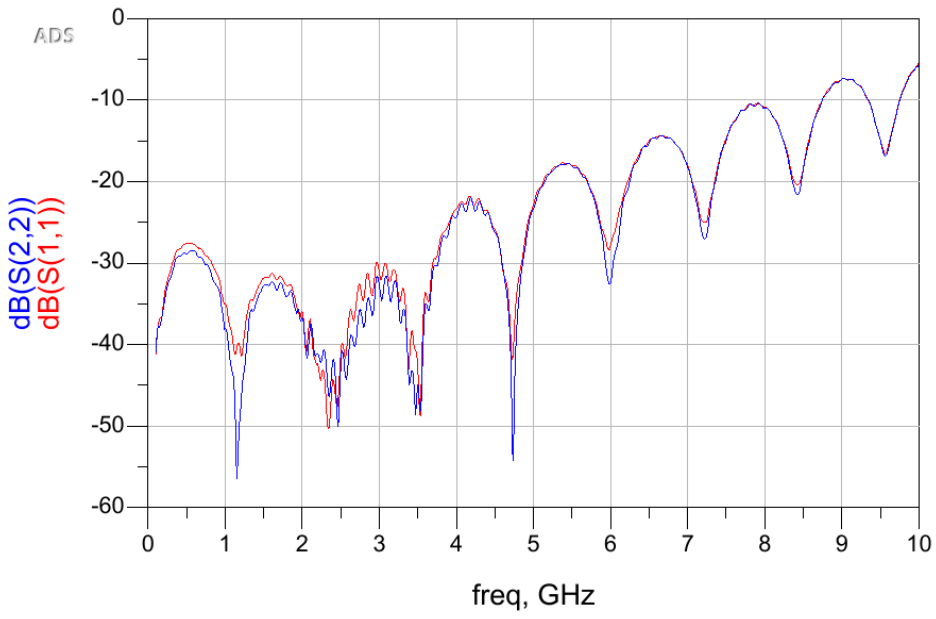

Figure B.19: S11 S22 graphs from experiment for adaptation analyse - 1.58mm

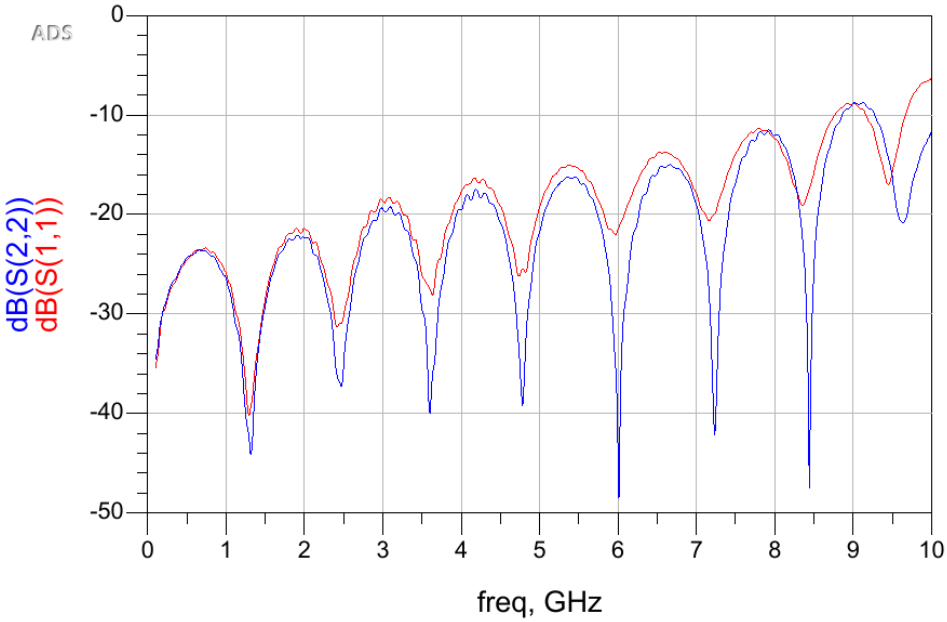

Figure B.20: S11 S22 graphs from experiment for adaptation analyse - 1.88mm

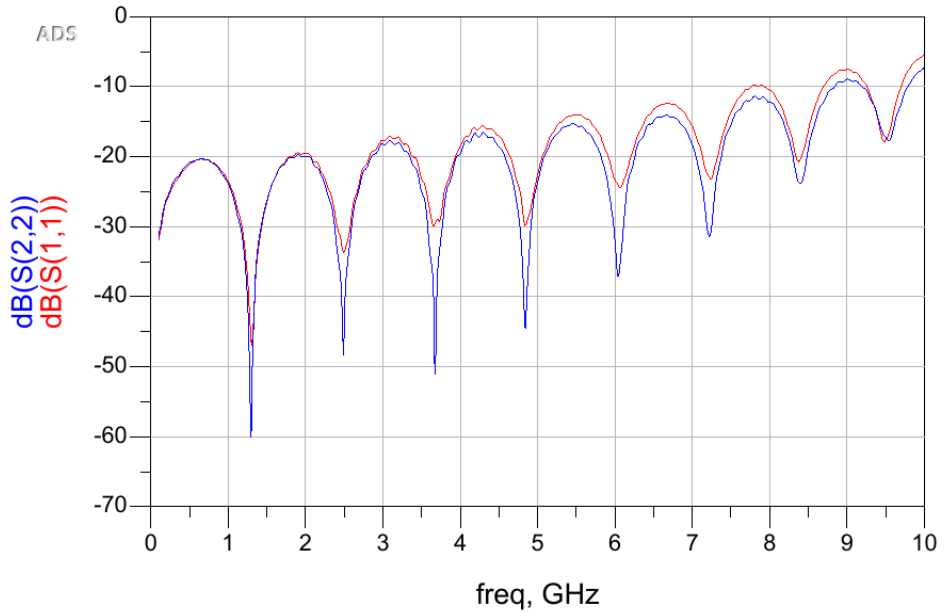

Figure B.21: S11 S22 graphs from experiment for adaptation analyse - 1.98mm

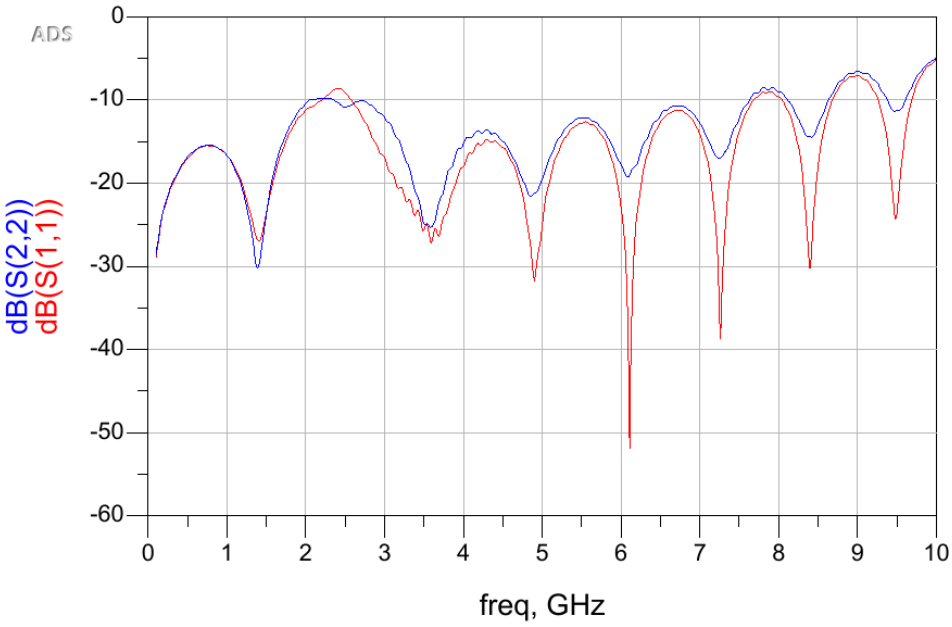

Figure B.22: S11 S22 graphs from experiment for adaptation analyse - 2.18mm

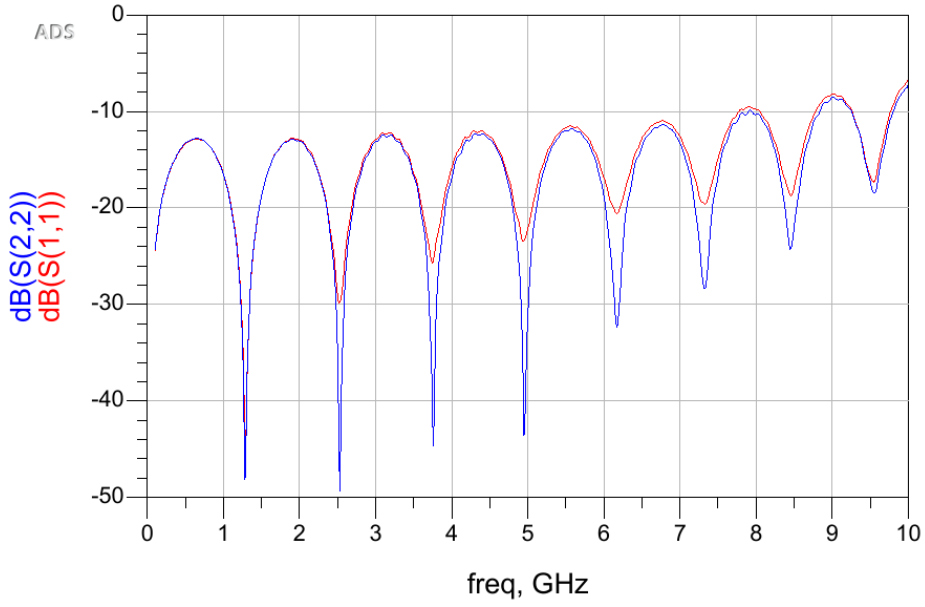

Figure B.23: S11 S22 graphs from experiment for adaptation analyse - 2.48mm

Appendix C- SMA tests

C.1 Graphs of input reflection coefficient - comparison

Figure C.1 has the incorrect data as referred in the throughout of this work, consequently the MLIN line placed in the remaining figures of this chapter, was not inserted.

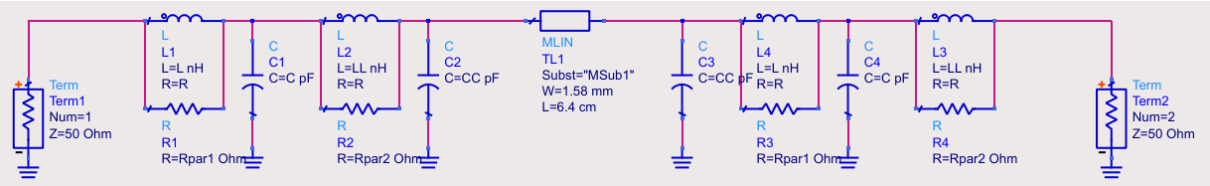

Figure C.1: SMA model to test MLIN

In the figures of this chapter, lines _ exp (black and green lines) is related to the values obtained experimentally, micro (blue and red line) is the Figure C.1, with MLIN's width value altered of each Figure. The pink line is the behaviour or the ADS' MLIN line for the respective widths. Figure C.1 missing values are represented in Figure 7.26.

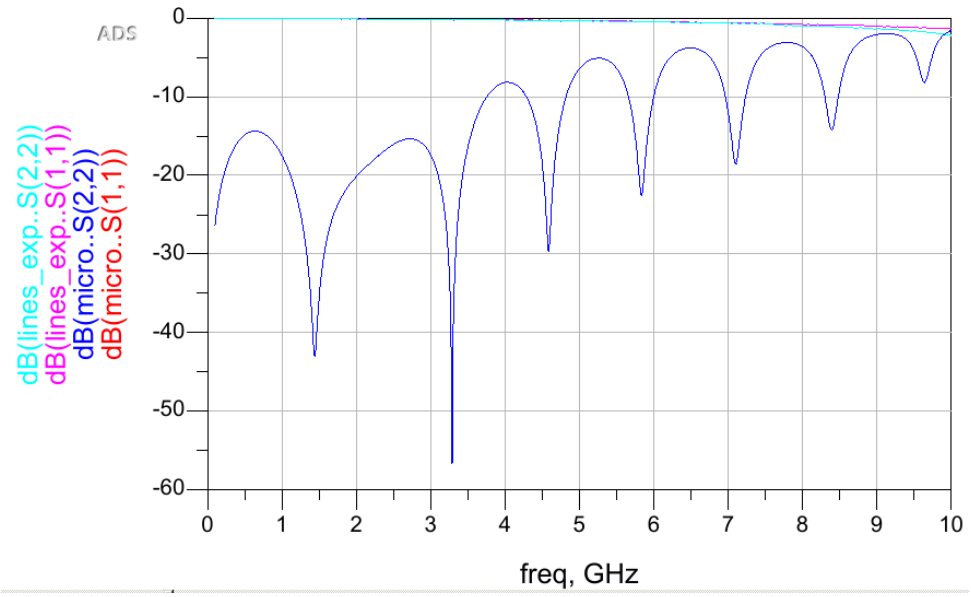

Figure C.2: SMA model applied to MLIN of 1.28mm

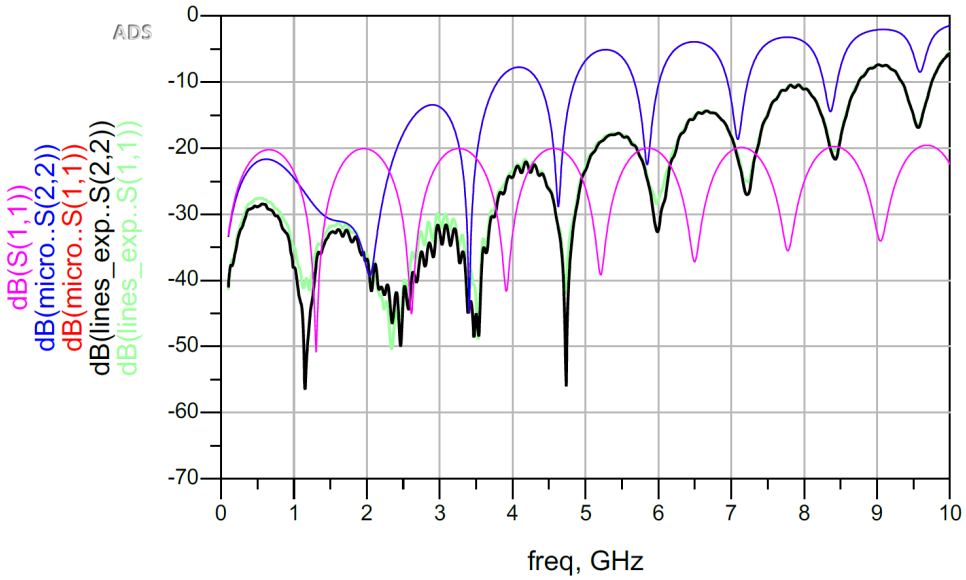

Figure C.3: SMA model applied to MLIN of 1.58mm

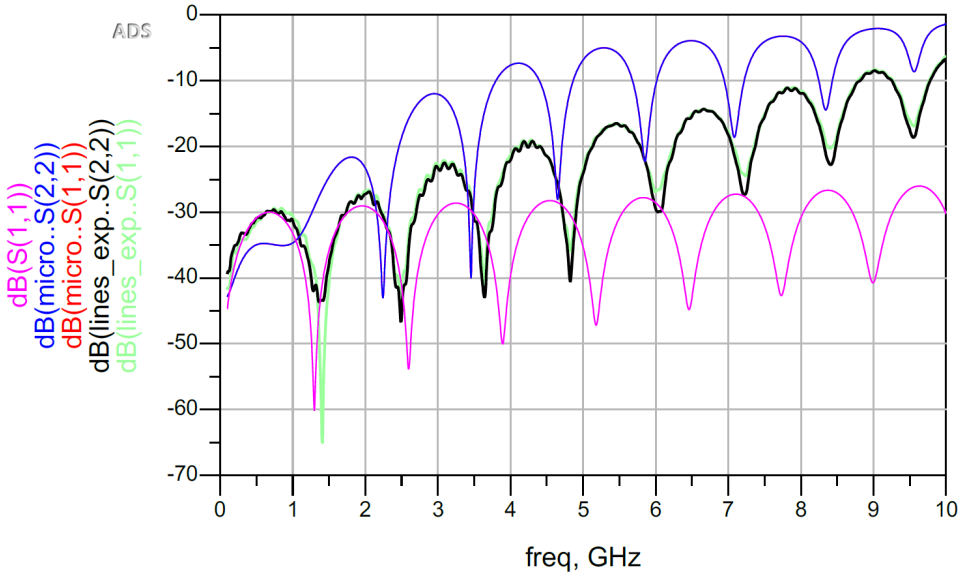

Figure C.4: SMA model applied to MLIN of 1.78mm

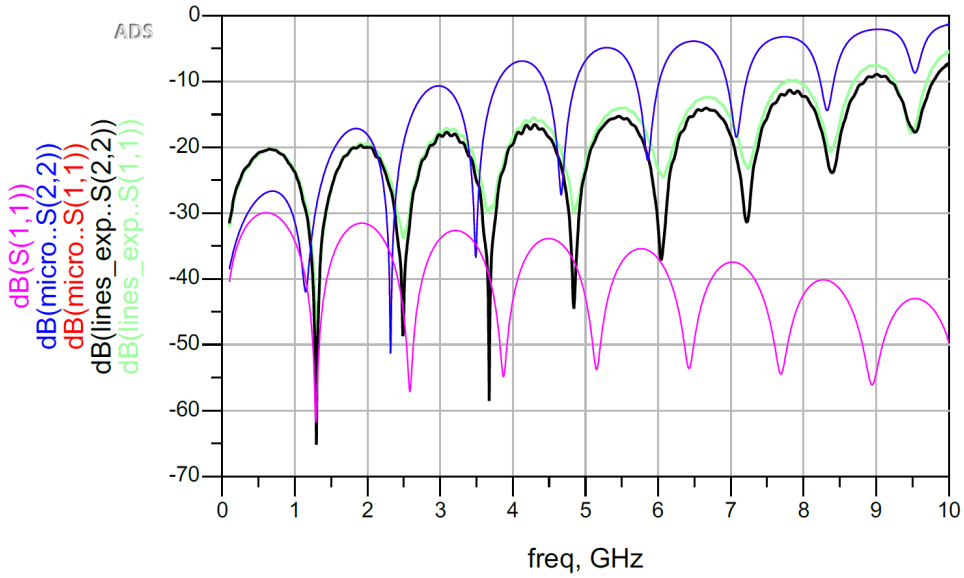

Figure C.5: SMA model applied to MLIN of 1.98mm

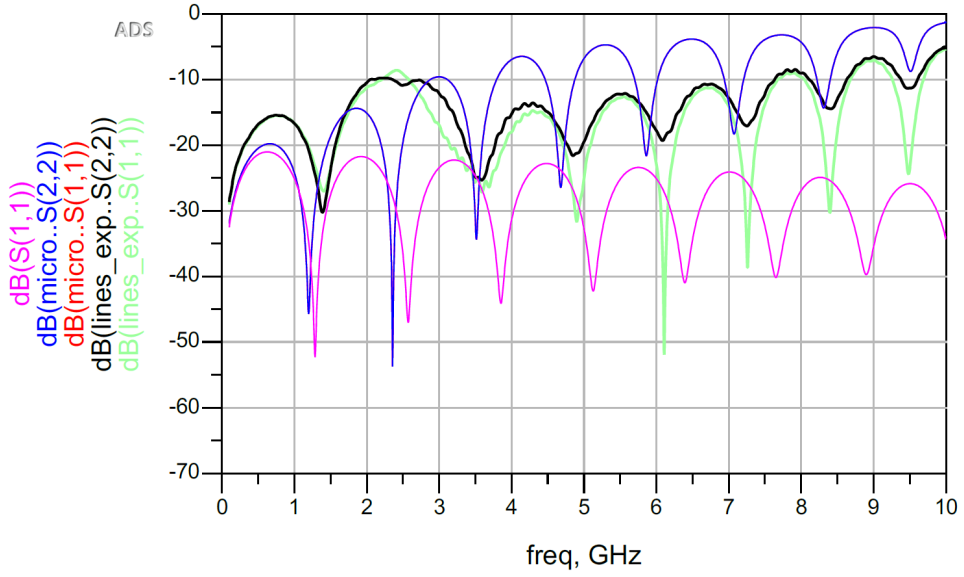

Figure C.6: SMA model applied to MLIN of 2.18mm

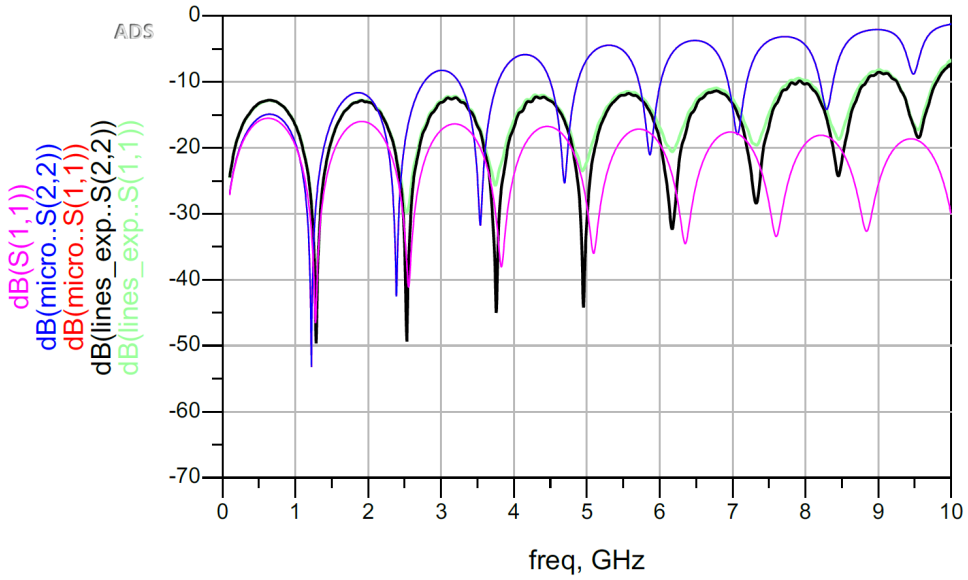

Figure C.7: SMA model applied to MLIN of 2.48mm

C.2 Graphs of insertion loss

In this section, pink line is the behaviour of a simple line with the respective widths, blue line is the experimental results and red line is the results of the model applied.

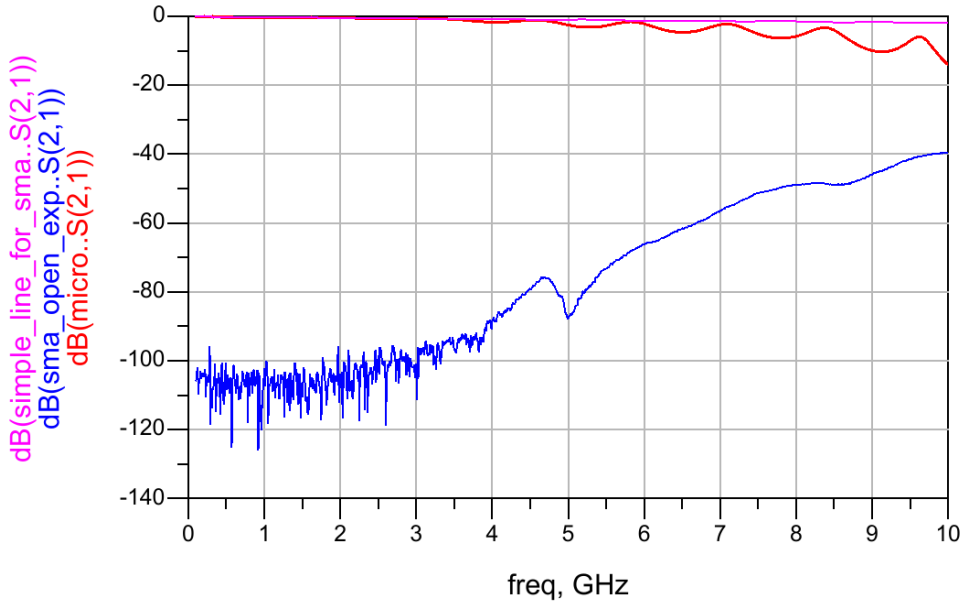

Figure C.8: SMA model applied to MLIN of 1.28mm - Insertion loss

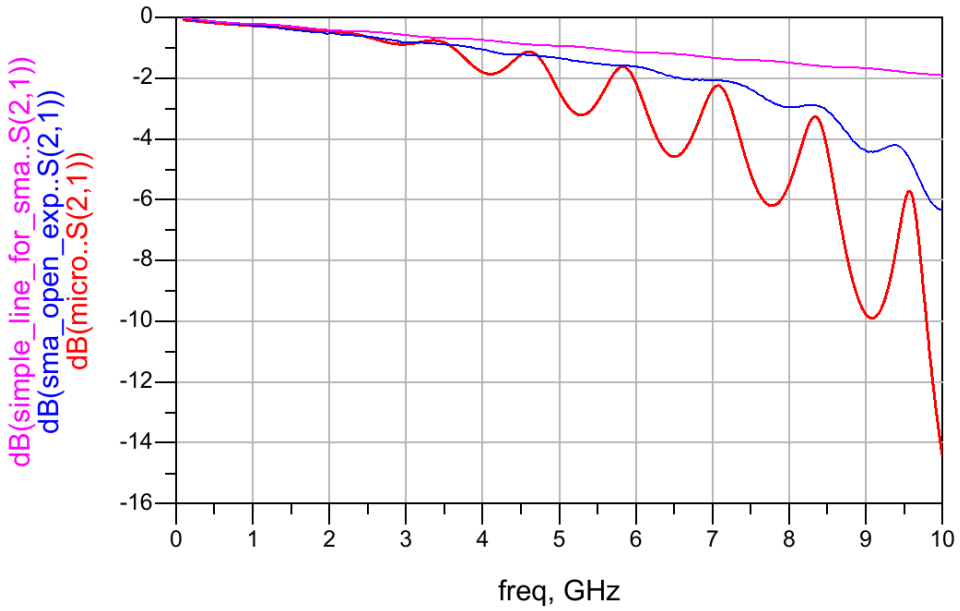

Figure C.9: SMA model applied to MLIN of 1.58mm - Insertion loss

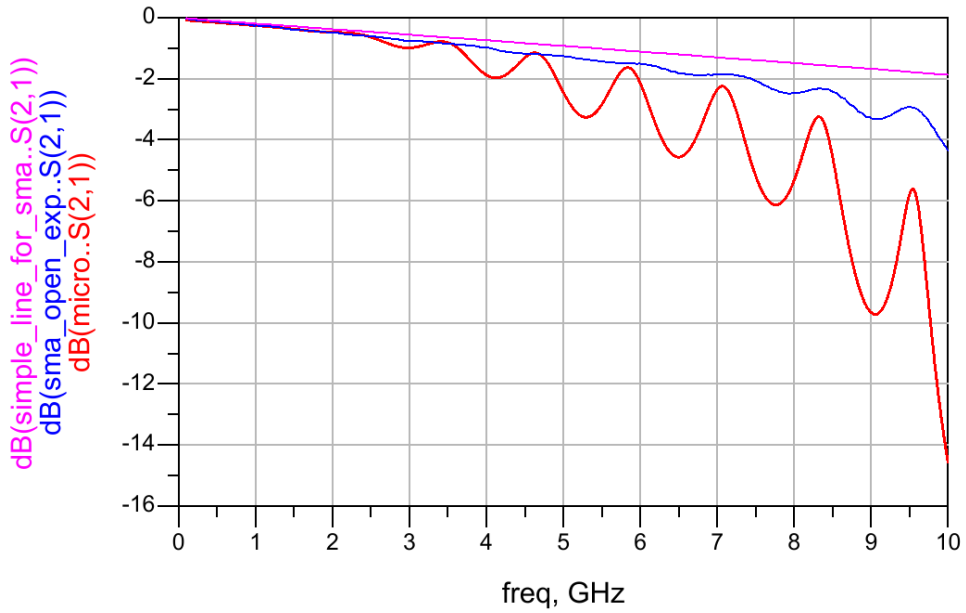

Figure C.10: SMA model applied to MLIN of 1.78mm - Insertion loss

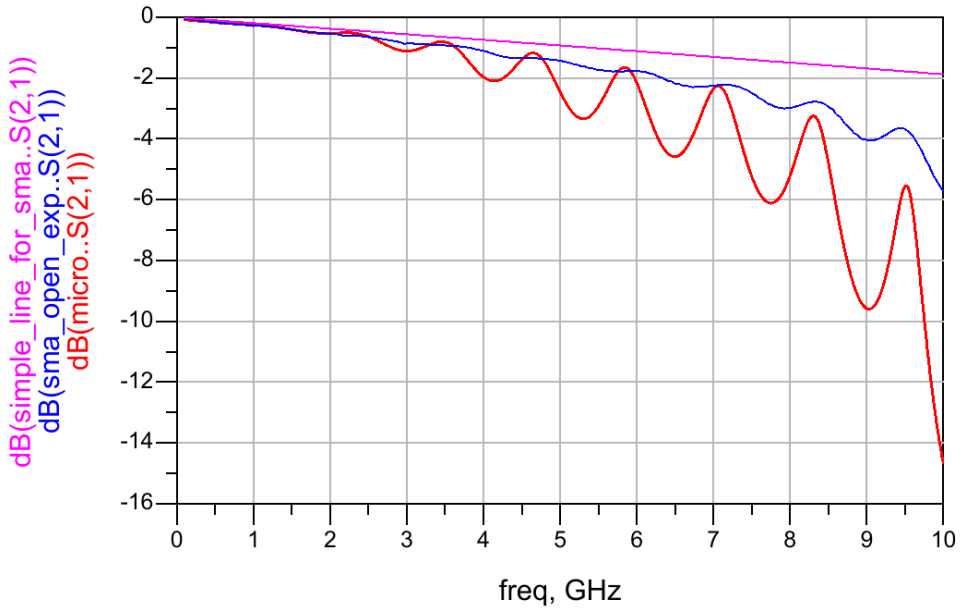

Figure C.11: SMA model applied to MLIN of 1.98mm - Insertion loss

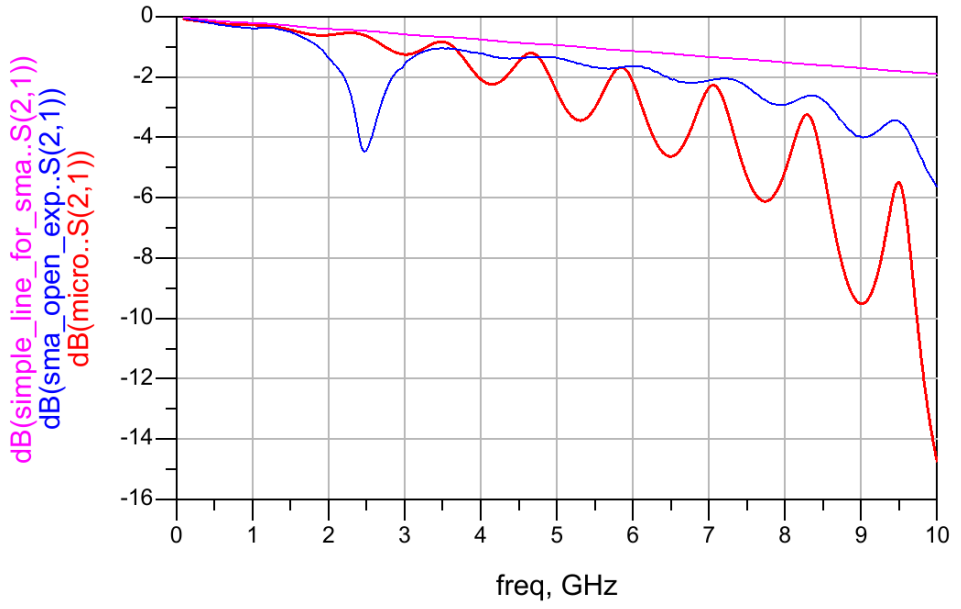

Figure C.12: SMA model applied to MLIN of 2.18mm - Insertion loss

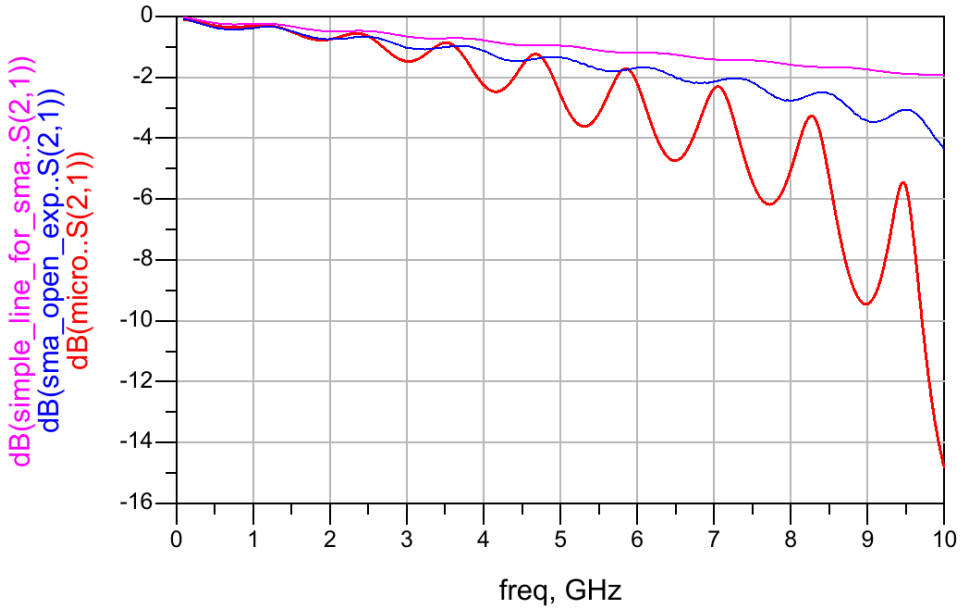

Figure C.13: SMA model applied to MLIN of 2.48mm - Insertion loss

C.3 Schematic's, of Figure 7.32, results for SMA test and verification

In the figures of this chapter, "lines_exp" (black and pink lines) is related to the values obtained experimentally and "Deemb_SMA" (blue and red lines) is referred to schematic from Figure 7.32.

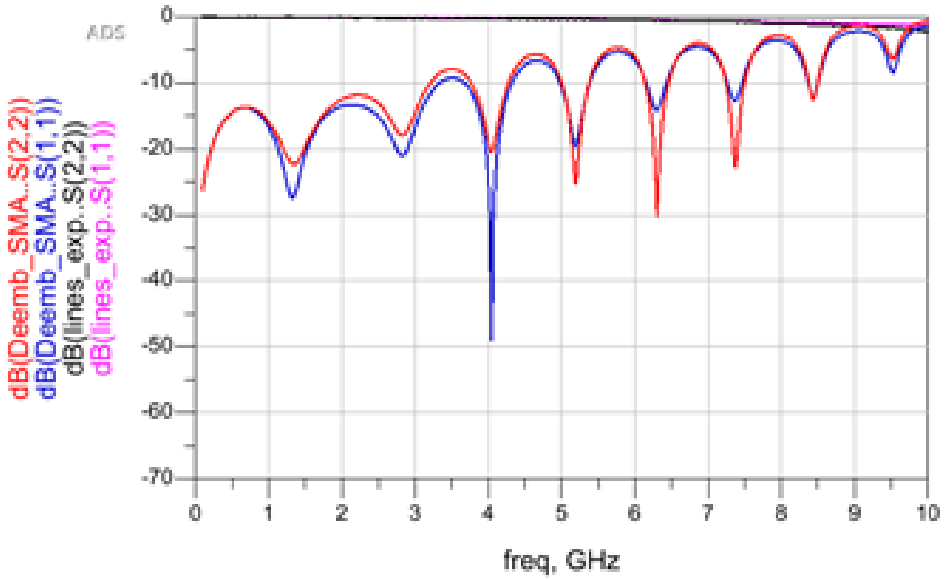

Figure C.14: SMA's model verification - 1.28mm

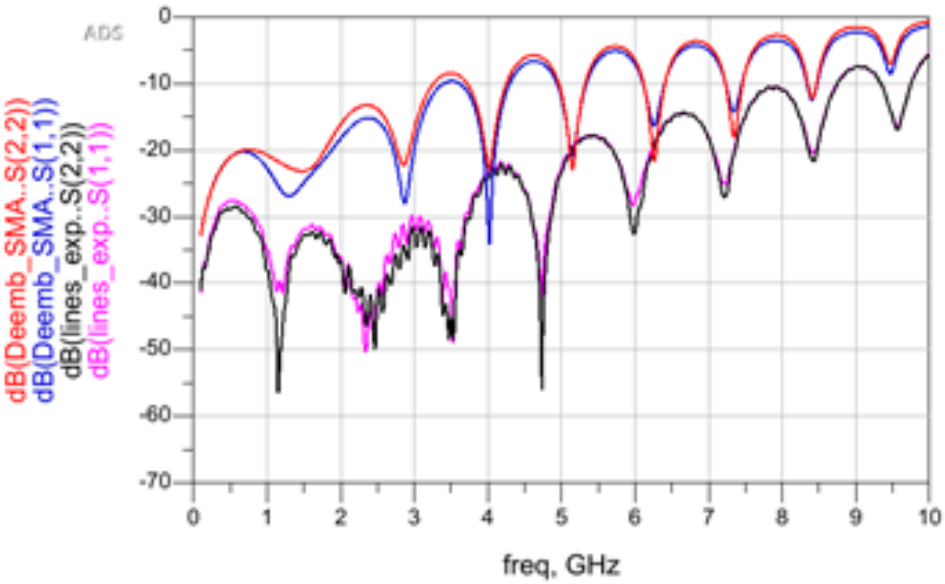

Figure C.15: SMA's model verification - 1.58mm

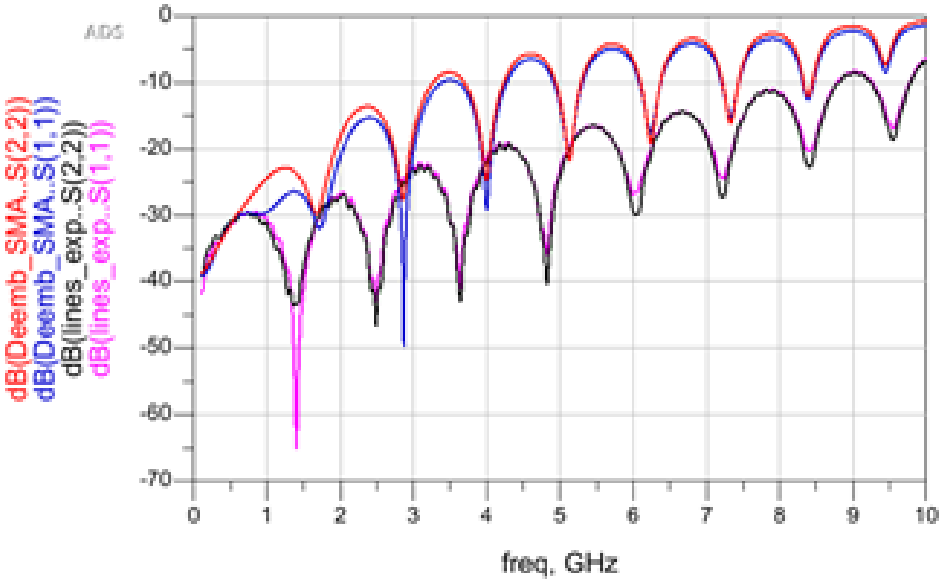

Figure C.16: SMA's model verification - 1.78mm

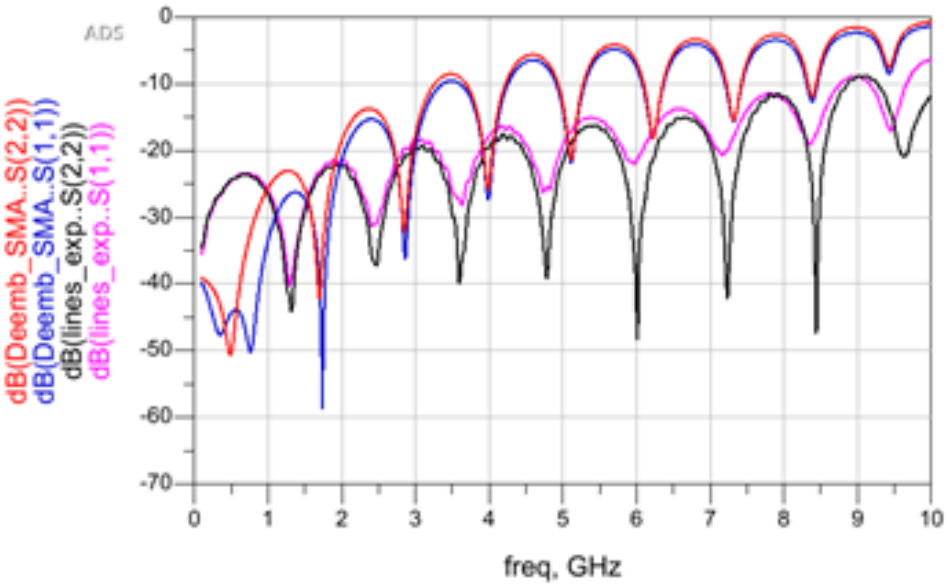

Figure C.17: SMA's model verification - 1.88mm

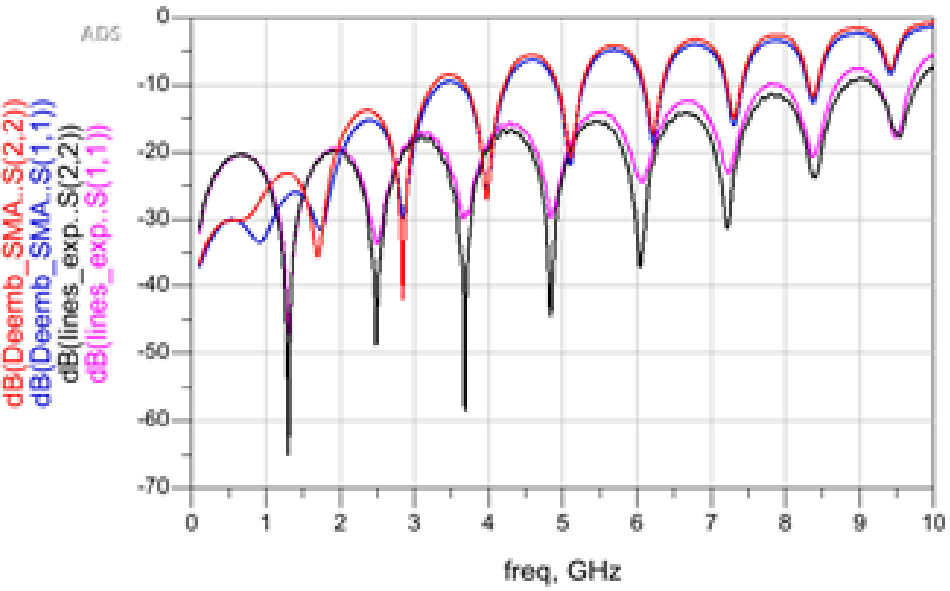

Figure C.18: SMA's model verification - 1.98mm

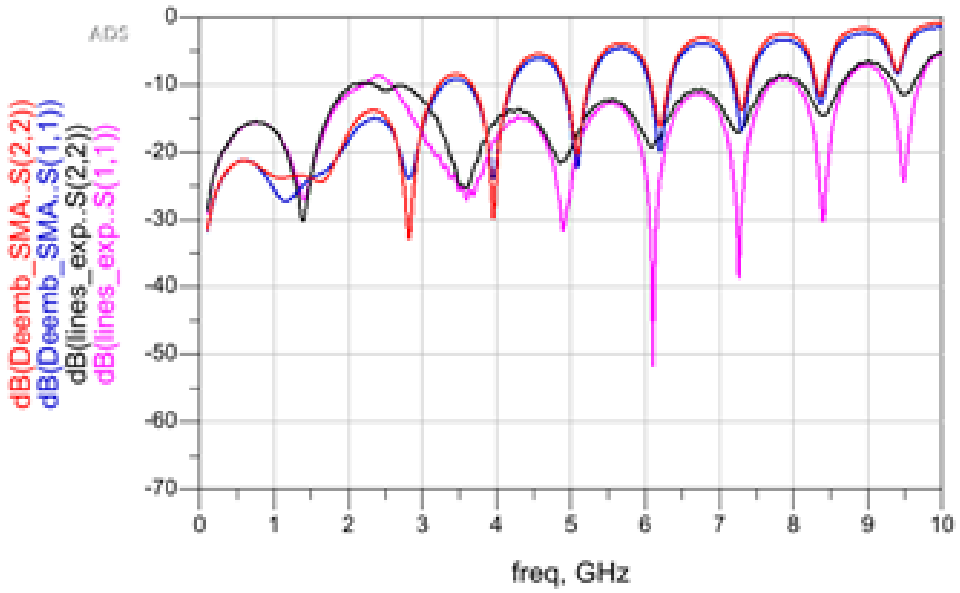

Figure C.19: SMA's model verification - 2.18mm

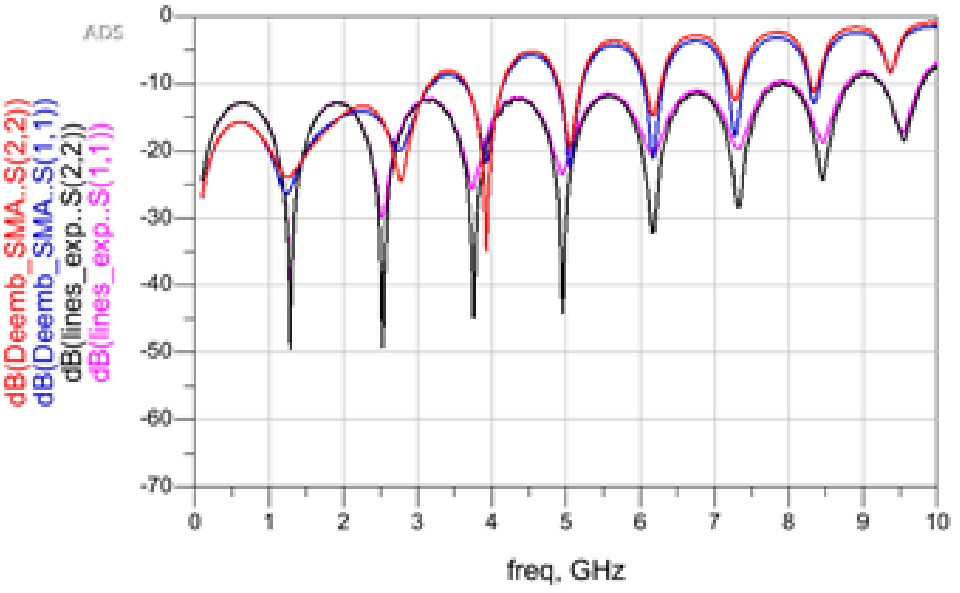

Figure C.20: SMA's model verification - 2.48mm

Appendix D- Test Fixture tests

D.1 Input reflection coefficient - results' comparison from VNA and ADS with applied model

In the figures of this section, the blue line corresponds to the experimental data and the red line to the model applied.

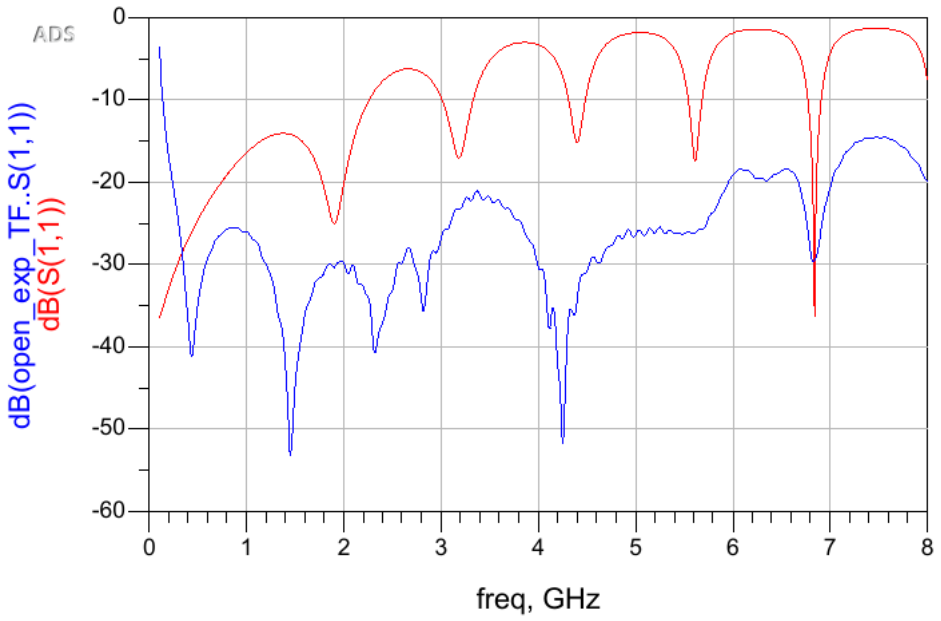

Figure D.1: TF model applied to MLIN of 1.58mm

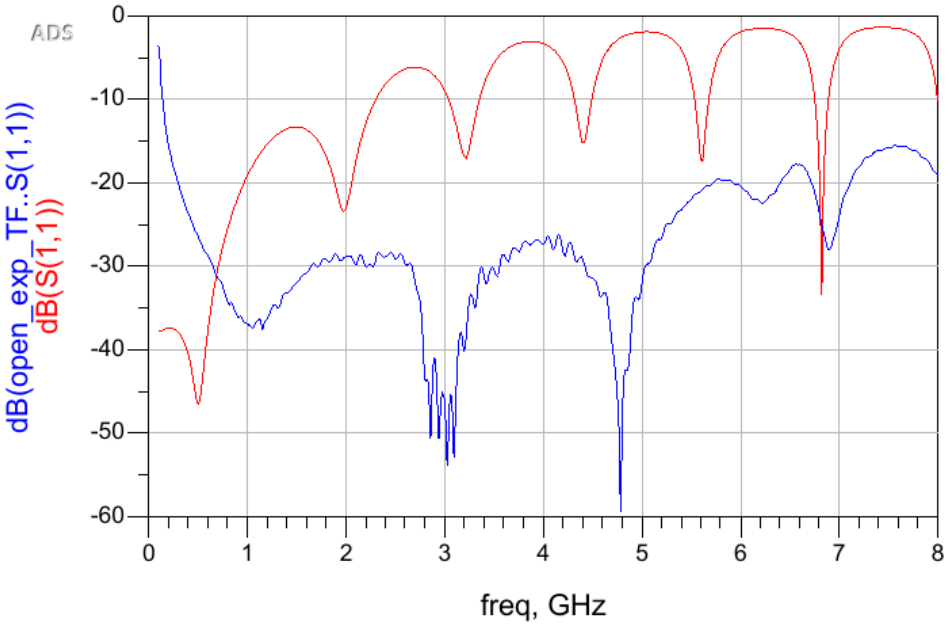

Figure D.2: TF model applied to MLIN of 1.78mm

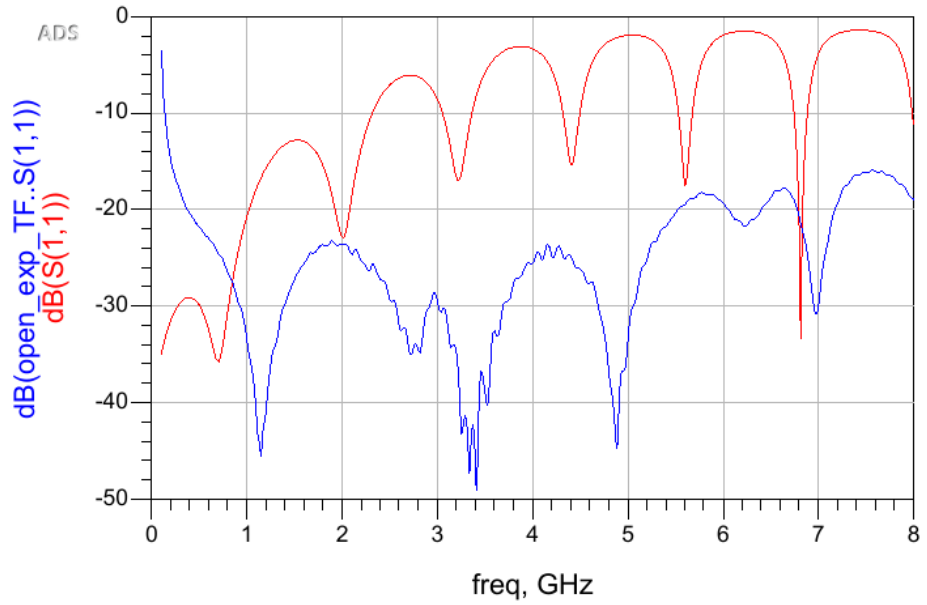

Figure D.3: TF model applied to MLIN of 1.88mm

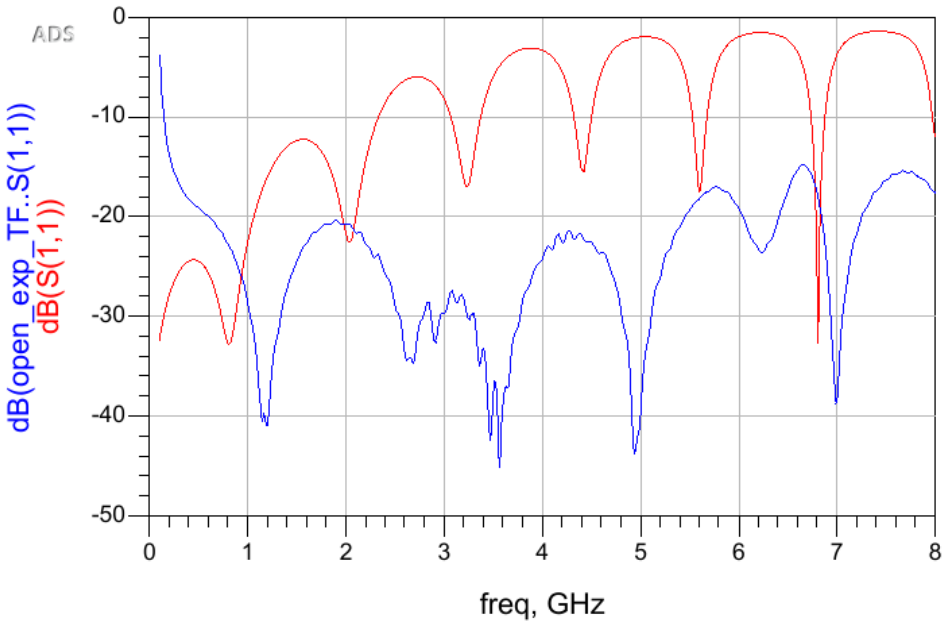

Figure D.4: TF model applied to MLIN of 1.98mm

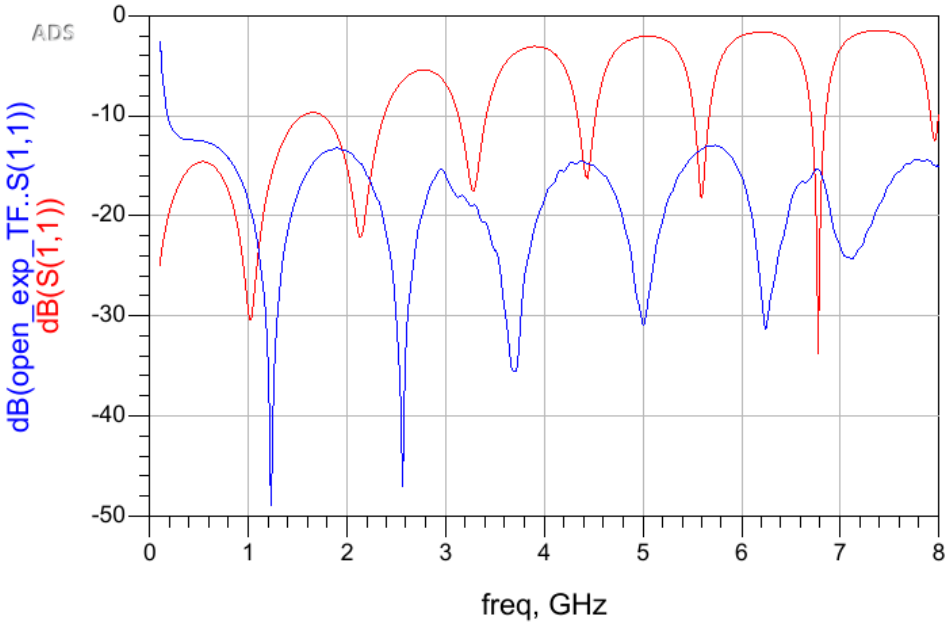

Figure D.5: TF model applied to MLIN of 2.48mm

D.2 Insertion loss results acquired directly from VNA

In this section are presented the results obtained experimentally.

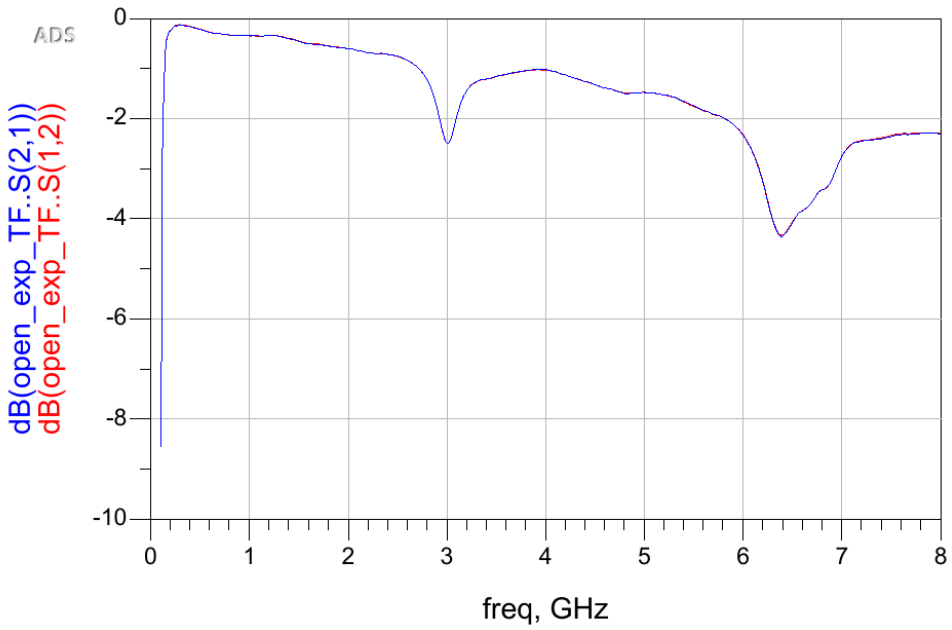

Figure D.6: S_{12} and $S_{21} from$VNA with transmission line's width of 1.28mm

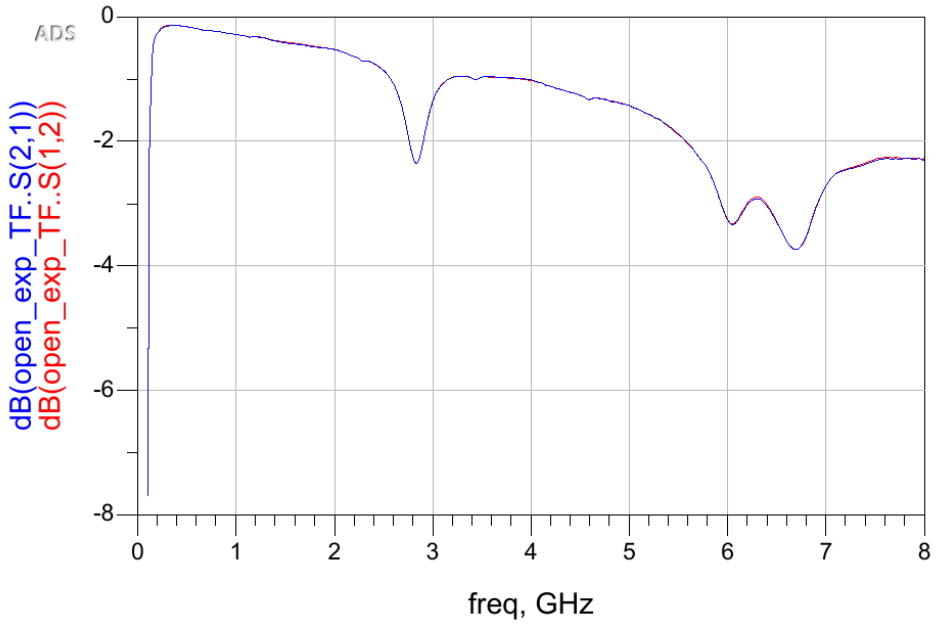

Figure D.7: S_{12} and $S_{21} from$VNA with transmission line's width of 1.58mm

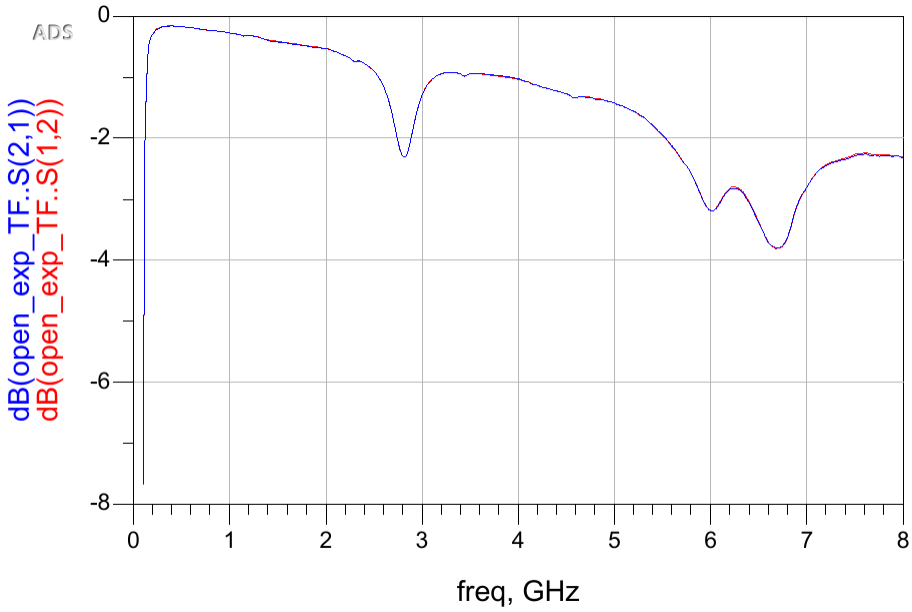

Figure D.8: S_{12} and $S_{21} from$VNA with transmission line's width of 1.78mm

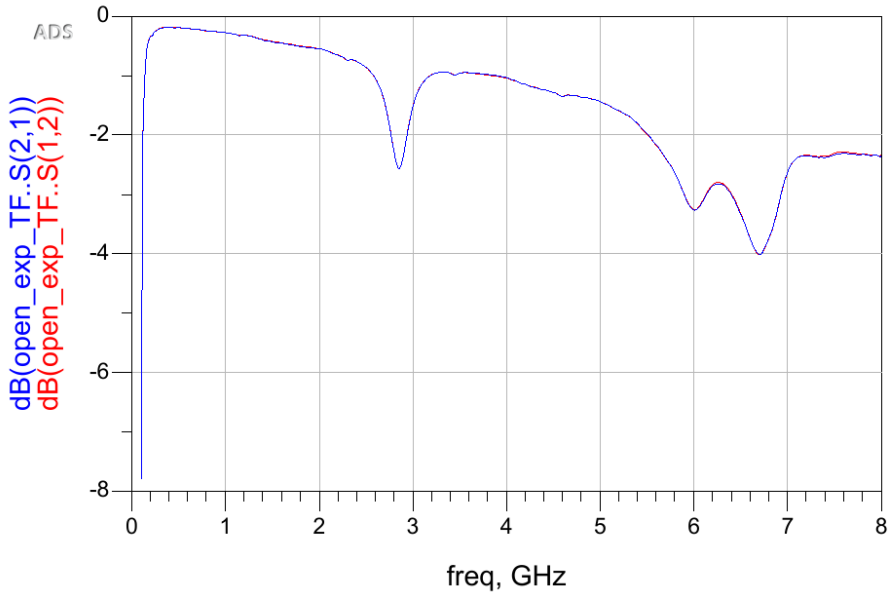

Figure D.9: S_{12} and $S_{21} from$VNA with transmission line's width of 1.88mm

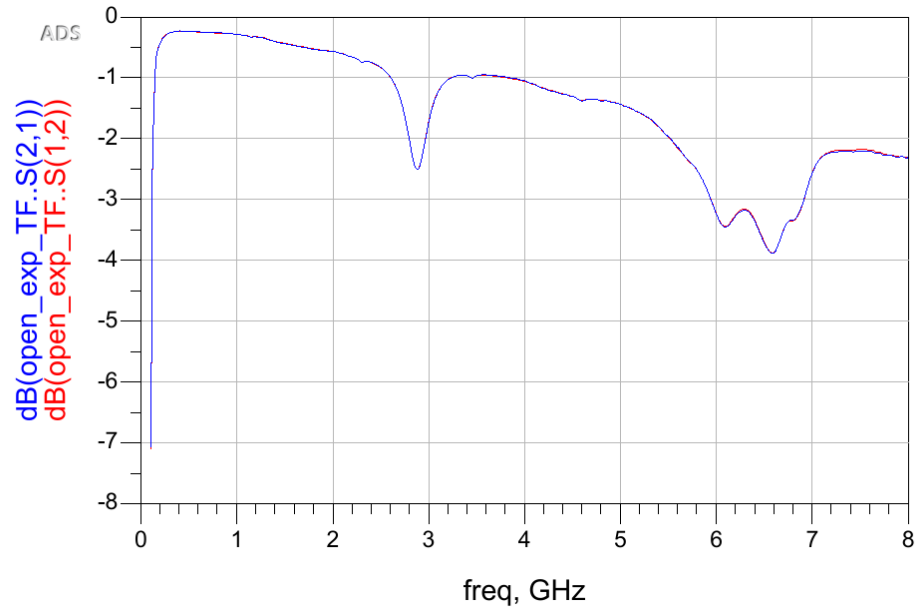

Figure D.10: S_{12} and $S_{21} from$VNA with transmission line's width of 1.98mm

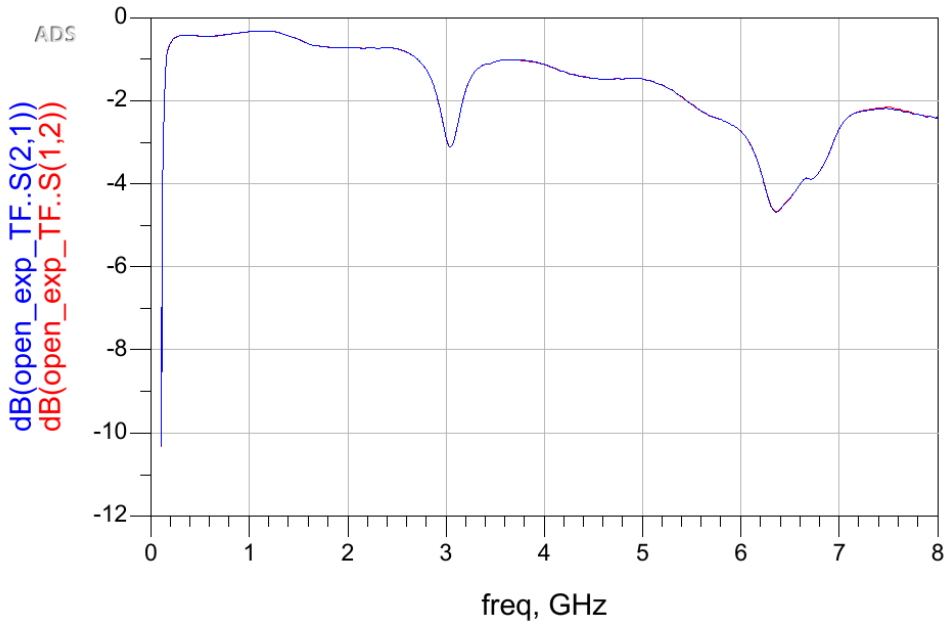

Figure D.11: S_{12} and $S_{21} from$VNA with transmission line's width of 2.48mm

Appendix E- ADS Figures

E.1 S-parameters S11 and S12 in Smith Chart from ADS - frequency sweep

In this section are presented the simulated results of a microstrip line, both insertion loss (in blue) and input reflection coefficient (in red). Considering it is a lossless line in ADS, line of S_{11} is the same as S_{22} and S_{12} the same as S_{21}.

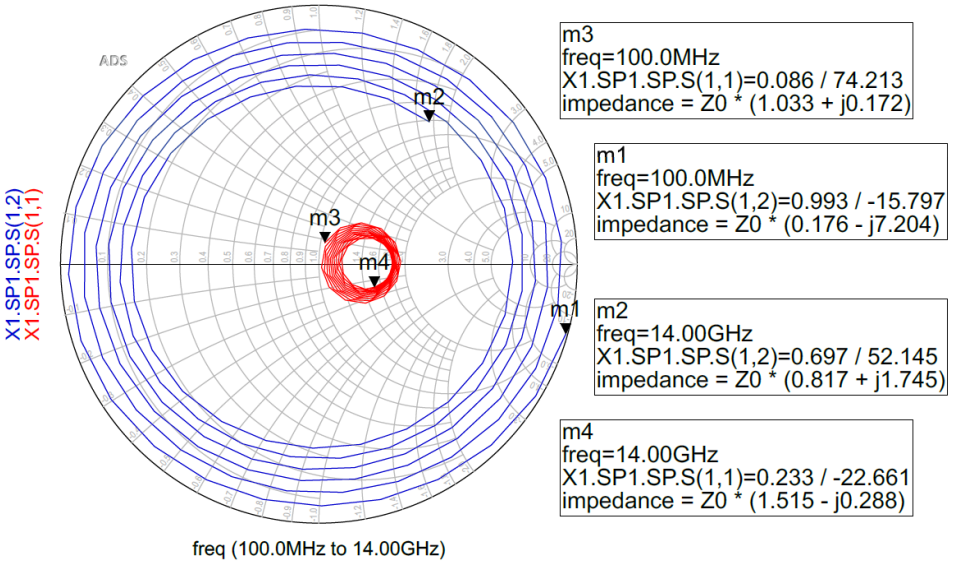

Figure E.1: S-parameters S_{11} and S_{12} described with Smith Chart from ADS - line of 1.28mm of width

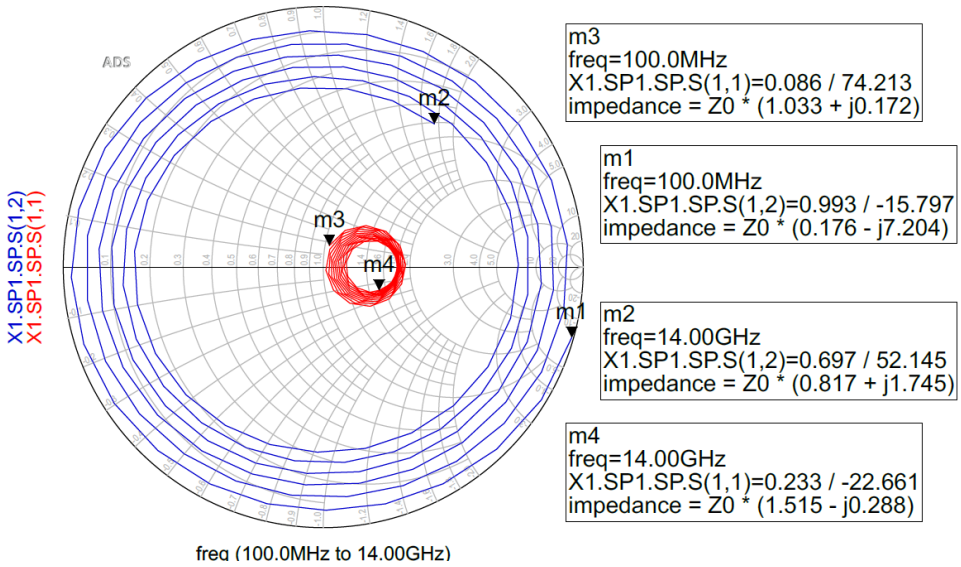

Figure E.2: S-parameters S_{11} and S_{12} described with Smith Chart from ADS - line of 1.58mm of width

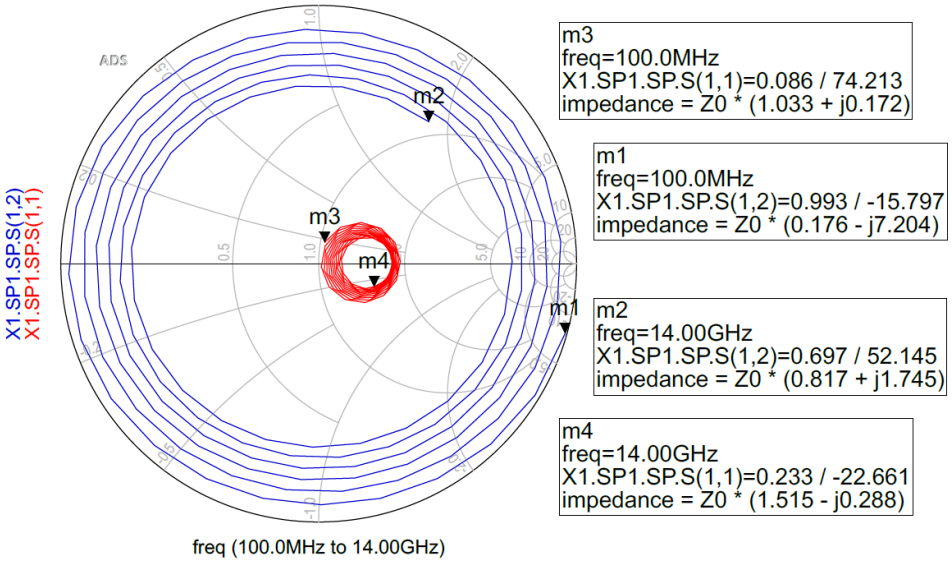

Figure E.3: S-parameters S_{11} and S_{12} described with Smith Chart from ADS - line of 1.78mm of width

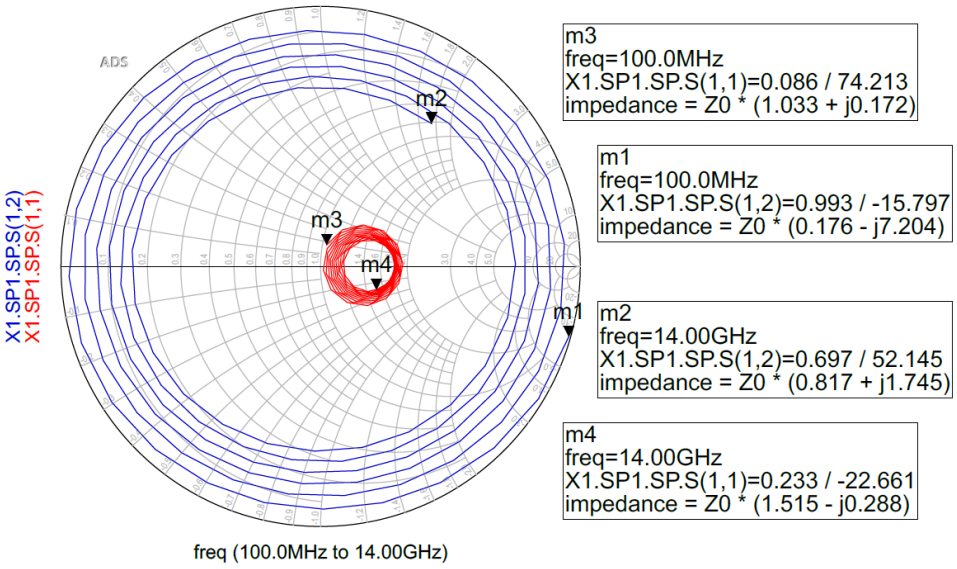

Figure E.4: S-parameters S_{11} and S_{12} described with Smith Chart from ADS - line of 1.98mm of width

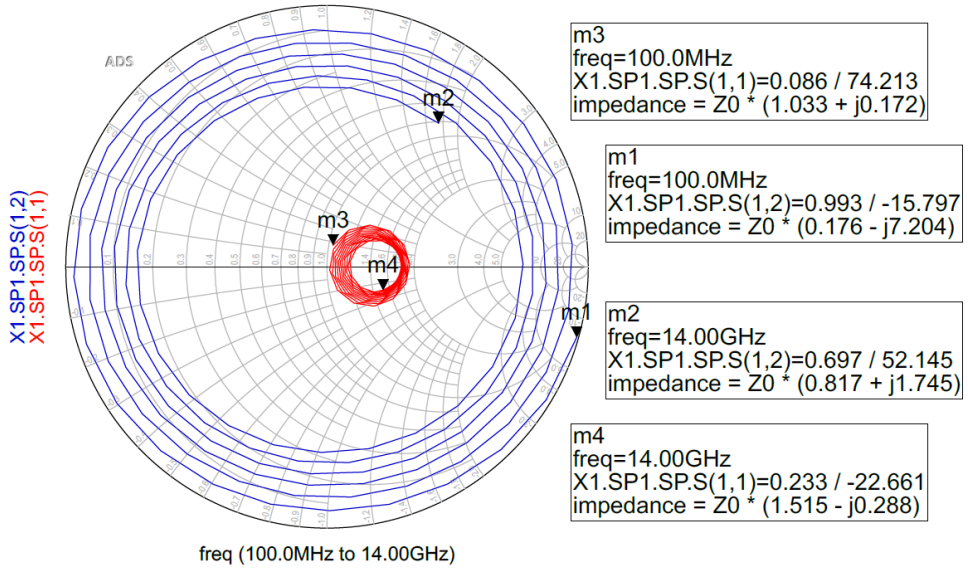

Figure E.5: S-parameters S_{11} and S_{12} described with Smith Chart from ADS - line of 2.18mm of width

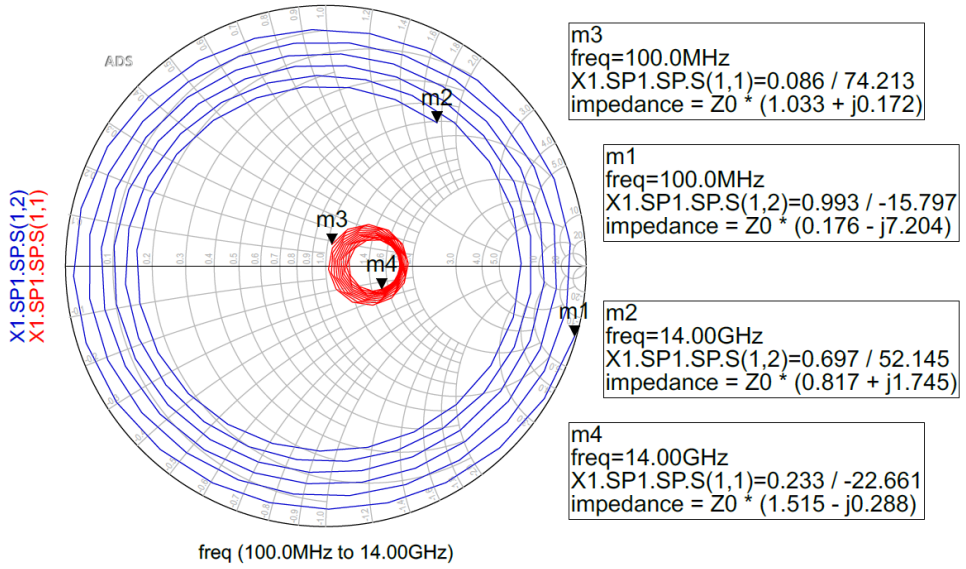

Figure E.6: S-parameters S_{11} and S_{12} described with Smith Chart from ADS - line of 2.48mm of width